
# NAVAL POSTGRADUATE SCHOOL

**MONTEREY, CALIFORNIA**

# THESIS

**APPLICATION OF COPPER INDIUM GALLIUM DISELENIDE PHOTOVOLTAIC CELLS TO EXTEND THE ENDURANCE AND CAPABILITIES OF UNMANNED AERIAL VEHICLES**

by

William R. Hurd

September 2009

Thesis Advisor: Sherif Michael
Second Reader: Todd Weatherford

| REPORT DOCUMENTATION PAGE | | Form Approved OMB No. 0704-0188 |
|---|---|---|



| 1. AGENCY USE ONLY *(Leave blank)* | 2. REPORT DATE | 3. REPORT TYPE AND DATES COVERED |
|---|---|---|
| | September 2009 | Master's Thesis |

**4. TITLE AND SUBTITLE**
Application of Copper Indium Gallium Diselenide Photovoltaic Cells to Extend the Endurance and Capabilities of Unmanned Aerial Vehicles

**5. FUNDING NUMBERS**

**6. AUTHOR(S)** William R. Hurd

**7. PERFORMING ORGANIZATION NAME(S) AND ADDRESS(ES)**
Naval Postgraduate School
Monterey, CA 93943-5000

**8. PERFORMING ORGANIZATION REPORT NUMBER**

**9. SPONSORING /MONITORING AGENCY NAME(S) AND ADDRESS(ES)**
N/A

**10. SPONSORING/MONITORING AGENCY REPORT NUMBER**

**11. SUPPLEMENTARY NOTES** The views expressed in this thesis are those of the author and do not reflect the official policy or position of the Department of Defense or the U.S. Government.

**12a. DISTRIBUTION / AVAILABILITY STATEMENT**
Approved for public release; distribution is unlimited

**12b. DISTRIBUTION CODE**

**13. ABSTRACT (maximum 200 words)**

In this thesis, we investigate the advantages of modifying current military Unmanned Aerial Vehicles (UAV) with available thin-film photovoltaic (PV) cells to increase their endurance, and/or capabilities. The approach taken was to explore available off-the-shelf flexible solar technology and to integrate it in a proof-of-concept model for testing and analysis. A physically similar commercially available battery-powered plane was used to demonstrate the materials and methods by which the RQ-11B (Raven) Small Unmanned Aerial Vehicle (SUAV) could be modified. This research extends academic and private pursuit of solar flight to near-term improvement of military SUAV. Besides increasing on-station time of reconnaissance assets, this research also displays the additional advantage of enabling systems on the ground to "self-charge." This will enable tactical units to operate further afield, untethered from conventional power sources. Beyond the proof-of-concept, findings are extended to other potential military uses and greater improvement through new or modified UAV design.

**14. SUBJECT TERMS**
Thin-Film Photovoltaics, CIGS, Unmanned Aerial Systems, UAV, Solar Plane, Maximum Power Point Tracker (MPPT), Lithium Polymer

**15. NUMBER OF PAGES**
151

**16. PRICE CODE**

| 17. SECURITY CLASSIFICATION OF REPORT | 18. SECURITY CLASSIFICATION OF THIS PAGE | 19. SECURITY CLASSIFICATION OF ABSTRACT | 20. LIMITATION OF ABSTRACT |
|---|---|---|---|
| Unclassified | Unclassified | Unclassified | UU |

NSN 7540-01-280-5500

Standard Form 298 (Rev. 2-89)
Prescribed by ANSI Std. 239-18

THIS PAGE INTENTIONALLY LEFT BLANK

**Approved for public release; distribution is unlimited**

# APPLICATION OF COPPER INDIUM GALLIUM DISELENIDE PHOTOVOLTAIC CELLS TO EXTEND THE ENDURANCE AND CAPABILITIES OF UNMANNED AERIAL VEHICLES

William R. Hurd
Lieutenant, United States Navy
B.S., Old Dominion University, 2003

Submitted in partial fulfillment of the
requirements for the degree of

**MASTER OF SCIENCE IN ELECTRICAL ENGINEERING**

from the

**NAVAL POSTGRADUATE SCHOOL**
**September 2009**

Author: William R. Hurd

Approved by: Sherif Michael
Thesis Advisor

Todd Weatherford
Second Reader

Jeffrey B. Knorr
Chairman, Department of Electrical and Computer Engineering

THIS PAGE INTENTIONALLY LEFT BLANK

# ABSTRACT

In this thesis, we investigate the advantages of modifying current military Unmanned Aerial Vehicles (UAV) with available thin-film photovoltaic (PV) cells to increase their endurance, and/or capabilities. The approach taken was to explore available off-the-shelf flexible solar technology and to integrate it in a proof-of-concept model for testing and analysis. A physically similar commercially available battery-powered plane was used to demonstrate the materials and methods by which the RQ-11B (Raven) Small Unmanned Aerial Vehicle (SUAV) could be modified. This research extends academic and private pursuit of solar flight to near-term improvement of military SUAV. Besides increasing on-station time of reconnaissance assets, this research also displays the additional advantage of enabling systems on the ground to "self-charge." This will enable tactical units to operate further afield, untethered from conventional power sources. Beyond the proof-of-concept, findings are extended to other potential military uses, and greater improvement through new or modified UAV design.

THIS PAGE INTENTIONALLY LEFT BLANK

# TABLE OF CONTENTS

THIS PAGE INTENTIONALLY LEFT BLANK

# LIST OF FIGURES

THIS PAGE INTENTIONALLY LEFT BLANK

# LIST OF TABLES

THIS PAGE INTENTIONALLY LEFT BLANK

# LIST OF ACRONYMS AND ABBREVIATIONS

| | |
|---|---|
| AFSOC | Air Force Special Operations Command |
| AGL | Above Ground Level |
| Ah | Ampere-Hour |
| AM | Air-Mass |
| ARPA | Advanced Research Projects Agency |
| a-Si | Amorphous Silicon |
| BATMAV | Battlefield Air Targeting Micro Air Vehicle |
| BDA | Battle Damage Assessment |
| BIPV | Building Integrated Photovoltaics |
| CdTe | Cadmium Telluride |
| CIGS | Copper Indium Gallium Diselenide |
| COTS | Commercial Off-The-Shelf |
| CZ | Czochralski |
| DARPA | Advanced Research Projects Agency |
| EO | Electro-Optical |
| ESA | European Space Agency |
| ESC | Electronic Speed Control Circuit |
| ETHZ | Swiss Federal Institute Of Technology Zurich |
| FCS | Future Combat System |
| FF | Fill Factor |
| GaAs | Gallium Arsenide |
| GCS | Ground Control Station |
| gMAV | Gasoline Micro Air Vehicle |
| GSE | Global Solar Energy |
| HALE | High-Altitude Long-Endurance |
| HVT | High-Value Targets |
| InP | Indium Phosphide |
| IR | Infrared |
| $I_{SC}$ | Short-Circuit Current |
| ISR | Intelligence, Surveillance, And Reconnaissance |
| IV | Current-Voltage |
| J | Joules |
| JCTD | Joint Comparative Technology Demonstration |
| JDAM | Joint Direct Attack Munition |
| LiPo | Lithium Polymer |

| | |
|---|---|
| Li-S | Lithium-Sulfur |
| LOS | Line Of Sight |
| MPPT | Maximum Power Point Trackers |
| Ni-Cd | Nickel Cadmium |
| Ni-mh | Nickel Metal Hydride |
| NREL | National Renewable Energy Laboratory |
| $P_M$, $P_{MPP}$ | Maximum Power Point |
| PV | Photovoltaic |
| PVPC | Photovoltaic Power Converters |
| RPV | Remotely Piloted Vehicle |
| RTF | Ready-To-Fly |
| SAR | Synthetic Apparature Radar |
| SOF | Special Operations Forces |
| STC | Standard Test Conditions |
| SUAV | Small Unmanned Aerial Vehicle |
| SWE | Staebler-Wronski Effect |
| TFPV | Thin-Film Photovoltaic |
| TFSC | Thin-Film Solar Cells |
| UAV | Unmanned Aerial Vehicles |
| UCAS-D | Unmanned Combat Air System Demonstration |
| $V_{OC}$ | Open-Circuit Voltage |
| Wh | Watt-Hour |

# EXECUTIVE SUMMARY

There are over 11,000 battery-powered UAVs in service or planned by the United States military. These systems provide tremendous benefit, but they have significant power restrictions that constrain their utility. These UAVs typically have an endurance of thirty minutes to two hours, after which time they must land so the batteries can be recharged, or so that another single-use battery can be installed. The retrieve-prepare-relaunch cycle can be far greater than the on-station time for the asset, and greatly reduces the utility of these systems to the intelligence gatherer, or war fighter.

These limitations cannot be solved merely by increasing battery sizes to extend missions or by including additional batteries in a system kit. The battery size must be a compromise between the additional endurance gained compared to the loss of payload volume and weight devoted to the larger battery. Increasing the size and number of battery packs also puts a greater strain on teams and individuals that use these systems. Each additional kilogram of weight and cubic centimeter of volume needed takes away from other needed equipment and supplies.

Present SUAV capabilities are already limited and advances in battery and lighter-weight materials technology are not keeping pace with ever-increasing needs for additional onboard electronics. The lack of sufficient power is expected to impact the use of these systems in the coming years.

The objective of this research was to investigate the improvement in battery-powered UAV performance through the additional of thin-film photovoltaic (TFPV) cells. We wanted to extend the range and endurance of tactical UAVs to increase mission effectiveness and improve the success and safety of our troops.

A secondary aim of this research was to demonstrate improved flexibility in deployment of tactical UAVs through the addition of TFPV. When not in flight, wing-mounted solar cells can recharge UAV batteries or other electronics, reducing the need

for an external power supply like a vehicle or generator. This "silent self-charge" capability might be of particular interest to Special Operations Forces (SOF) in remote locations.

This thesis selected the RQ-11 Raven as a target modification and flexible TFPV cells made from copper indium gallium diselenide (CIGS) after comparison of available alternatives. It compared solar-enhanced to battery-only performance through laboratory, stationary outdoor, and flight-testing. Since an RQ-11 was unavailable, a remotely piloted vehicle (RPV) of similar size was used as a proof-of-concept test platform. Additionally, the best CIGS could not be obtained, so heavier, less efficient CIGS cells from a flexible battery charger were tested.

Stationary and in-flight baseline battery endurance was established through constant throttle testing. Next, pre-installation tests showed that with 8% efficient CIGS, the endurance of the test plane could be extended up to three times its pre-solar baseline. Finally, using a constant-throttle flight to approximate the mission profile of a UAV, the aircraft flew 2.5 times longer with solar cells than without. Additionally, on-ground testing showed that the batteries used in this aircraft could be recharged between flights in as little as two hours.

Comparison between our test aircraft and the RQ-11 revealed that, although the Raven is much heavier and has greater power consumption due to its payload, similar endurance improvements might be seen using better 11% rather than 8% CIGS cells, much improved construction, and a maximum power point tracking circuit. Lastly, this thesis estimated the cost of such a solar modification to be less than $1,000 per aircraft, about 3% of the initial cost of a single Raven.

Improved solar-modified UAVs will potentially benefit the Department of Defense, the Intelligence Community and other users of UAVs. There are many additional applications of solar-modified UAVs, such as border, port, and maritime observation, agriculture and forestry, and wildfire monitoring.

# ACKNOWLEDGMENTS

To my wonderful wife Megan, and children Patrick and Katherine—thank you for your unwavering support. You made this possible.

Thank you also to my thesis advisor Dr. Sherif Michael and second reader Dr. Todd Weatherford, both of whom agreed to assist with my thesis, even after having taught me in several classes. Professor Michael provided guidance and showed great patience as my advisor.

I would also like to thank lab managers Jeffrey Knight and James Calusdian, who helped me with many of the practical aspects of my design and assembly.

Lastly, thank you to Thin-Film Flyer pilot Don Meeks, who volunteered so many hours. He ensured that the plane was tested in the safest way possible, out of the unskilled hands of the author.

THIS PAGE INTENTIONALLY LEFT BLANK

# I. INTRODUCTION

## A. BACKGROUND

The military uses thousands of Unmanned Aerial Vehicles (UAVs) that run on batteries and the number will only continue to climb. There are over 11,000 battery-powered UAVs in service or planned by the United States military [1]. Though these systems have provided tremendous benefit, they have significant restrictions that constrain their utility. Foremost among these limitations is energy. The payload, speed, and altitude primarily determine the power used in flight, and the duration of flight defines the total energy needed in the design and use of Small Unmanned Aerial Vehicles (SUAV).

These electrically powered SUAVs typically have an endurance of thirty minutes to two hours, after which time they need to be retrieved so the batteries can be recharged, or so that another single-use battery can be installed. The retrieve-prepare-relaunch cycle can be far greater than the on-station time for the asset, and greatly reduces the utility of these systems to the intelligence gatherer, or warfighter. SUAV capabilities are limited by in-flight stored power and the proximity of a nearby charging source.

These limitations cannot be solved merely by increasing battery sizes to extend missions and by including additional batteries in a system kit. The battery size must be a compromise between the additional endurance gained compared to the loss of payload volume and weight devoted to the larger battery. Increasing the size and number of battery packs also puts a greater strain on teams and individuals that are meant to benefit from these systems. Each additional kilogram of weight and cubic centimeter of volume needed takes away from other needed equipment and supplies.

Present SUAV capabilities are already limited, and advances in battery and lighter-weight materials technology are not keeping pace with ever-increasing needs for additional onboard electronics. The lack of sufficient power is expected to impact the use of these systems in the coming years.

> Future expectations for long-duration employment of unmanned systems cannot be supported by current energy sources. The volume and length of mission times required when combined, exceed the ability of current technology to support. This may lead to a decrease in the capabilities actually fielded, either in quantity or in length of mission capabilities. [1]

This leads to the obvious need for alternate means of storing energy, methods of conserving power, and generation or capture of additional energy while in fight. One of the most practical and promising means of extending SUAV flight is through the use of solar cells.

Universities, private ventures, and hobbyists have pursued solar flight for decades. The commercial and academic studies have generally focused on the development of futuristic prototypes or proof-of-concept vehicles without regard to near-term practical applications. On the other end of the spectrum, remote controlled aircraft hobbyists have experimented with existing commercial off-the-shelf (COTS) solar technology as a primary power source, or as an augment to batteries. There are currently no solar powered military UAVs. There are plans for a High-Altitude Long-Endurance (HALE) UAVs, including the Vulture program sponsored by the Defense Advanced Research Projects Agency [2].

## B. OBJECTIVE

In this research, we investigated the potential advantages of modifying current military Unmanned Aerial Vehicles with available thin-film photovoltaic (PV) cells in order to increase their endurance, and/or capabilities. Key factors in determining the practicality of this approach are the cost-benefit analysis (increased flight time versus initial and recurring costs), maintenance required, need for additional training, special handling and storage needs, and potential negative impact on flight parameters.

This research will potentially benefit the Department of Defense, the Intelligence Community as well as other users of UAVs. There are many additional applications of solar-modified UAVs, such as border, port, and maritime observation, agriculture and forestry, and wildfire monitoring.

The greatest near-term benefit to the military would be extended range and endurance of tactical UAVs to the war fighter and supporting intelligence activities. This would increase mission effectiveness and improve the success and safety of our troops, particularly Special Operations Forces (SOF) in remote locations without dedicated external air intelligence, surveillance, and reconnaissance (ISR) support. We wanted to demonstrate, not only improved flight characteristics, but also improved flexibility in deployment of tactical UAVs. When not in flight, wing-mounted solar cells can still be used to charge the UAV or other electronics, reducing the need for troops to plug-in to a power source, or carry additional batteries.

The aim of this research was to compare, procure, and test thin-film solar cells applied to a SUAV, or reasonably comparable Remotely Piloted Vehicle (RPV) and to compare the solar-enhanced aircraft characteristics to baseline battery-only attributes.

Beyond application of current technology on existing SUAVs, we also sought to extrapolate findings to investigate the potential benefit of applying the same solar cells to larger UAVs and other novel military applications.

## C. RELATED WORK

Since the first solar flight in 1974, there have been dozens of projects devoted to achieving sustained solar-powered aircraft [3]. There have been large and small-scale aircraft, flying exclusively on solar power, or using solar to augment onboard batteries. Of the recent projects that most closely relate to this research one the most notable have been AC Propulsion's SoLong in 2005 [4]. In 2006, André Noth of the Swiss Federal Institute of Technology Zurich (ETHZ) began test flights of the Sky-Sailor. In 2008, he flew the plane for 27 hours and landed with a fully charged battery [5]. Another member of the design team developed a small-scale adaptation, using the same design process with the Sun-Surfer in 2007 [6].

## D. APPROACH

The focus of this research was to research commercial-off-the-shelf (COTS) thin-film solar cells, power converters, and other necessary components that can configured for efficiency and weight conservation, and optimized for application to military UAVs. Ideally, the research would produce a solar-adapted prototype UAV of an existing military model. This was not possible due to time constraints and lack of available UAVs upon which to experiment. However, existing SUAVs were the basis for selection of COTS RPV and testing methods.

Of current United States SUAVs, the Raven (RQ-11B) appeared to be the best candidate for modification, not because it has the best surface area to weight ratio, but because thousands of them are already in use by the U.S. Armed Services and allies. We wanted to examine the SUAV whose modification would have the greatest operational impact for a significant number of years.

## E. ORGANIZATION

- Chapter II reviews the history of solar flight, and focuses on recent and relevant advances and will examine the current military UAV inventory.
- Chapter III will review the theory of operation of solar cells, and compare available thin-film photovoltaic technology.
- Chapter IV will explore existing and additional power components needed to integrate solar cells onto a UAV including batteries, regulators, charge control, and solar optimization circuits.
- Chapter V will cover the design and physical assembly of the aircraft components.
- Chapter VI is a presentation of the testing methods and results, to include laboratory, stationary outdoor, and flight tests.
- Chapter VII gives conclusions, and makes recommendations for extension of the current research.

# II. AIRCRAFT

## A. HISTORY OF SOLAR FLIGHT

On September 17, 1974, a new era of flight began when the Sunrise (Figure 1) made the world's first flight exclusively powered by solar cells. Astro Flight designed the aircraft under contract from the Advanced Research Projects Agency (ARPA) as a one-third scale model of a proposed aircraft.

Figure 1. Sunrise I, 1974 (From [7]).

Sunrise was not only the first solar plane, but also a concept for a perpetual or very long duration flight. The idea was to fly the plane at a very high altitude, above the cloud cover and high winds to expose the solar cells to the greatest amount of sunlight. It would then glide and descend slowly throughout the night until sunrise permitted it to regain altitude. This was obviously the first attempt to prove the concept of a High-Altitude, Long-Endurance (HALE) aircraft [3].

Another significant step in the annals of solar aviation was the flight of the Solar Riser, a manned aircraft (Figure 2). It did not have the ability to sustain flight on solar alone, instead power provided by its solar cells was used to charge a battery which enabled it to fly at approximately 12 m altitude for 0.8 km [8].

Figure 2. Solar Riser, 1979 (From [5]).

The next two significant solar aircraft were manned. First was the Gossamer Penguin, shown in Figure 3, which is a scaled-down version of the human-powered Gossamer Albatross II. This was the first solar aircraft powered in flight directly from the sun, that carried a human pilot. In this case, the human in question was a 13-year-old boy, the son of AeroVironment founder Dr. Paul MacCready. With a pilot that weighed only 80 lbs (36.3 kg), the plane was flown very low to the ground and for short distances [9].

Figure 3. Gossamer Penguin (From [5]).

With knowledge gained from the Gossamer Penguin project, and sponsorship from DuPont, AeroVironment and AstroFlight again teamed up to produce the Solar Challenger, shown in Figure 4. Specifically designed for solar flight as opposed to an adapted version of some other aircraft, it had large flat wings to accommodate a greater number of solar cells, and a robust structure to withstand greater winds. The plane flew across the English Channel on July 7, 1981 [5].

Figure 4. Solar Challenger (From [10]).

Solar flight has continued to improve in all aspects as photovoltaic cells have become lighter and more efficient and batteries have continued to improve in energy density. There have been many other significant achievements in solar aviation, but in the interest of brevity, we will focus on those that relate closely to the topic of this research. In 2008, André Noth wrote an in-depth review of the entire history of solar flight, which includes a comprehensive table of all known projects [5].

## B. RECENT SOLAR UAV RESEARCH

As performance has increased, so has cost decreased (Figure 5), enabling greater access, and innovation in the field of study.

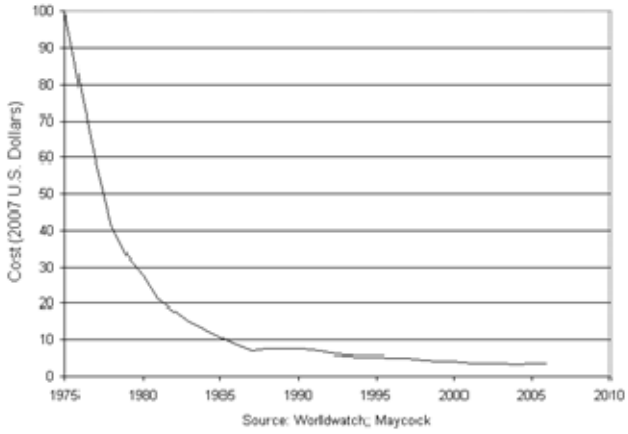


Figure 5. World Average Photovoltaic Module Cost per Watt (From [11]).

Solar airplanes have moved further from high-end academic exercises or materials exhibitions and closer to realistic and practical production models.

### 1. High-Altitude Long-Endurance

High-Altitude Long-Endurance (HALE) UAVs represent one of the most promising applications of thin-film solar cells for military or commercial surveillance and communications systems. From the first solar-powered airplane, designers have sought to create aircraft that operate at very high altitudes to take advantage of the best solar exposure and the ability to descend slowly during the night [3].

AeroVironment continued to develop the most notable solar HALE UAVs, often working with NASA. Continuing from the Solar Challenger, these aircraft include the Pathfinder, Pathfinder-Plus, Centurion, and Helios, shown in Figure 6.

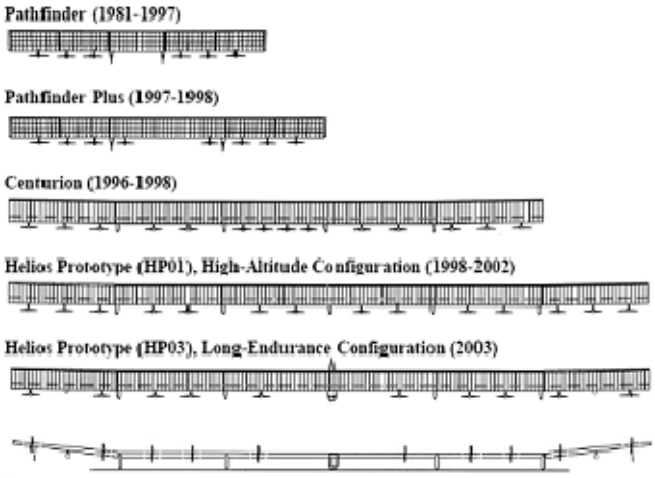


Figure 6. AeroVironment Solar HALE Evolution (From [12]).

Pathfinder flew to a solar-powered record of 50,000 feet in 1995, and after moving to Hawaii and undergoing additional improvements, flew to 70,500 feet in 1997. Pathfinder Plus was a larger version that featured two additional motors. In August of 1998, it flew to 80,200 feet. Next came the Centurion, with 14 motors, and a wingspan of 206 feet. The Centurion was originally intended to demonstrate flights at greater than 100,000 ft. altitude, and the Helios was to fly for at least 96 hours at 50,000 ft. In 1998, the Centurion made several low-altitude test flights [12].

Due to budget cuts, the Centurion was modified in 1999, and renamed Helios. NASA and AeroVironment agreed to abandon the lower-altitude test program and focus on the Centurion's original objectives. After a series of test flights and configuration changes, a high-altitude version of the Helios achieved a record-setting altitude of 96,863 ft. in August 2001. This was a record not only for solar planes, but also for all winged aircraft in horizontal flight. Unfortunately, a catastrophic crash in June 2003 effectively ended the program that funded the NASA/AeroVironment program, but it was viewed as having proved the HALE concept. A NASA report on the Helios mishap stated:

> Although more knowledge can and should be pursued as recommended in this report, an adequate knowledge base now exists to design, develop, and deploy operational HALE systems. [12]

Though budget cuts appear to have stalled NASA's solar HALE efforts, the research has continued. In July 2008, the Zephyr, from the British defense company Qinetiq, underwent U.S. Joint Comparative Technology Demonstration (JCTD) at Yuma Proving Grounds in Arizona. This aircraft carried a U.S. communications payload and flew for a record 82 hours and 37 minutes [13].

The Zephyr (Figure 7) is extremely lightweight, with a wingspan of 18 meters, but only weighing 30 kg (about 60 ft., 66 lbs.). Two emerging technologies have contributed to the lightweight construction, and therefore long endurance, of this aircraft. It uses lithium sulfur batteries, which have a much higher energy density per mass (350-400 Wh/kg), than lithium ion batteries (200–225 Wh/kg) [14]. The other main improvement in the planes power-to-weight ratio was achieved using thin-film solar cells. In this case, the aircraft was powered by amorphous silicon cells manufactured by United Solar Ovonic [15].

Figure 7. QinetiQ's Zephyr Solar UAV (From [15]).

Another ongoing solar HALE UAV project is the DARPA Vulture. This aircraft is envisioned as being capable of flying for over five years to provide intelligence, surveillance, and reconnaissance (ISR), and communications [16].

### 2. Small Solar/Battery Powered UAVs

Over the past five years, there have been a growing number of corporate and academic research projects, aimed at producing perpetual or long-endurance UAVs.

#### *a. SoLong*

On June 1–3, 2005, the solar UAV SoLong (Figure 8) flew for 48 hours and 11 minutes. This aircraft was designed and flown by AC Propulsion chairman Alan Cocconi. SoLong featured a 4.75 m wingspan, 12.8 kg weight, and 1,200 Wh battery [4]. It used SunPower Corporation A-300 silicon solar cells, which have been measured by the National Renewable Energy Laboratory (NREL) at an efficiency of 21.5% under standard test conditions [17].

Figure 8. 2005 Alan Cocconi with AC Propulsion's SoLong (From [4]).

### *b. Sky-Sailor*

The project that produced the Sky-Sailor solar airplane began as a European Space Agency (ESA) study. The goal was to determine whether continuous solar flight on Mars is viable for unmanned exploration. André Noth, then a PhD candidate, used this topic for his doctoral research. Dr. Noth and the Sky-Sailor team first developed a flexible design methodology for solar planes. The premise was to construct a rigorous model that would take into account some 30 constant, variable, and mission-dependent factors by which a solar plane could be evaluated and optimized. A multidisciplinary approach helped to produce a detailed model that takes into account electrical, mechanical, and physical factors [5]. For his Master's internship project, Niels Diepeveen tested the optimization method for scalability through the Sun-Surfer project (Figure 9) in January through March of 2007 [6].

Figure 9. Niels Diepeveen with Sun-Surfer in 2007 (From [6]).

The Sky-Sailor (Figure 10) was unlike the much larger HALE solar UAVs that flew above the cloud cover and had a significant altitude from which to descend during the night. It was also significantly different from the slightly larger SoLong plane, which took advantage of rising warm air, or "thermals" to assist the battery and solar cells. The Sky-Sailor was tested under level flight at only 200 m above ground level (AGL). On June 20, 2008, the Sky-Sailor demonstrated the ability for continuous flight, completing a flight of more than 27 hours [5].

Figure 10. André Noth with Sky-Sailor in 2008 (From [5]).

## C. MILITARY UAVS

### 1. History

With the advent of the first automatic gyroscope stabilizer, UAVs were first developed in World War I. These earliest unmanned flights were akin to modern cruise missiles. The first radio-controlled UAV was a converted U.S. Navy Curtis N-9 trainer (Figure 11) that was capable of carrying a 300 lb. (136 kg) bomb 50 miles [18].

Figure 11. Curtiss / Sperry Aerial Torpedo 1918 (From [18]).

Another significant UAV from WWI was the Kettering Bug, shown in Figure 12. Though it lacked the radio control of the Curtis model, this was an original design, rather than an adaptation of an existing craft. The Kettering Bug had a wingspan of only six feet, used a two-stroke engine, and was capable of carrying a 250 lb. (113 kg) bomb. The "aerial torpedo" was launched from a set of tracks, flew straight a predetermined distance, then crashed to earth. The war ended before it was used in combat [19].

Figure 12. Kettering Bug 1918 (From [19]).

The first reusable UAV was the Queen Bee, developed in the United Kingdom for Royal Navy anti-air gunnery training. From 1935–1947, the Royal Navy and Royal Air force used 380 of these aircraft. Another innovation during the war was the conversion of PB4Y-1 Liberators and B-17s to fly unmanned using television guidance systems [18].

Figure 13. Queen Bee Reusable Target UAV 1935 (From [18]).

The AQM-34 Ryan Firebee UAV, shown in Figure 14, flew more than 34,000 daytime and nighttime missions over Southeast Asia from 1965–1975. These UAVs were air launched and controlled by a DC-130, and deployed a parachute to land [18].

Figure 14. DC-130 with Two AQM-34 Ryan Firebees (From [20]).

The Israeli military modified and used 12 Firebees during the Yom Kippur War of 1973. They were used, not only for reconnaissance, but also as decoys. The Egyptians fired all 43 of their missiles at the Israeli drones. The Firebees were incredibly successful in this role as they evaded 32 of the missiles, and shot down 11 others with onboard Shrike air-to-air missiles [18].

During the remainder of the 1970s and into the 1980s, Israel emerged as the leader in UAV technology. The first of two notable UAVs they produced was the Scout. It was relatively small (13 ft. wingspan), and made of fiberglass, so it was very difficult to track, and even harder to destroy. The UAVs were capable of transmitting real-time video, and were incredibly effective in identifying Syrian RADAR sites for destruction by bombers. The second important Israeli UAV produced during this period was the Pioneer [18].

The U.S. Navy was disappointed in the ineffectiveness of naval gunfire support and airstrikes and the ability to conduct battle damage assessment (BDA) safely during operations in Libya, Grenada, and Lebanon [21]. The Navy sent a contingent to investigate the shortfalls of strikes against Syrian Army positions near Beirut. During this fact-finding mission, the team came away with a great appreciation for the effectiveness of Israeli UAVs in conducting targeting and BDA missions. They recommended the U.S. military should adopt similar UAV systems for these roles to increase mission effectiveness. This would keep pilots and much higher-cost aircraft out of these high-risk missions at a fraction of the cost [22].

The Secretary of the Navy agreed with the recommendation and ordered an rapid acquisition program to get these assets to the fleet. This resulted in the RQ-2 Pioneer aircraft, with a wingspan of 16.9 ft (5.15 meters), speed of 100-plus mph (161 kph) and the ability to carry a 65–100 lb. (29–45 kg) payload in excess of greater than 100 miles (185 km). The Pioneer can be launched from pneumatic rails or with rocket-assist, and can be recovered by net at sea or on a small, unimproved landing site ashore (Figure 15).

Figure 15. Shipboard Launch and Recovery of RQ-2A Pioneer (From [23][24]).

U.S. maritime and ground forces including operations in Bosnia, Yugoslavia, and Somalia have used the Pioneer. It was incredibly successful in directing naval gunfire, as witnessed during Operation Desert Storm. During one famous incident, Iraqi forces signaled their surrender to a low-flying RQ-2 that was spotting targets for the 16-inch guns of the USS Wisconsin (BB 64). Knowing the Pioneer's presence signaled an accurate and devastating impending strike, the soldiers used anything they could, including bed sheets, to signal their surrender [21].

From that point, the United States quickly became a leading user and producer of UAVs. As shown in Figure 16, the use of UAVs has grown exponentially since the attacks of September 11, 2001.

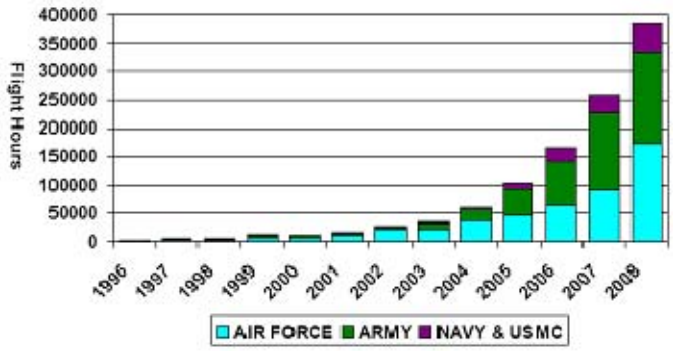


Figure 16. DoD UAS Flight Hours by Fiscal Year (From [25]).

These figures are particularly staggering when the fact that man-portable small UAVs (less than 10 lbs., 4.5 kg) are not included in the flight hours. The numbers of this type of UAV grew from 40 in 2002, to nearly 6,000 in 2008 (Table 1) [25].

| UAS | # of UAS | | Change in # (2002 - 2008) | UAS | # of UAS | | Change in # (2002 - 2008) |
|---|---|---|---|---|---|---|---|
| | 2002 | 2008* | | | 2002 | 2008* | |
| **Theater & Tactical (> 10 lbs)** | | | | **Small (< 10 lbs)** | | | |
| Pioneer | 34 | 0 | -34 | Dragon Eye | 40 | 672 | **632** |
| Silver Fox | | 53 | **53** | Raven A & B | | 4995 | **4995** |
| ScanEagle | | 13 | **13** | gMAV | | 54 | **54** |
| Shadow 200 | 24 | 252 | **228** | WASP | | 116 | **116** |
| Hunter | 41 | 41 | **0** | **Sub-Total** | **40** | **5837** | **5797** |
| I-Gnat/Warrior A | | 18 | **18** | | | | |
| Predator MQ-1B | 22 | 109 | **87** | **Grand Total** | **167** | **6358** | **6191** |
| Reaper MQ-9 | | 26 | **26** | Note: Small unmanned aircraft systems (SUAS), those weighing less than 10 lbs, have been included. The greatest increase in numbers of aircraft is due to SUAS. SUAS are listed separately. Numbers listed are for aircraft, not systems. Systems are composed of varying numbers of aircraft. | | | |
| Global Hawk | 6 | 9 | **3** | | | | |
| **Sub-Total** | **127** | **521** | **394** | | | | |
| * As of Oct 1, 2008 | | | | | | | |

Table 1. Change in Fielded Number of UAS 2002–2008 (From [25]).

### 2. Current United States UAVs

UAVs have obviously become much more prevalent in today's military. Unmanned surveillance and combat is widely seen as the future of operations. Missions that are best suited to UAVs are commonly described as "dangerous, dirty, or dull." The United States Congress recognized in 2001 the growing need for unmanned systems and mandated their increased use. In the 2001 Defense Authorization, they declared:

> It shall be a goal of the Armed Forces to achieve the fielding of unmanned, remotely controlled technology such that—(1) by 2010, one-third of the aircraft in the operational deep strike force aircraft fleet are unmanned.

Today's UAVs are incredibly diverse in size, capabilities, and mission employment. They can provide visual or thermal imagery, signals intelligence, targeting, and even the ability to strike High-Value Targets (HVT) in denied or remote areas. Though they often perform missions that manned aircraft can accomplish, UAVs eliminate the risk to pilots and aircrew, and often do so at a much lower cost.

UAVs have evolved into robust and highly reliable multi-mission capable aircraft. Each of the Armed Services employs UAVs for missions such as security, surveillance, targeting, and guidance. In the conflicts in Iraq and Afghanistan, they have saved many lives, "providing the Warfighter with evidence that IEDs have been planted on convoy routes, warning troops of ambushes, assisting troops in contact, and permanently removing HVAs from the battle." [1]

Apart from military applications, unmanned aircraft can be used in a myriad of ways by civilians for research, public safety, and commercial interests. Though it's not possible to detail every use, some of these applications include: search-and-rescue missions, fires detection and tracking, observing agriculture, wildlife, icebergs, hurricanes, aerial mapping, communications, and border security.

In the future, there may be even greater demand in the civilian sector for UAVs with superior capabilities and longer endurance. There are undoubtedly more suitable applications for use of thin-film photovoltaic cells as civilian aircraft can be easier to optimize for performance, as they do not need to meet the same levels of reliability and survivability.

Though the current research has wide potential for civilian and military UAVs alike, it focused primarily on military aircraft. In particular, it examined application of thin-film solar cells on the UAVs that, if improved, would most benefit the U.S. military in the near term. To that end, we reviewed current and forthcoming aircraft in the U.S. inventory to narrow the scope of the project.

Previously, several of the U.S. military services have categorized UAVs into different "tiers" or "classes." The latest DoD UAS Roadmap and other recent literature do not indicate agreement or adherence to named tiers, so we review UAVs by size, or similar employment.

There are of course many other UAV programs in various stages of development that don't fit into these existing classifications, including the Navy's Unmanned Combat Air System Demonstration (UCAS-D) [26], but we focus on those that are planned or in use in significant numbers.

### *a. Large/High Altitude/Strike*

These are the largest and probably most well known UAVs in today's inventory. Included are the Improved Gnat (I-Gnat) /Warrior Alpha, Predator (MQ-1), Reaper (MQ-9), Global Hawk (RQ-4), and the Hunter (MQ-5). Long-endurance drones like these have become indispensible to today's military. They have been providing commanders with persistent surveillance over a battlespace or theatre since the mid-1990s.

The lineage of several of these systems can be traced to DARPA's AMBER program (Figure 17). The medium-altitude unmanned aircraft first flew in 1986, but was not initially taken on as a program of record by the armed services. However, Desert Storm showed the significance of bringing this capability to the battlefield quickly [27].

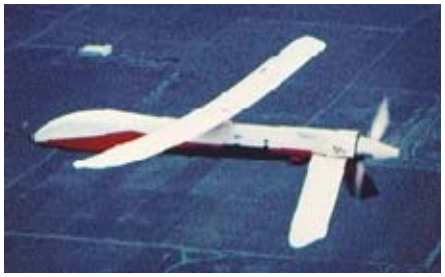

Figure 17. DARPA's AMBER Developed by Leading Systems 1986 (From [28]).

Based on the AMBER aircraft, the Gnat 750 (Figure 18) was developed to help bridge an identified ISR gap [27]. Later, a larger, more capable Gnat, the Improved Gnat-Extended Range (I-Gnat-ER) was produced. This includes the 2007 addition of strike capability. This configuration is now known as the "Warrior Alpha" [1].

Figure 18. General Atomics Gnat 750 (From [29]).

Of course, the AMBER's "descendants" did not end there. General Atomics acquired Leading Systems, which was the birthplace of AMBER, and produced the Predator derived from this basic design. The RQ-1 Predator began flying surveillance missions in 1995, and has been flown over Bosnia, Kosovo, Iraq, and Afghanistan. The Predator's designation was changed from RQ-1 to MQ-1 in 2001, indicating its new capabilities as a multi-mission aircraft versus reconnaissance only. The newer MQ-1 is 27 feet long (8.2 m) with a wingspan of 55 feet (16.8 m). It can carry a payload of 450 lbs. (204 kg), fly for over 24 hours, or 16 hours with weapons attached. The MQ-1 is powered by a 115 hp engine and can fly to 25,000 ft (7.62 km). The Predator was fitted with a laser designator so it can provide targeting for precision munitions, and it can be equipped with two AGM-114 Hellfire missiles [1].

The last piece of the AMBER/Gnat/Predator lineage is the MQ-9 Reaper, originally called the Predator B. It is a significantly larger and has a gross weight nearly five times that of the RQ-1, shown in Figure 19. The primary mission of the Reaper is to act as a "persistent hunter-killer for critical time-sensitive targets" [1]. It accomplishes this through the ability to carry much larger payloads than the Predator, up to 3750 lbs. (1,701 kg). This allows the aircraft to deliver GBU-12 Laser Guided Bombs, GBU-38 Joint Direct Attack Munition (JDAM), in addition to Hellfire Missiles.

USAF

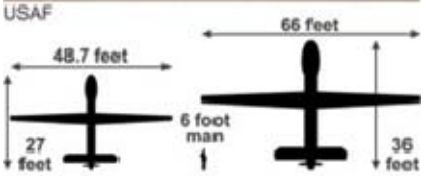


| Predator | | Reaper |
|---|---|---|
| 115 | Horsepower | 900 |
| 135 mph | Top speed | 300 mph |
| 25,000 | Max. altitude | 50,000 |
| 450 lbs | Payload | 3,750 lbs |
| 2 Hellfire laser-guided missiles | Armaments | 2 Hellfire missiles and heavier laser-guided bombs |
| 454 miles | Range | 1,878 miles |
| 2,250 lbs | Takeoff weight | 10,500 lbs |
| $40 million | Cost | $69.1 million |

Source: Department of Defense
By Frank Pompa and Chris Fruitrich, USA TODAY

Figure 19. Predator/Reaper Comparison (From [30]).

The next step in the evolution of this platform may be the Predator C (Avenger), shown in Figure 20. This jet-powered, stealthy UAV was developed by General Atomics and test flown in April 2009 [31].

Figure 20. General Atomics Aeronautical Predator C “Avenger” (From [32]).

Another system that falls into this general category is the MQ-5 Hunter (originally the RQ-5). Though these systems were only produced in small numbers under a joint service program until 1996, they have been retrofitted with modern avionics and the ability to carry munitions.

The last active member of this category is the RQ-4 Global Hawk. Similar to the AMBER/Gnat/Predator program, the RQ-4 Global Hawk began as a DARPA demonstration and was transferred to the Air Force [27]. The Global Hawk flew for the first time in 1998, and became a full-scale production model in 2001. It normally flies at very high altitude, providing theater-wide ISR. Its sensors include electro-optical (EO), infrared (IR), and synthetic apparature Radar (SAR). Due to its ability to fly at 65,000 ft (19.8 km), robust sensor package, and ability to keep pilots out of danger, the Global Hawk was selected to replace the U-2 [33]. Like the Predator, the Global Hawk has a larger, more capable variant, the RQ-4B. A size comparison of the enhanced model to the original is shown in Figure 21.


Figure 21. Global Hawk Variants (From [34]).

### *b. Medium*

According to the Marine Corps, these aircraft are "designed to support divisions, regiments, battalions, and MEUs" [35]. The Navy uses the ScanEagle in this role (Figure 22). The ScanEagle is approximately 40-pound (18-kg), has an endurance of over 15 hours, and normally flies at about 60 mph (97 kph) up to 15,000 feet. The Marine Corps has used the ScanEagle, and the previously described Pioneer (RQ-2), but in 2006 selected the Army's Shadow (RQ-7) to replace it. The Army selected the Shadow (Figure 23) for Brigade-level support in 1999. Like the ScanEagle, it is rail-launched, but it is a great deal heavier. The Shadow can fly faster (127 mph, 204 kph), carrying much heavier payloads than the ScanEagle (60 lbs., 27 kg), but only for five to six hours.

Figure 22. ScanEagle Shipboard Launch (From [36]).

Figure 23. Shadow (RQ-7) Launch (From [37]).

### *c. Small/Tactical*

These are small-unit tactical aircraft, powered by batteries. They can be man carried, and launched by hand. They provide units with low-level ISR, such as in mountainous or urban environments where a small-unmanned aerial system (SUAS) with a "birds-eye" view can conduct "close-range aerial observation over the next hill, ahead of convoys or a few blocks away in cities without endangering personnel" [38]. These systems use a laptop computer as a ground control station (GCS) and weigh approximately five pounds (2.27 kg).

Though they lack the endurance and firepower of some of their more famous brethren, these UAVs "have proven their worth at Company and Platoon level, giving short-term line of sight (LOS) ISR capability to individual soldiers and also extending the reach of soldiers providing base perimeter defense" [1].

Due to their low cost and portability, the United States' SUAV inventory dwarfs of that of that larger systems. As of 2008, there were nearly 6,000 SUAVs in the military's inventory, with many more on the way. Since the Air Force's transition from the Desert Hawk, and the Marine Corps' switch from the Dragon Eye, the RQ-11 Raven is the only remaining active production line. The Raven will survive as the "Joint" SUAV as these other UAVs are phased out.

AeroVironment's RQ-14 Dragon Eye first flew in 2000 (Figure 24). Following a 40-unit operational assessment, the USMC awarded a full-production contract to AeroVironment and BAI Aerosystems. The Dragon Eye weighs less than five pounds (2.27 kg), has a wingspan of just less than 4 feet (1.2 m), and can fly for 45–60 minutes. A second variant, called the RQ-14B Swift was simply an RQ-11A Dragon Eye that used a Raven Ground Control Station (GCS). Production is complete on these systems, but as of October 2008, there were still 672 systems in use.

Figure 24. U. S. Marine Launching an RQ-14 Dragon Eye (From [39]).

By far the most prevalent SUAV is the RQ-11 Raven, shown in Figure 25. The Raven was developed from the Flashlight and Pathfinder aircraft in 2002 and was selected as an interim solution for the Army in 2004. It provides color electro-optical

imagery as well as infrared, and is normally flown at a mission altitude near 500 feet (152 m). As of October 2008, there were already nearly 5,000 Ravens fielded, with 5,000 more to come. This makes the Raven the most widely used UAV in history.

Figure 25. Soldier Hand-Launch of RQ-11 Raven (From [40]).

We will focus on the Raven in following chapters as the UAV of choice for solar modification since its use is so widespread, and it looks to be the SUAV program for the U. S. military for the foreseeable future. Table 2 gives an overview of the physical and performance characteristics of the Raven.

| RQ-11 Raven | | | |
|---|---|---|---|
| Weight | 4.2 lb | Payload Capacity | 11.2 oz |
| Length | 36 in | Engine Type | Direct Drive Electric |
| Wingspan | 55 in | | |

**Performance:**

| | | | |
|---|---|---|---|
| Ceiling, MSL | 15,000 ft | Endurance | 90 min |
| Normal Operating Altitude, AGL | 500 ft | Cruise Speed | 26 kts |
| Radius | 10 km (LOS) | | |

Table 2. RQ-11 Raven Characteristics [From [1]).

### *d. Micro UAVs*

There are two significant micro-UAV programs in the DoD, with many more on the horizon. The first is the Battlefield Air Targeting Micro Air Vehicle (BATMAV). The specific aircraft that functions in this role is the Wasp III, manufactured by AeroVironment. The Wasp III (Figure 24) is small, very lightweight (1

lb), and was developed for Air Force Special Operations Command (AFSOC). Combat Controllers can easily transport this UAV to provide force protection and to help guide friendly air strikes while staying further from enemy positions. [1]

Figure 26. AeroVironment Wasp III MAV (From [41]).

The second notable micro-UAV is the gMAV, or Gasoline Micro Air Vehicle (Figure 25). DARPA funded and Honeywell developed this ducted-fan man-packable unit. It is 16.5 pounds (7.5 kg) and can be operated by a single soldier, though it is often carried to a location in a vehicle prior to deployment [42]. The program is still under evaluation, but has been operated in Iraq by the Pennsylvania Army National Guard's 56th Stryker Brigade Combat Team. This followed gMAV missions supporting the 25th Infantry Division that were flown by Honeywell operators.

Figure 27. Honeywell gMAV Ducted Fan Micro Air Vehicle (From [43]).

### *e. Vertical Take Off and Landing (VTOL) UAV (VTUAV)*

The last U.S. military UAV we review is the MQ-8 Fire Scout. The MQ-8 is an unmanned helicopter, based on the Schweizer Model 333 manned helicopter. The Navy awarded Northrop Grumman a contract to develop the RQ-8A in February 2000. In 2003, the Army selected the Fire Scout for its Future Combat System (FCS). In 2004, the Navy formalized a contract for an MQ-8B variant for use aboard the Littoral Combat Ship. In 2006, the two Fire Scouts autonomously landed aboard the USS Nashville (LPD-13) a total of nine times. This marked the first time an unmanned helicopter landed and launched on a moving U.S. ship [44]. This is displayed in Figure 28.

Figure 28. Fire Scout Landing on USS McInerney (FFG-8) (From [45]).

## D. CHAPTER SUMMARY

In this chapter, we described the history of solar flight, described some of the most recent research on the subject, and presented an overview of current U. S. military UAVs. Of these UAVs, the RQ-11 Raven appears to be the most relevant to the present effort to improve a UAV using thin-film solar cells due to its use of battery power, relatively short flight endurance, and large numbers of aircraft in use. Most of the UAVs described in this chapter are shown in Figure 29, an overview of the existing and projected major UAV systems in the United States.

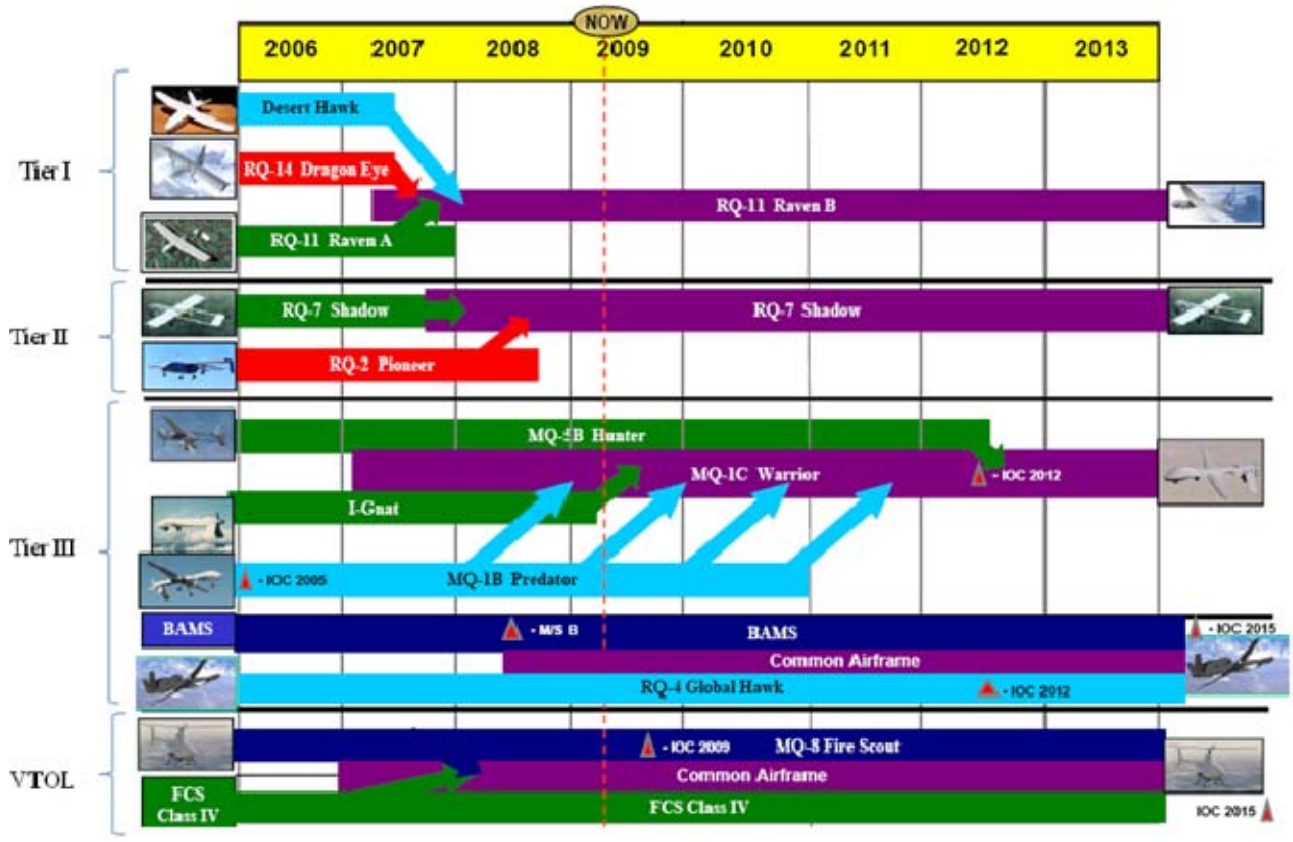


Figure 29. DoD UAS Convergence Plan (After [25]).

THIS PAGE INTENTIONALLY LEFT BLANK

# III. PHOTOVOLTAICS

## A. THEORY OF OPERATION

From as far back at the seventh century B.C., solar energy has been used to start fires, to heat water, and even to cook food. The ability for solar energy to be converted to electrical energy was found in 1839 when Edmond Becquerel discovered the Photovoltaic Effect. Over one hundred years later, in 1954, the first silicon photovoltaic (PV) cell was developed at Bell Labs. This first cell was able to convert 4% of the Sun's energy into electricity [46].

From those humble beginnings, solar energy has shown incredible growth. Figure 30 shows the total worldwide photovoltaic production from 1975–2007. Solar power has become more popular with each passing year due to: rising fossil fuel energy costs, the search for renewable energy sources due to concerns for the environment, and the rapidly decreasing cost of solar energy.

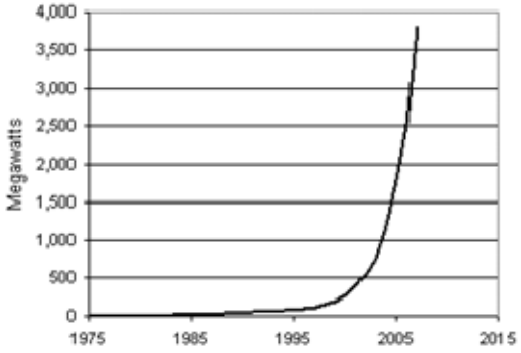


Figure 30. World Annual Photovoltaic Production 1975–2007 (From [47]).

Because silicon solar cells are the simplest and most prevalent solar cells, we use them as the foundation for explaining the photovoltaic effect and factors that affect solar cell performance.

### 1. Semiconductors

Solar cells are p-n junctions like diodes. Like diodes, they are usually made from silicon, which "makes up 25.7% of the earth's crust by weight" [48]. Silicon is a Group

IV semiconductor, which means it has four electrons in its outermost or valence shell. When elements like silicon form regular, rigid structures called crystals, they "prefer" to have their outermost electron shell full. In crystalline silicon, if it is pure or "intrinsic," each of the four valence electrons forms a covalent bond between an adjacent silicon atom. These shared electrons allow each atom to have eight in their valence shell, so they are stable. If some of the Group IV silicon is replaced, or "doped" by a Group V element such as phosphorus, shown in red in Figure 31(a), then four of the electrons from the phosphorous will form covalent bonds with the nearest silicon atoms. Since Group V elements have five valence electrons, and the valence shell of the silicon and phosphorus are now both full with eight electrons each, there is one remaining electron from the phosphorus atom. This "extra" electron is represented by the "$e^-$" in Figure 31(a). This material is now referred to as an "n-type" semiconductor or "donor" material as it easily gives up the lightly bound electron.

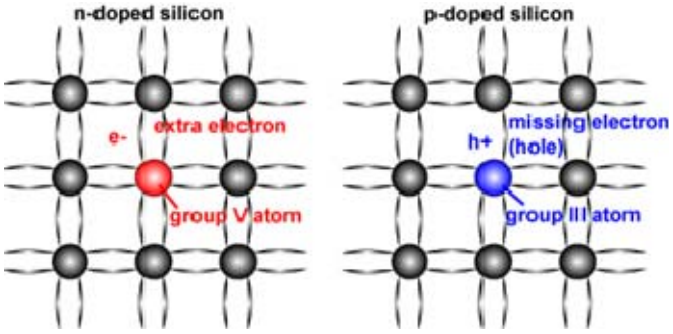


(a) (b)

Figure 31. Crystal Silicon Doping (From [49]).

A similar process takes place in the creation of a "p-type" semiconductor material. However, in this case, a Group III material like Aluminum is used, rather than Group V material. The three electrons form bonds with three adjacent silicon atoms, but one bond is left unfilled. This absence of an electron or "hole" is a spot that is easily taken by a free electron to complete the valence shell, thus the semiconductor is seen as "positive" or an "acceptor" material.

## 2. P-N Junction

One useful way to represent semiconductors in solid-state physics is with "energy band" diagrams. An energy band diagram is often useful in explaining the operation of semiconductor devices. Figure 32 shows a simple diagram that compares the energy bands of metals, semiconductors, and insulators.

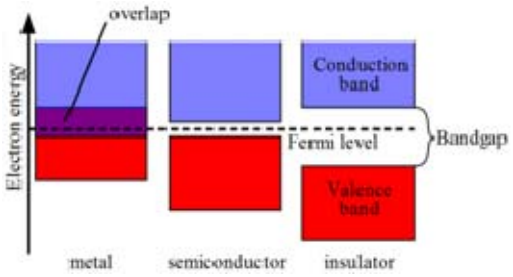


Figure 32. Simplified Energy Band Diagram Comparison (From [50]).

The first important aspect of the diagram is the bandgap, or energy gap of the material, often indicated by $E_G$. This is an electrical, rather than physical property, and indicates the amount of energy that must be imparted to an electron in the valence shell of a semiconductor for that electron to move to the conduction band. Conduction band electrons are "free" in that they are not bound to an atom. In an insulator, the valence band is full, and the conduction band is empty. It is relatively difficult to remove an electron from the valence band of these atoms when the bandgap ($E_G$) is large.

A semiconductor has a partially filled valence band, so $E_G$ is somewhere between the conductor and insulator. In metal, or other conductors, the valence and conduction bands are very narrow, or even overlap, so electrons can be easily freed from the valence shell. Figure 33 shows the bandgap at room temperature of silicon (Si), gallium arsenide (GaAs), and germanium (Ge). $E_C$ and $E_V$ are the conduction and valence band energies.

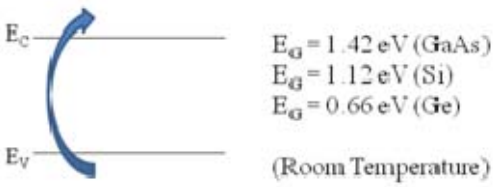


Figure 33. Bandgap of Common Semiconductors (After [51]).

Though energy band diagrams for semiconductors can be much more complicated, simplified energy band diagrams help us understand the most important aspects for the current discussion. Aside from the energy bandgap of the material, which is largely a function of the electron configuration of an intrinsic material, the Fermi level is the most important parameter of semiconductors.

An in-depth review of the development of Fermi levels is beyond the scope of this research. Simply put, the Fermi level is drawn from a probabilistic analysis and provides a numerical indication of the distribution of electron states within a material. In an intrinsic semiconductor, the Fermi level is centered in the bandgap. This is shown by the line $E_I$ in Figure 34(a). The Fermi level of an extrinsic or doped semiconductor is indicated by the line $E_F$ in Figure 34 (b) and (c). In short, the Fermi level's position in the energy gap is a quick indication of the type of conducting material.

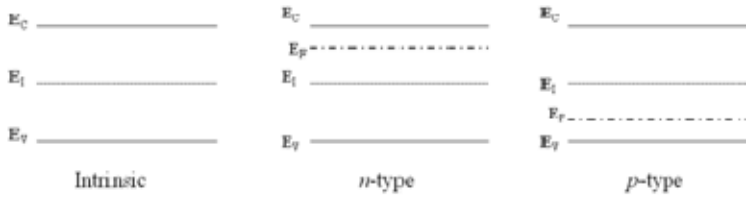


(a) (b) (c)

Figure 34. Intrinsic and Quasi-Fermi Levels in Semiconductors (From [51]).

When n-type and p-type semiconductors are joined, they form the most basic semiconductor device, the p-n junction, or diode. When these two materials are brought together the charge carriers, electrons and holes, diffuse across the junction, quickly come to a stable quiescent state. This is shown by the alignment of the Fermi levels on the energy band diagram (Figure 35). The resulting "band-bending" is an indication of the internal electrostatic field created within the device. The diffusion of charges causes a depletion region to form. The width of the depletion region is analogous to the height of the barrier indicated by "$qV_{bi}$" on Figure 35. In order for the barrier to be overcome to allow current to flow through the device, an external voltage is applied to "forward bias" the p-n junction. Of course, the reverse is also true. If the opposing polarity external voltage is applied, it increases the width of the depletion region, or height of the barrier, further inhibiting current flow.

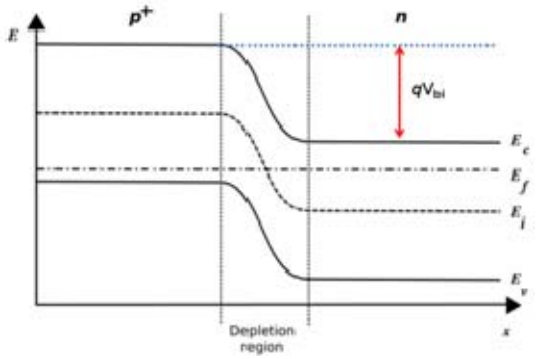


Figure 35. P-N Junction (After [52]).

### 3. Photovoltaic Effect

Without an external light source, solar cells conduct like a diode, indicated by the black line in Figure 36. Like a diode, the solar cell will conduct electricity when an external voltage of the correct polarity and magnitude. The forward-biasing of solar cells is very undesirable as they are meant to generate photocurrent for a load when they are reverse-biased. A blocking diode is connected between the solar cell and load to prevent the cell from conducting and discharging batteries, or damaging other loads.

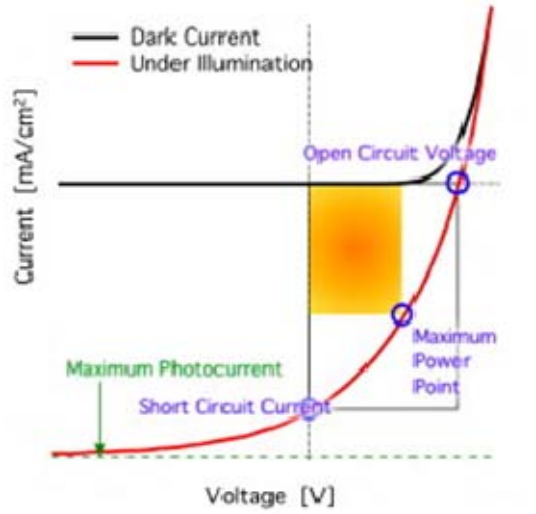


Figure 36. Solar Cell Light-Dark Current-Voltage (IV) Curve (After [53]).

The red line in Figure 36 shows the current of the solar cell when it is illuminated. This is also referred to as the "light" current-voltage (IV) curve and shows the current that is being supplied from the solar cell as a result of the photovoltaic effect.

Some of the photons that arrive at a solar cell are reflected from the surface. Others that enter but have low energy will pass through the cell. Some of the photons of the correct wavelength, and therefore energy greater than the semiconductor bandgap, enter a solar cell, and are absorbed. Recall that the bandgap of the semiconductor material differs based on the material and doping. These photons impart energy to electrons, freeing them from the valence shell, and creating an electron-hole pair. The formation rate of electron-hole pairs due to photons is referred to as the photogeneration rate. The internal electric field, or built-in voltage, causes electrons and holes to separate and move toward the front and back contacts of the cell and through the load to recombine (Figure 37).

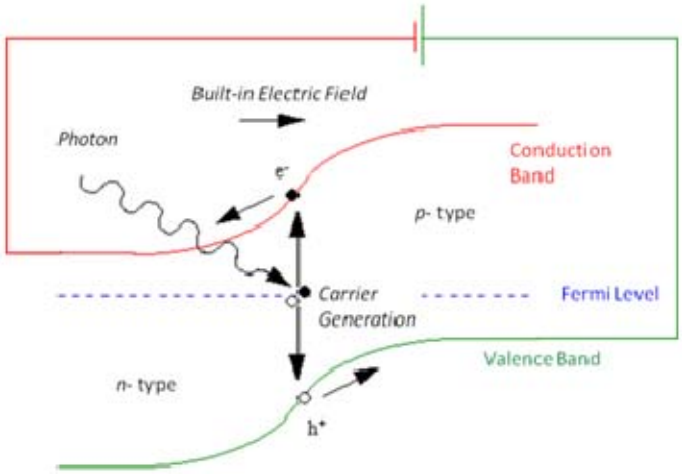


Figure 37. Energy Band Diagram of Photovoltaic Effect (After [54]).

Figure 38 is a physical representation of a solar cell demonstrating the generation of current by the photovoltaic effect.

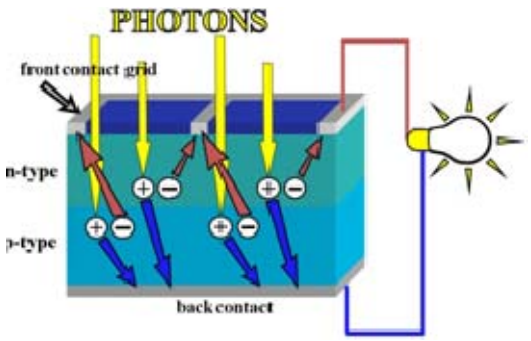


Figure 38. Simplified Solar Cell (From [55]).

## 4. Cell Performance

The first thing that affects a solar cell's efficiency is the bandgap ($E_G$) of the material of which it is constructed. As shown previously, the bandgap is determined by the intrinsic material and doping level. Some compounds can be "tuned" to respond to a particular band of the solar spectrum. Obviously, for a solar cell to produce the greatest amount of electricity for a given illumination level, the cell material used should be chosen based on the spectrum of light. As discussed, the energy of the photons ($E_P$) needs to be greater than that of the semiconductor bandgap ($E_G$) in order to be absorbed to create an electron-hole pair.

### *a. Energy Calculations*

The energy of the incoming photons in Joules (*J*) can be determined using [56]

$$E_p = hv \tag{3.1}$$

where $v$ is the frequency of the incoming radiation in Hertz (Hz) and $h$ is Planck's constant ($6.6262 \times 10^{-34}$ J-s). Since electromagnetic energy is usually referred to by its wavelength $(\lambda)$ rather than frequency, we do an easy substitution using the relationship

$$v = \frac{c}{\lambda} \tag{3.2}$$

Where $c$ is the speed of light in meters per second ($3 \times 10^8$ m/s) and $\lambda$ is the wavelength of radiation in meters.

Therefore, the energy of photons related to wavelength is

$$E_P = \frac{hc}{\lambda} \tag{3.3}$$

The bandgap of the most common photovoltaic cell (Si) is 1.12 *eV* or 1.79 × $10^{19}$ *J* (1*eV*=1.6 x $10^{-19}$*J*). When substituting into 3.3 and rearranging, we find this corresponds to

$$\lambda = \frac{(6.6262 \text{ x } 10^{-34})\,(3 \text{ x } 10^{8})}{1.79 \text{ x } 10^{-19}} = 1.11\mu\text{m} \tag{3.4}$$

We know that $E_P$ needs to be greater than $E_G$, and since the energy of radiation is inversely proportional to wavelength (3.3), the wavelengths of light that can be converted to electricity by a silicon solar cell must be less than 1.11 μm.

### *b. Solar Radiation*

Now that we have reviewed photovoltaic device operation principles, we need to look at the most important external factor in performance, the Sun's spectrum. For space and very-high altitude applications, the reference spectrum is Air-Mass Zero (AM 0). This is the radiation in space without atmospheric interference and results in a power density of approximately 1,360 watts per square meter (W/$m^2$). As shown in Figure 39, AM 1.0 is the spectrum of light through one Earth atmosphere when the Sun is at its zenith perpendicular to a point on the surface. Since AM 1.0 is extremely narrow in its applicability, a more realistic spectrum is used for comparing solar cells. The power density for AM 1.5 is approximately 1000 W/$m^2$ [57].

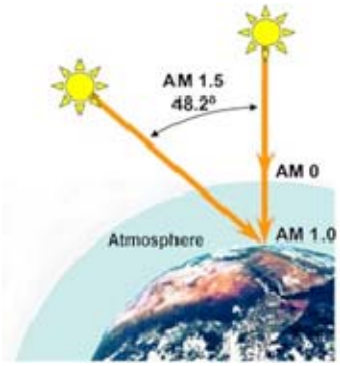


Figure 39. Solar Spectrum Air-Mass Numbers (From [57]).

The irradiance of the Sun is the radiant power incident to a surface per unit area, usually measured in watts per square meter ($W/m^2$). Figure 40 shows the difference between AM 0, the upper curve shown in yellow, and AM 1.5, the lower curve shown in red. Aside from a generally reduced power across the spectrum due to scattering and absorption, specific bands of energy are greatly attenuated by water vapor and carbon dioxide in the atmosphere. This is shown by the dramatic dips in irradiance called "Absorption Bands."

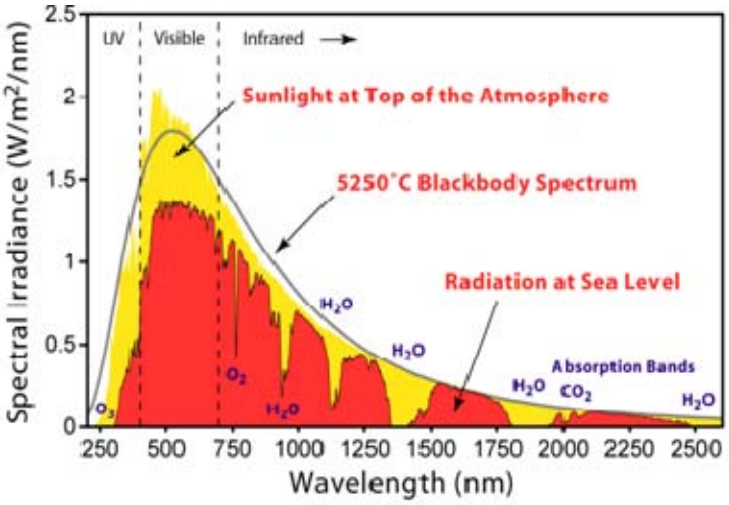


Figure 40. Solar Radiation Spectrum (From [58]).

### *c. Characterization of Solar Cells*

There are five parameters that are used most commonly to describe the electrical characteristics of a solar cell: open-circuit voltage ($V_{OC}$), short-circuit current ($I_{SC}$), maximum power ($P_M$, $P_{MPP}$, or simply MPP), energy conversion efficiency ($\eta$), and fill factor (FF). The most complete way to characterize a solar cell is through the use of a Current-Voltage, or "IV" curve, like the one shown in Figure 41. Solar cell performance is generally measure under standard test conditions (STC). This is defined as AM 1.5 (1000 $W/m^2$) at 25°C [59]. As the names implies, the open-circuit voltage ($V_{OC}$) of the cell is measured with an open circuit, and $I_{SC}$ is measured with the terminals of the cell electrically shorted. The resistance of the test load connected to the cell is varied over the full range from short to open and data collected to characterize the complete response.

As shown by the red line in Figure 41, the maximum power from the cell is not equal to the hypothetical maximum.

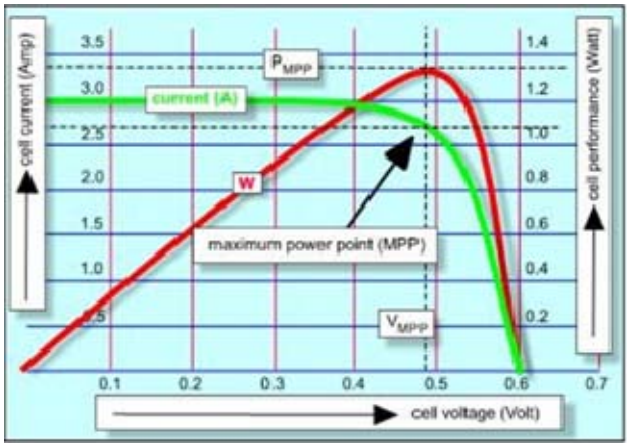


Figure 41. Solar Cell IV Curve and Power (From [60]).

Figure 42 shows that the actual maximum power from a solar cell is less than the theoretical maximum power, which is the product of $V_{OC}$ and $I_{SC}$.

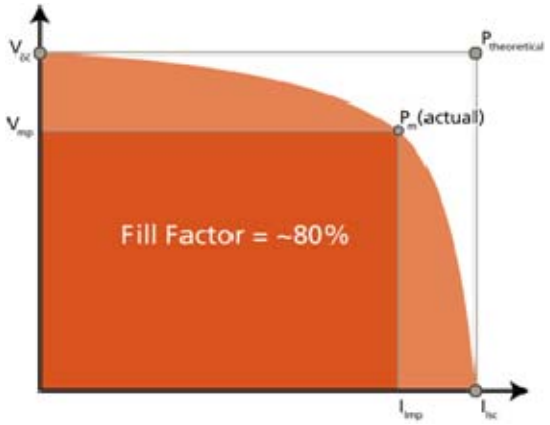


Figure 42. Solar Cell IV Curve Showing Fill Factor (From [61]).

The degree to which the actual output is less, is known as the fill-factor and is found using [56]

$$FF = \frac{V_{mp} I_{mp}}{V_{OC} I_{SC}} = \frac{P_{mp}}{V_{OC} I_{SC}} \tag{3.5}$$

The last basic parameter to describe is the energy conversion efficiency. This is a measure of the ability of the cell to convert electromagnetic energy of light or other radiation into electrical power from the cell. This is not a measure of the number of electron-hole pairs that are produced for a given number of photons, but rather an external measurement of the current that comes from the terminals of the cell, since recombination takes place within the cell limiting usable current. Maximum efficiency is found using [59] [56]

$$\eta = \frac{I_{SC} V_{OC} FF}{P_{light} A_a} = \frac{P_{out}}{P_{in}} \tag{3.6}$$

where $P_{light}$ is the power of incident photons ($W/m^2$), and $A_a$ is the solar cell aperture area ($m^2$).

### *d. Factors Affecting Performance*

Several factors can limit the numbers of photons that are absorbed, the number of electron-hole pairs that are created, and the number of charge carriers that "escape" from the bulk of the semiconductor to the cell's contacts and beyond. The first significant factor is reflection that is shown in Figure 43. In order to reduce reflection, texturing and anti-reflective coatings are applied to the surface. Lost efficiency from reflection can be reduced from as high as 36% to 5% using these methods [62]. The next factor, related to reflection, is self-shading. Some of the light that incident to the cell surface is reflected or absorbed by the cell's top conductors. This can result in a loss of up to 8% of incoming light. For this reason, the geometry of top conductors must be optimized to reduce shading while remaining large enough to allow charge carriers to be captured before they recombine within the semiconductor [62].

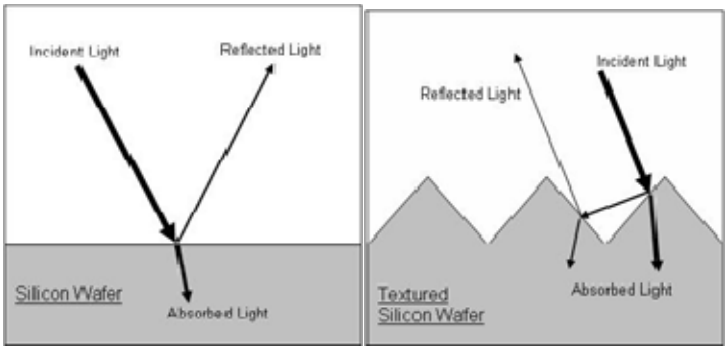


(a) (b)

Figure 43. Reflection from Surface (a) and Texturing to Reduce Reflection (b) (From [63]).

Increased temperature is the second major loss of efficiency in cells. This can be caused by increased ambient temperature in the operating environment or from incorrect photon energy. Low-energy photons that do need meet the bandgap energy, do not create an electron-hole pair, but can be absorbed by cell and converted into heat. Photons of energy greater than the semiconductor's bandgap are more likely to create an electron-hole pair, but the energy above that needed for photogeneration is also converted to heat.

These higher temperatures cause greater "lattice vibration" in the semiconductor crystalline structure which impedes the flow of charges. If there are greater numbers of charge-carriers created due to the heat, there is an increased chance that a photon-created charge carrier will interact with a heat-induced charge carrier and recombine. Electrons and holes recombining inside the semiconductor reduce the number that can create useful current outside the cell [62].

There are additional factors that lead to greater recombination rates are. The thickness of the semiconductor regions must be considered. There will be very little photocurrent produced if photogeneration rates are high, but charge carriers must travel long distances through the bulk to reach an electrical contact. Material defects like impurities and imperfect crystalline structure lead to "dangling bonds," missing covalent bonds, which act as additional recombination centers within the bulk of the cell [62].

### *e. Types of Cells*

As noted previously, different semiconductor materials have different bandgaps and therefore respond to different wavelengths of light. Figure 44 shows part of the periodic table of elements with the most commonly used semiconductor materials shown in blue. The earliest and most basic semiconductors and hence solar cells were made from silicon or germanium doped with a Group III or Group V element to make them *n* or *p* material. Another common group of semiconductors are called III–V compounds, such as gallium arsenide (GaAs), or Indium Phosphide (InP). Lastly, semiconductors and solar cells can be made from more exotic mixes of elements from I–VI. The two most common of these compounds used for photovoltaics are Cadmium Telluride (CdTe), and Copper Indium Gallium DiSelenide, commonly referred to as CIGS [49].

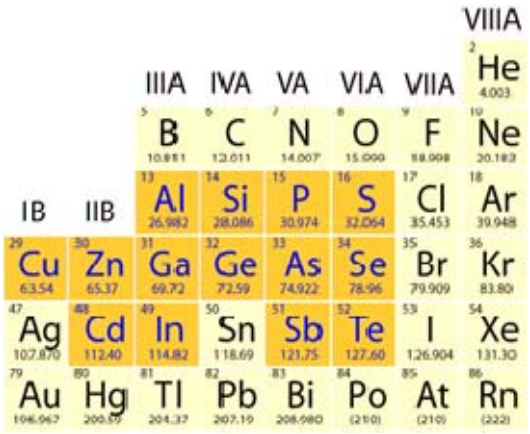


Figure 44. Periodic Table with Commonly Semiconductors (From [49]).

The most common material for solar cells is silicon, which can be used in three different forms. The first is single-crystal silicon (c-Si), the same form used in transistors, integrated circuits, and other common components. This is the most expensive, but also highest quality and most efficient form of single-junction silicon cell. The process of creating c-Si is called the Czochralski (CZ) process. A picture of various sizes of ingots, or "slugs" and wafers of c-Si and are shown in Figure 45 [49].

Figure 45. Single-Crystalline Silicon Ingots and Wafers (From [64]).

Multi-crystalline silicon is much simpler and cheaper to produce. The process involves pouring melted silicon into a cast and allowing it to cool. Unfortunately, this produces many small crystals of varying orientations. Between each of these crystals are "grain boundaries" (Figure 46) which produce regions of high recombination [49].

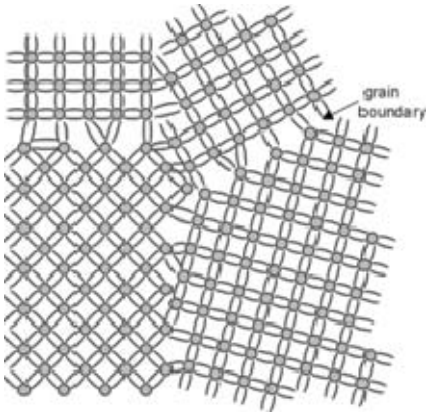


Figure 46. Multi-Crystalline Silicon with Grain Boundaries (From [49]).

The last form of silicon commonly used in solar cell production is called amorphous silicon (a-Si). Amorphous silicon can be produced very cheaply on flexible substrates, but due to its physical structure has a much higher level of recombination than either single or multi-crystalline silicon. Amorphous silicon will be discussed further in this chapter as thin-film silicon cells are compared for application to aircraft.

One of the most promising types of cells in use today is the multi-junction cell. These cells are stacks of single junction cells layered upon each other. The simplified structure and external quantum efficiency of an example of these is shown in Figure 47. The manufacture of these cells is much more complicated and costly than other technologies, so their use has been somewhat limited to applications that require very high efficiencies such as satellites and terrestrial concentrators. As shown in Figure 47, the top cell, in this case InGaP, is designed to absorb blue light, which has the highest energy and shortest wavelength. The longer wavelength light then passes through to the InGaAs layer where green light causes photogeneration. The lowest energy radiation passes through to the lowest layer, made from Ge [65].

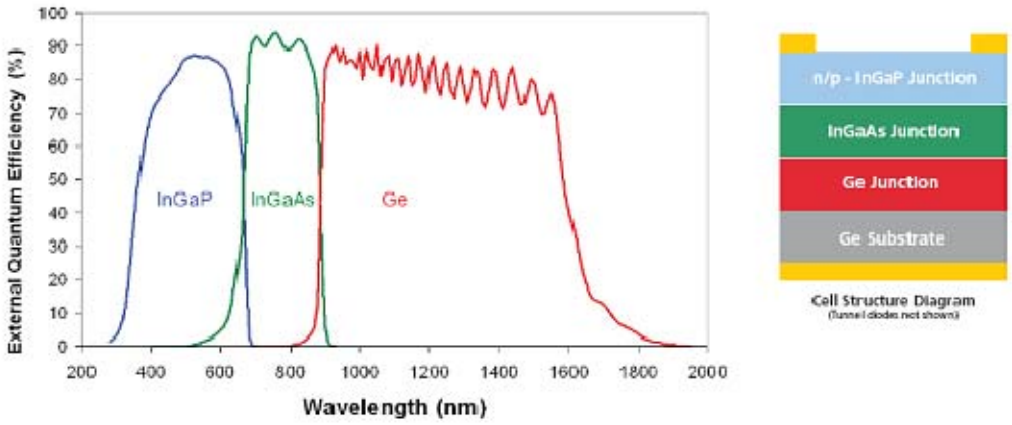


Figure 47. Triple-Junction Solar Cell Efficiency and Simplified Structure (From [65]).

## B. ADVANTAGES OF THIN-FILM FOR AIRCRAFT

The focus of this research is the application of thin-film cells to unmanned aerial vehicles to supplement the onboard power system, so the remainder of this chapter will compare the various types of thin-film cells to rigid cells and to one another. It is assumed throughout that some type of solar cells will be used on UAVs. Since rigid cells have been used almost exclusively in related research, we will focus on the advantages of TFPV compared to the traditional rigid choices.

Though thin-film cells have low efficiencies compared to crystalline solar cells, they are low cost, low mass, and very flexible (Figure 48), which makes them very attractive for aviation use.

Figure 48. Example of Thin-Film Solar Cell (From [66]).

Additionally, in comparison with rigid, single, or multi-junction silicon solar cells, thin-film solar cells (TFSC), or thin-film photovoltaics (TFPV) offer the ability to cover a much greater percentage of available wing and fuselage surface area due to their inherent flexibility. Provided they are light enough, solar cells should be placed on as great a proportion of the total surface area as possible. In order for rigid cells to wrap around the contours of a wing section or other surface, they need to be constructed or modified into smaller pieces. Unfortunately, the result is a great number of cells that need to be connected, with each connecting bus or wire adding weight without contributing additional power. On the other hand, TFSC can easily conform to existing aircraft shapes with very little concern for the preexisting aerodynamics of the aircraft, and much less extra wiring than small rigid cells would require.

Another important advantage of thin-film cells is that they have a much greater specific power per mass. This is fundamental to aviation applications, as mass is one of the most restrictive parameters for aircraft design and operations. Compared to rigid alternatives, lower mass solar arrays also means that supporting structures can be less robust which yields even greater weight savings. For small, less rugged UAVs, the wing and fuselage outer skin could be made thinner or even be replaced by the cells themselves as a cover material.

Cost is the final and perhaps greatest advantage that thin-film arrays present compared with crystalline silicon cells. Thin-film cells are cheaper to manufacture than crystalline Si or GaAs because, largely, they use a reduced amount of raw materials, and are manufactured with less energy through low-temperature deposition. As shown in Figure 49, second-generation photovoltaics, which include TFPV, are less expensive than crystalline cells (first generation).

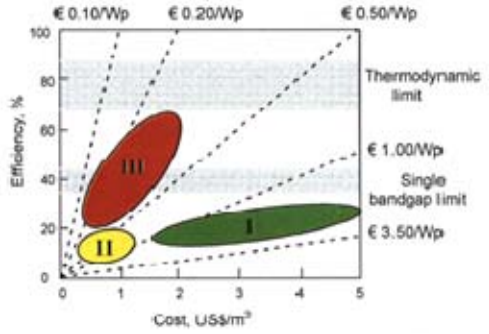


Figure 49. Costs and Efficiencies of Photovoltaic Technology Generations (From [67]).

Third-generation photovoltaics, which include many concepts that build upon thin-film technology, should prove to yield much greater efficiencies for even lower costs. Based on a June 2009 survey of commercially available cells, the lowest available priced crystalline silicon cells are $2.80 per watt, while the lowest priced thin-film cells are only $1.76 per watt [68].

Additionally, a program to modify existing UAVs would be less expensive if TFSC were used, rather than rigid cells. As discussed previously, rigid cells are heavier for a given power provided, so existing wings and other structures might have to be replaced, or reinforced to accommodate the greater weight. The additional electrical connections for a rigid cell configuration would also require additional materials and labor costs.

## C. ALTERNATIVE ANALYSIS

In order to determine the best of the three feasible options, an in-depth review of the alternatives is required. This starts with efficiency, as do most discussions of solar cells, and then discusses additional characteristics for consideration, such as: cost, specific power, drawbacks, et cetera.

### 1. Efficiency Comparison of Alternatives

The three main available types of thin-film cells are: copper indium gallium diselenide (CIGS, $Cu(In_{1-x}Ga_x)Se_2$), cadmium telluride (CdTe), and amorphous silicon (a-Si). There are other thin-film technologies that show promise, such as organic cells, and dye-sensitizing cells, but the research is not yet as mature and they are not commercially available. A comparison of CIGS, CdTe, and a-SI follows, to determine which provides the greatest benefit versus rigid solar cell modification of UAVs.

The first significant parameter for solar cells is efficiency. The cell-efficiency determines the dimensions of the potential thin-film replacement array compared to the smaller size required for a more efficient rigid configuration. A major determining factor of a solar cell's efficiency is the bandgap of the semiconductor material. As Figure 50 indicates, crystalline silicon cells (shown in blue) respond to a wider range of wavelengths than the existing thin film alternatives. Amorphous silicon can harvest more energy from the shorter-wavelength higher-power blue and green spectrum, but is relatively narrow across the spectrum. CdTe and CIGS have a broader spectral response compared to a-SI, but not as wide as c-Si.

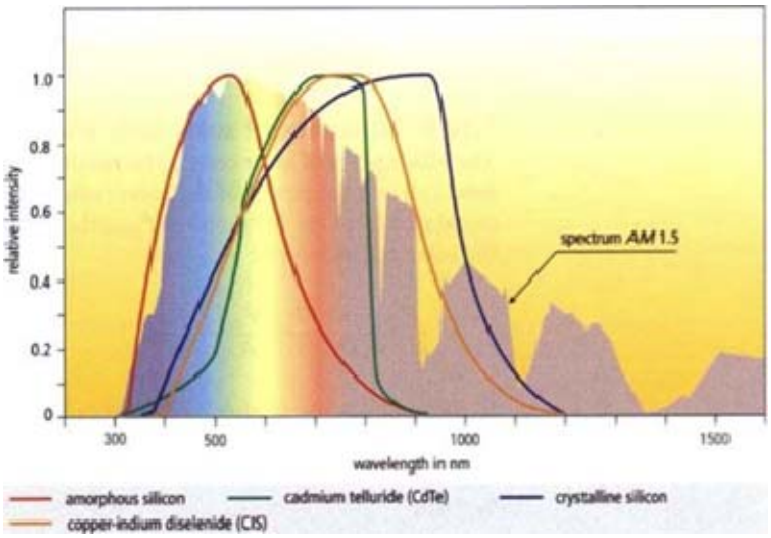


Figure 50. Spectral Response of Thin-Film Photovoltaics and Crystalline Silicon (From [69]).

Table 3 shows the current best research cell efficiencies of the three alternatives. Though these are research efficiencies, there is a strong correlation between the efficiencies shown and those of the commercially available for the same technologies. A recent NREL survey of efficiencies for production line solar cells listed the following values: CIGS (11.2), CdTe (10.8), and a-Si (8.5) [70].

| device type | $\eta$ [%] | $J_{sc}$ [mA/cm$^2$] | $V_{oc}$ [V] | ff [%] | area [cm$^2$] |
|---|---|---|---|---|---|
| CIGS | 19.9±0.3 | 35.5 | 0.692 | 81.0 | 0.419 |
| CdTe | 16.5±0.5 | 25.9 | 0.845 | 75.5 | 1.032 |
| a-Si | 9.5±0.3 | 17.5 | 0.859 | 63.0 | 1.07 |

Table 3. Maximum Recorded Efficiencies for Thin-Film Solar Cells (From [71]).

As shown in Figure 51, the latest record-setting cells for a-Si and CdTe were produced in 1999 and 2001 respectively. In addition, both are below the efficiency of CIGS, which has continued to improve steadily year-by-year. Also of note is that single-junction crystalline Si cells have not seen improvement in research cell efficiency since 1999, but multi-junction cells have improved dramatically in the past decade. Though these multi-junction cells have research efficiencies above 40%, it is important to note

that this is under concentration. The greatest 1-sun efficiency shown is 33.8%, and currently used production multi-junction cells for space applications have an average of approximately 28% [72][73].

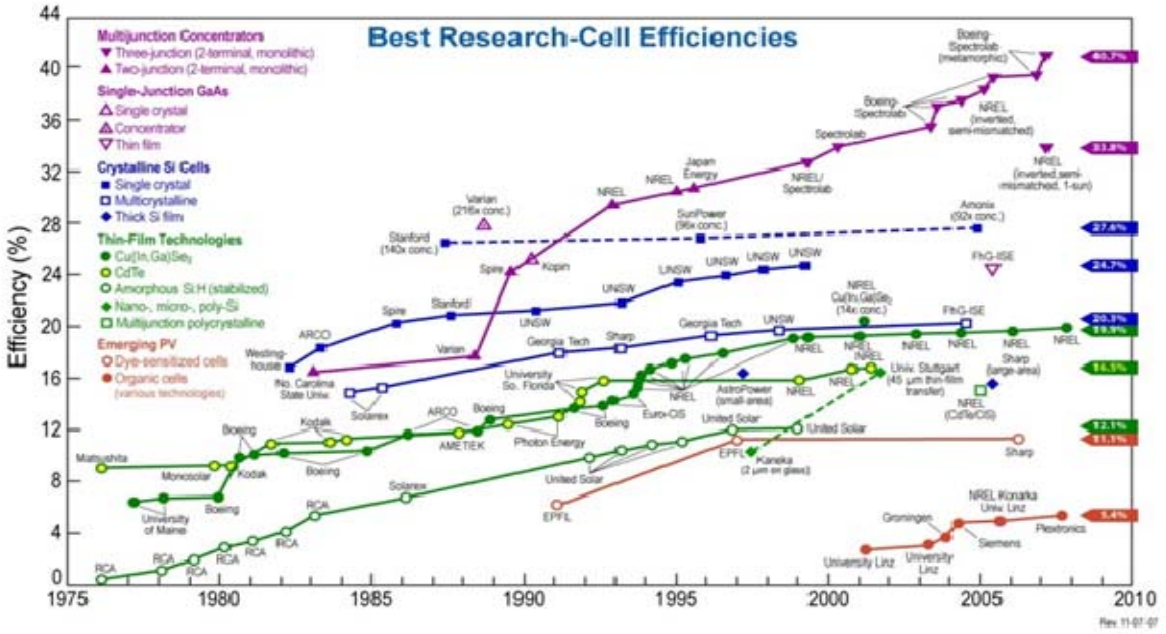


Figure 51. Best Research Cell Efficiencies (From [74]).

### 2. Amorphous Silicon

Amorphous silicon is a low cost alternative to traditional silicon cells. It is a non-crystalline material constructed through vapor deposition. Though not as efficient, it is much easier to produce, and requires much less silicon. Due to its amorphous nature, it is not limited by the lattice-matching requirement of crystalline silicone, so it can be used to form multi-junction cells more readily. In fact, most production a-Si cells are multi-junction [75].

Amorphous Silicon requires low heat for deposition and is inherently flexible (Figure 52). This means it is possible to manufacture it using roll-to-roll processes that increase throughput and decrease cost. Amorphous silicon can also be deposited on many different substrates for different applications, including clear plastic, since it does not require lattice matching, and has low-heat requirements during manufacture.

Figure 52. Amorphous Silicon (From [76]).

Due to its appeal for solar aircraft applications, Powerfilm Solar has a product specifically targeted for use on radio-controlled airplanes [77]. While there are many benefits to using a-Si in aircraft, there are also a number of significant drawbacks. First, as shown previously, a-Si has a lower efficiency than crystalline Si, and is the lowest efficiency of either of the other thin-film alternatives.

The other significant drawback of a-Si cells that must be addressed is the Staebler-Wronski Effect (SWE). Amorphous silicon is commonly referred to as "hydrogenated amorphous silicon" or "a-Si:H," due to the presence of hydrogen, which has been identified as a key component in the efficiency of a-Si cells. This phenomenon was first identified in 1977, but there are still several different theories to explain its cause. The most accepted model is that when a weak Si-Si bond is broken through photo-excitation, "back-bonded H atom prevents restoration of the broken bond by a bond switching event" [78]. The result of the SWE is that over time, when exposed to light, a-Si can lose up to 25% of its conversion efficiency. This does not affect either of the remaining alternatives, CdTe or CIGS.

### 3. Cadmium Telluride

Cadmium Telluride is a very promising material for use in TFPV, but also has some significant technical hurdles to overcome for continued improvement. CdTe is a direct bandgap material and has a very high absorption coefficient. The bandgap of CdTe is ~1.5 eV which is nearer to the Shockley-Queisser theoretical maximum efficiency

point (1.4 eV) than either a-Si, or CIGS [71]. As previously shown in the Table 3, and Figures 51, the efficiency of CdTe is better than that of a-Si, though not as good as CIGS. The cost of CdTe cells is competitive with that of a-Si, and better than CIGS [71].

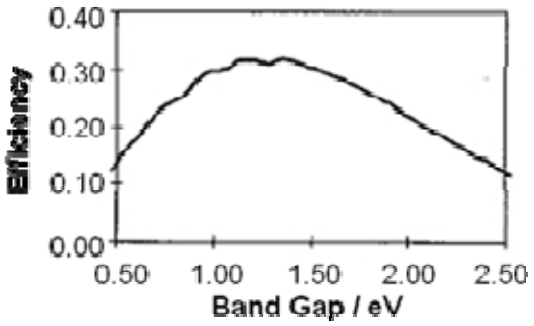


Figure 53. Theoretical Solar Cell Maximum Efficiency (From [59]).

Though CdTe is currently being produced in relatively large quantities, there are several drawbacks to pursuing it for future space applications. As seen in Figure 51, research efficiency improvements have plateaued. This is largely due to scaled-back investment in CdTe innovation. There has been an ongoing debate waged largely in Europe regarding the safety of Cd in the manufacture of solar cells. Cadmium is a toxic substance suspected as a carcinogen, but the NREL among others have concluded that the public's perception of the hazard posed is much greater than that which is realistically posed. Though this may be so in most applications such as space, or fixed terrestrial sites, it may be of greater concern for application to small UAVs as they will be handled frequently and probably suffer damage in an operational environment. Another material related concern in regards to CdTe is the relative scarcity of Tellurium. A surge in production would drive up demand, which could cause the price to increase [79]. The last significant issue with improvement of CdTe cells is efficient carrier extraction. As shown in Figure 54, the top electrode is in contact with the CdTe. Unfortunately, there is no metal with a work function to match properly the bandgap of CdTe. There are methods to implement intermediate layers to provide better matching and transport, but they tend to decrease the overall device performance and stability.

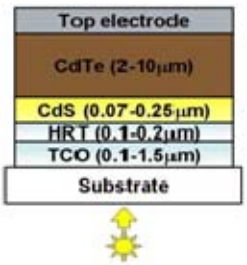


Figure 54. Typical Configuration for a CdTe Cell (From [71]).

### 4. Copper Indium Gallium Diselenide

The last production model TFSC to consider is CIGS. As shown previously, CIGS has the best overall efficiency, and has shown continued improvement. Compared to rigid alternatives, CIGS is also very lightweight and flexible, as shown in Figure 55. For these and other reasons detailed, CIGS is the best current option to supplant rigid single or multi-junction silicon cells for future solar UAV designs.

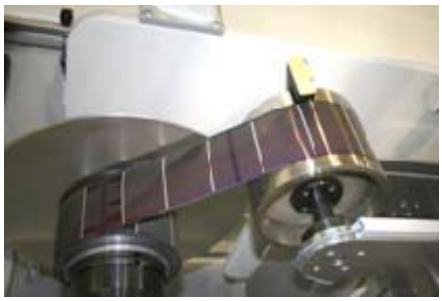

Figure 55. Roll-to-Roll Manufacture of CIGS Solar Cells (From [80]).

### 5. Emerging Alternatives

The emerging technologies of organic cells, dye-sensitizing cells, and thin multi-junction cells among others all show promise but are not currently viable alternatives for widespread UAV use.

## D. SELECTED THIN-FILM TECHNOLOGY

Copper indium gallium diselenide (CIGS) is the best option for use in unmanned aircraft and other aerospace applications. As shown previously, it has the greatest research and production cell efficiency amongst the thin-film alternatives, and continues

to improve annually. Copper indium selenide (commonly CIS) was initially used in thin-film cells, with a bandgap of approximately 1.04 eV, but it was found that by substituting gallium for a portion of indium, the bandgap could be engineering to 1.67 eV. This means that theoretically CIGS bandgap could be adjusted to the Shockley–Queisser limit for optimal power output. However, the engineered bandwidth of CIGS is, in practice limited to 1.3–1.4 eV since the lattice mismatch between the CIGS and CdS layers, shown in Figure 56, becomes too great above this point [81].

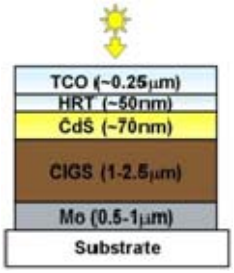


Figure 56. Typical CIGS Construction (From [81]).

Another significant advantage of CIGS for UAV application is that it is very lightweight, and potentially much lighter. CIGS has the highest specific energy of any solar cell, achieving 559 W/kg on titanium substrate and 919 W/kg on polyimide. Because CIGS is manufactured through vapor deposition at lower temperatures and using roll-to-roll techniques, it can be made cheaply and on many different substrates [82]. For some applications titanium or stainless steel substrates can be used for greater strength, conductivity, or shielding. In other instances, where weight and flexibility need to be optimized, polyimide would be the best option.

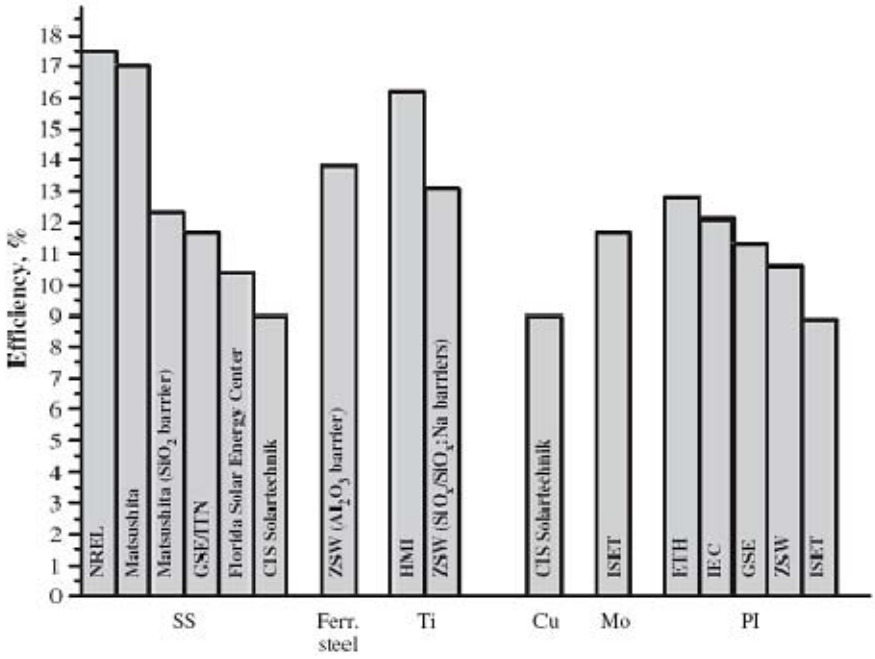


Figure 57. Efficiency of Thin-Film CIGS on Various Substrates (From [82]).

CIGS cells typically contain a small amount of the toxin cadmium in the CdS layer that forms the junction with the CIGS. Fortunately, no carriers are produced in the CdS, so it can be made as thin as possible to permit greatest number of photons to pass into the CIGS layer.

Because CIGS is relatively easy to bandgap engineer and manufacture, it shows the greatest promise for continued improvement in efficiency and specific power. Figure 58 shows that CIGS can be doped with higher levels of gallium nearer the back contact. The resulting increase in the conduction band level creates a field that reduces recombination. Improvements in this process will spur the development of even thinner CIGS layers as recombination losses are controlled [81].

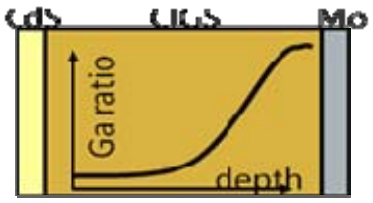


Figure 58. Graded Bandgap by Varying Ga Ratio in CIGS (From [81]).

## E. CHAPTER SUMMARY

In this chapter, we reviewed basic semiconductor theory; how semiconductors are tailored for specific functions. Next, we looked at how solar cells are constructed from p-n junctions, including the physical and energy-band description of the photovoltaic effect. We compared the more common rigid crystalline solar cells to flexible thin-film cells, and compared each of three TFSC to each other: a-Si, CdTe, and CIGS. After further review of some of the advantages and disadvantages of each of these technologies, we explained why CIGS thin-film solar cells would be the best choice for a high-efficiency, low-cost modification of existing UAVs, like the RQ-11 Raven.

# IV. POWER INTEGRATION

## A. OVERVIEW

In addition to adding solar cells to existing UAVs, it is important to consider the most efficient, cost-effective way for the power from those cells to be stored and used. This chapter will review some of the components and methods for coupling and using power in order from the solar cells, through additional circuits, to the motor, battery, or other load.

It is prudent to review energy conversion devices before delving into the specifics of power integration. Small UAVs (SUAVs) like our target model, the RQ-11 Raven, operate on battery power. They use onboard circuitry to connect the battery to the motor; monitor the battery voltage; and power servos, transmitter, receivers, cameras and other payloads. The power source, a battery, converts stored chemical energy to electrical energy for use by onboard electronics and for conversion to mechanical energy by the motor. As Table 4 indicates, the conversion from stored chemical energy to electrical energy is about 90% efficient.

| Energy Conversion Device | Energy Conversion | Typical Efficiency, % |
|---|---|---|
| Electric heater | Electricity/Thermal | 100 |
| Hair drier | Electricity/Thermal | 100 |
| Electric generator | Mechanical/Electricity | 95 |
| Electric motor (large) | Electricity/Mechanical | 90 |
| Battery | Chemical/Electricity | 90 |
| Steam boiler (power plant) | Chemical/Thermal | 85 |
| Home gas furnace | Chemical/Thermal | 85 |
| Home oil furnace | Chemical/Thermal | 65 |
| Electric motor (small) | Electricity/Mechanical | 65 |
| Home coal furnace | Chemical/Thermal | 55 |
| Steam turbine | Thermal/Mechanical | 45 |
| Gas turbine (aircraft) | Chemical/Mechanical | 35 |
| Gas turbine (industrial) | Chemical/Mechanical | 30 |
| Automobile engine | Chemical/Mechanical | 25 |
| Fluorescent lamp | Electricity/Light | 20 |
| Silicon solar cell | Solar/Electricity | 15 |
| Steam locomotive | Chemical/Mechanical | 10 |
| Incandescent lamp | Electricity/Light | 5 |

Table 4. Efficiencies of Common Energy Conversion Devices (From [83]).

As noted, battery-powered aircraft must convert chemical energy to electrical energy (battery) then to mechanical energy (motor and gearbox). According to the average conversion efficiencies for these processes, 10% of the stored energy is lost when electrical energy is extracted from the battery, and another 10% lost at the motor. Therefore, if 100 watts are stored, only 81 watts are produced at the output of the motor. This does not take into account additional loses in wiring, regulation and control circuits, or other mechanical coupling such as gearboxes.

For a solar UAV modification, taking into account these conversion losses, it is extremely important to consider how to extract the greatest power from the solar cells and how to best couple it to the load(s). Once the electrical energy from the solar cells is properly converted and/or regulated it should be used to directly power the load(s) if possible. Otherwise, large percentages of the collected solar energy could be lost in conversion, negating potential benefits.

For example if CIGS solar cells are connected in series so that they only charge the battery directly, they will convert approximately 10% of the Sun's energy to electricity. There will be a 10% efficiency loss in charging the battery, another 10% loss when extracting power from the battery, and another 10% loss in the final mechanical conversion. So if the solar cells are applied to a large wing area of 1 $m^2$ the sun will provide 1000 W (AM 1.5), but only about 73 watts of mechanical energy will be produced.

$$1000 \text{ W} \times 0.1 \times 0.9 \times 0.9 \times 0.9 = 72.9 \text{ W} \quad (4.1)$$

Conversely, if the solar cells are connected in parallel with the battery, they can power the motor directly. This would result in a theoretical power of

$$1000 \text{ W} \times 0.1 \times 0.9 = 90 \text{ W} \quad (4.2)$$

## B. SOLAR ARRAYS

Solar cells are almost never used individually, but rather they are wired in panels or arrays to "build-up" the voltage or current to a usable level (Figure 59). One of the important solar design consideration, discussed in chapter III, is the need to protect the

solar cells from forward biasing. For this reason, “blocking” diodes are used, which prevents batteries from discharging through the solar cells rather than the load (Figure 59).

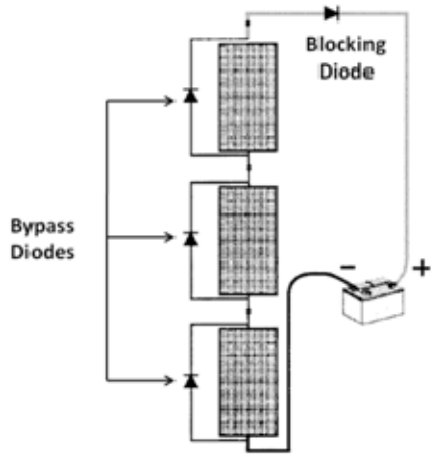


Figure 59. Solar Array with Blocking and Bypass Diodes (After [84]).

This figure also shows the last important element in solar array design, the use of “bypass” diodes. These diodes are used to combat the effects of “shading” or panel malfunction. Solar arrays like that in Figure 59 connect multiple cells or panels in series to create a higher voltage. The main concern with this configuration is that when one of the cells is shaded, the current through all of the cells is severely reduced or even eliminated. A diode in parallel with each of the panels allows current to still flow, though the voltage is reduced by the amount of the lost cell and the amount dropped by the diode. This is taken into account when designing the system.

## C. SOLAR POWER OPTIMIZER

Solar cells produce different amounts of current and voltage depending on ambient sunlight (irradiance), angle of incidence, temperature, internal and external resistance, and a number of other factors. The two principle determinants of varying solar cell output are temperature and irradiance. These have previously been discussed in Chapter III. Figure 60 shows how both of these factors impact the output power.

One of the effects of higher temperatures is greater light absorption, which slightly increases short-circuit current. However, the decrease in voltage far outweighs the increase in current. Higher temperatures impart greater energy to the electrons within the semiconductor crystalline structure. Thus, they are essentially easier to free from the valence shell because the added heat has imparted to them greater energy. The voltage of solar cells is driven by the energy bandgap of the semiconductors, so when added heat reduces the bandgap, the voltage decreases [85]. The solid I-V curve lines in Figure 60 show this effect. The loss of efficiency due to temperature, known as "temperature coefficient" of CIGS solar cells is approximately -.04%/°C. [82]

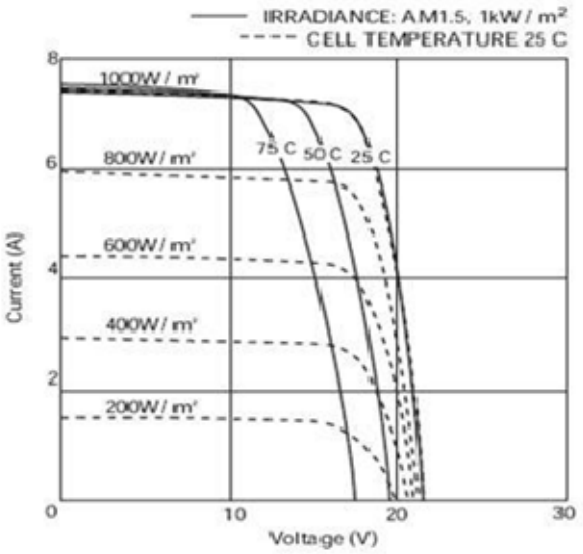


Figure 60. Temperature and Irradiance Effect on I-V Curve (From [86]).

Irradiation is the most significant cause of variation in solar cell output power. The dashed lines in Figure 60 show the effect of reduced irradiation. This effect is much simpler to understand; the output of a solar cell decreases when the incident radiation decreases. This decrease can be due to the movement of the sun, environmental factors like clouds, airborne dust, natural shading, and in the case of this research, movement of the solar cells themselves.

Ideally, a solar cell will be operated under constant radiation from a perpendicular source at a set distance, but that is not realistic. Terrestrial solar cells produce uneven power due to many factors. The number of hours of sun and intensity of the light varies with the seasons, obviously more so in locations further from the equator. In locations near the equator, there is significant irradiance for nearly twelve hours a day. In more northern latitudes, such as in Kabul Afghanistan (34.3°N), the amount of sun per day varies from over twelve hours during the summer to eight in the winter. Though on average the sun shines for twelve hours per day, the average intensity of the light is lower further from the equator. Figure 61 is a map that shows the world average solar "insulation" (incident solar radiation). Obviously, the earth's atmosphere has a big impact on insulation; otherwise, the map would show uniform bands of strengthening intensity from the poles to the equator.

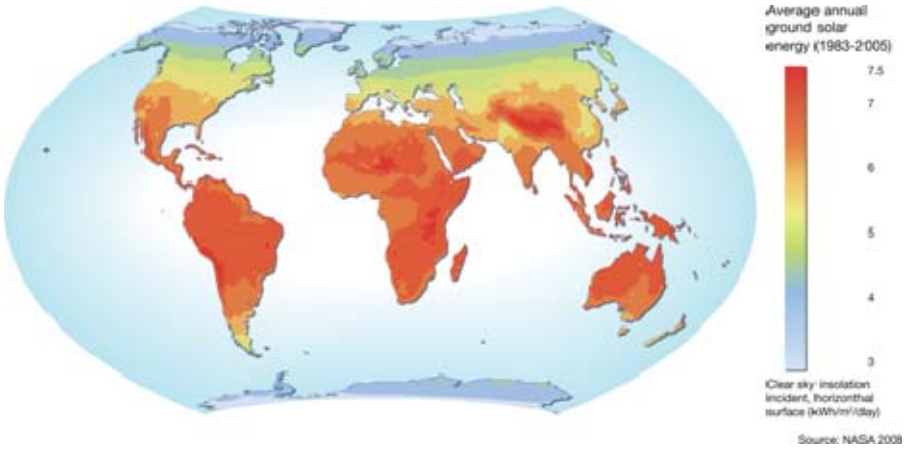


Figure 61. Average Annual Ground Solar Energy 1983–2005 (From [87]).

For a ground solar installation, the best way to adapt to changing angles of incidence is to use a solar tracking array. Tracking systems are obviously more expensive initially. For fixed terrestrial installations, solar arrays are angled to optimize solar power throughout the year. As shown in Figure 62, the amount of power generated by a solar array increases significantly when panels are installed on a favorable angle.

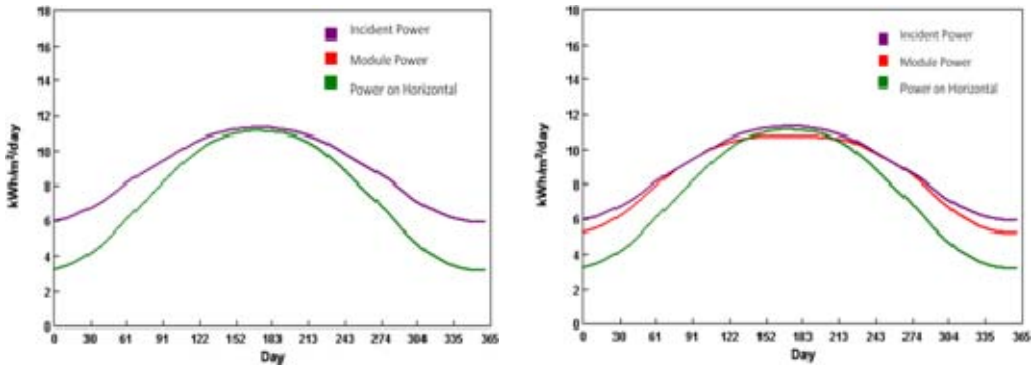


(a) (b)

Figure 62. Daily Solar Insolation at 34°N Latitude with Solar Array Angled at 0° (a), and 29° (b) (After [49]).

In order to convert the greatest proportion of light into electricity, solar panels are often installed with optimizing circuits called maximum power point trackers (MPPT) or Photovoltaic Power Converters (PVPC). We will use the more common MPPT during our discussion.

The MPPT is primarily a DC-DC converter that permits the solar cells to operate at their maximum solar conversion efficiency. It then converts the voltage to a necessary level to power the load. The MPPT should have its output voltage set for the battery or other load that is connected, but should accept input voltages over a relatively wide range.

As shown in Figure 60, the voltage and current of a solar cell can vary widely depending on irradiance and temperature. This means that for a UAV or other aircraft installation, the maximum power point of the cells, ($P_{mpp}$) will change continuously. This variation will be significant compared to terrestrial installation due to ever changing angles of incidence, altitude, and convection cooling (from wind across the aircraft in flight). As with other solar installations, without an MPPT the solar cells on a UAV will be forced to operate at the battery voltage [88].

Figure 63 shows the I-V curve for a Global Solar 12-watt solar battery charger connected directly to an 11.1 V lithium polymer (LiPo) battery. Lithium polymer batteries will be discussed later in this chapter, and the configuration for Figure 63 will be

discussed in “design” in Chapter V. The normal operating voltage range for an 11.1 V Lithium polymer battery (9.5–12.5 volts) is superimposed on this figure to demonstrate the operating point of the solar cells if not corrected by an MPPT.

Two temperature curves are displayed in Figure 63, each with three significant points highlighted. The blue line represents the I-V curve of the solar array under standard test conditions (1000 W/m$^2$, 25°C). Points (1) and (2) are the operating power points ($P_{op}$). If the battery is being discharged while the solar cells are connected, such as by a motor or other load while in flight, the $P_{op}$ will start at (2), and move to point (1) as the battery’s voltage decreases. The initial $P_{op}$ will be approximately 10.6 W and drop to around 9 W. The average power drawn from the solar array over the battery discharge cycle will be approximately 10 W. Compare this to the maximum power point of approximately 11.25 W. Lightweight MPPTs have been designed to operate at up to 96% efficiency [5], but for the sake of this discussion, we will use the power consumption of the specific MPPT used in the proof-of-concept testing (Chapters V and VI). If the MPPT increases the power from the solar cells by 1.25 W and consumes 0.25 W, the net gain is 1 W, or 10%.

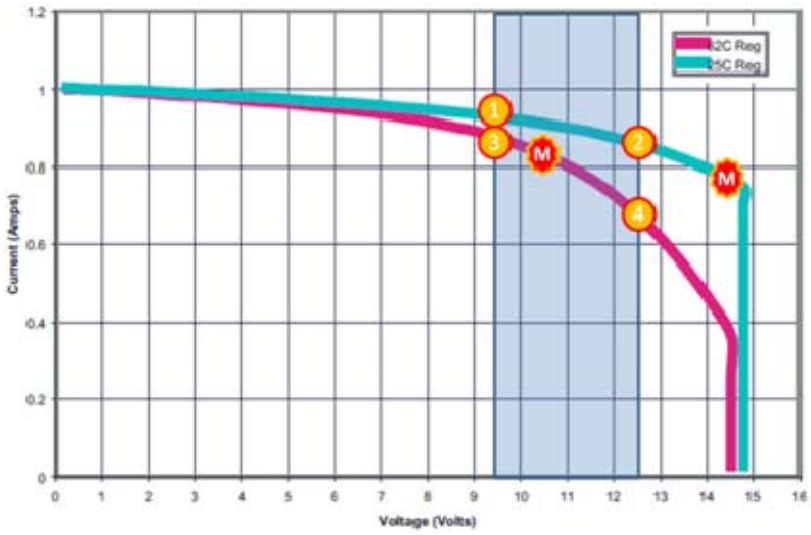


Figure 63. Maximum Power Point and Operating Power Points at 25°C and 62°C (After [89]).

The second line in Figure 63 shows the I-V curve of the solar cells operating at 62°C, as will be shown subsequently, this is much higher than measured temperatures during experimentation. The $P_{mpp}$ in this case falls between the two $P_{op}$ (3) and (4). The difference between the maximum power and the operating power over this range is only about 0.17–0.27 W, so the same MPPT would not be beneficial, so a more efficient model such as the one used in Sky-Sailor should be used [5].

In micro or small UAVs, the added weight of the MPPT is often not justified by the increased solar efficiency. In that case, careful attention must be paid to matching the solar cell voltage to the battery voltage. This may lead to less than optimal solar cell coverage of the surface area.

Other important roles played by a well-designed MPPT are: DC-DC conversion, voltage regulation, and charge control. These functions can all be incorporated on a single circuit board or module for weight, energy, and cost savings.

### 1. DC-DC Converter

Even without an MPPT, a DC-DC converter may be necessary to provide an interface between the solar cells and battery or load. This is most likely due to restrictive geometry of the available aircraft surfaces compared to the solar sizes. If solar cells cannot be resized to put a greater number in series, the output voltage may be lower than that of the battery. In this case, they will never provide additional power so a converter is needed to raise the voltage.

### 2. Voltage Regulator

Depending on the sensitivity of the battery and other connected electronics, voltage regulation will be more or less important. If a DC-DC converter is used, voltage regulation should be inherent in the design. A smooth, stable voltage from the solar cells, MPPT, or converter will help prevent damage from voltage ripple or spikes and reduce noise in the system.

### 3. Charge Control

To prolong battery life and prevent damage or accidents, recharging must be monitored and controlled. The most commonly used batteries, variations of lithium ion, must be charged safely through control of the charging current and maximum voltage. There are also several different methods for charging lithium ion cells that must be selected based on the application [90].

Lithium Polymer batteries, like those used in the RQ-11 Raven, are manufactured in cells of 3.7 volts each. In general, they should not be charged to greater than 4.2 V per cell, or allowed to discharge to less than 3.0 V. Therefore, in the example configuration discussed, an 11.1 V Li-Po battery is made from three cells of 3.7 V wired in series. This Li-Po pack should be charged to no greater than 12.6 V (4.2 V x 3 cells), and discharged to no less than 9.0 V (3.0 V x 3 cells).

Cell balancing is another important consideration for Li-Po batteries. These battery packs normally have a "tapped" connector that permits monitoring and balancing of individual cells. As previously stated, Li-Po cells have an upper and lower voltage, which should not be exceeded. Deep discharging, below the critical voltage of 3.0 V per cell can damage the cell and limit its performance. It is even more critical to prevent over-charge. If 4.2 V per cell is exceeded, the battery can catch fire, or explode [91].

### 4. Previous Designs

Dr. Noth developed an excellent MPPT design, shown in Figure 64, for use in his Sky-Sailor project.

Figure 64. Sky-Sailor MPPT (From [5]).

Randyll Fernandez tested a promising lightweight design, the PVPC from Atira Technology at the Naval Postgraduate School. This small circuit did not require external microprocessor control lines, and increased power from solar cells by 55% in one day-long test, and by 197% in a second [92].

## D. BATTERIES

This research is focused on improving Small UAVs through the integration of solar cells. As shown in Chapter II, primary (single use), or more often secondary (rechargeable) batteries, power these man-packable aircraft. The following excerpt from the 2005 UAS Roadmap describes the primary challenges of electric UAVs:

> Recent improvements in the ability to recharge lithium-based batteries have resulted in significant logistics improvements for users in the field. Further improvements are needed in power-to-weight ratios for the next generation of batteries to improve the performance and endurance of these small platforms on a single charge. Currently, most battery operated MAV have a fraction of an hour of endurance, while mini-UA fair only slightly better, only because they can carry larger numbers of the same lithium-based batteries. [93]

Though energy density improvements continue, as Figure 65 demonstrates, batteries still cannot rival the non-reversible energy storage provided by liquid fuels such as gasoline.

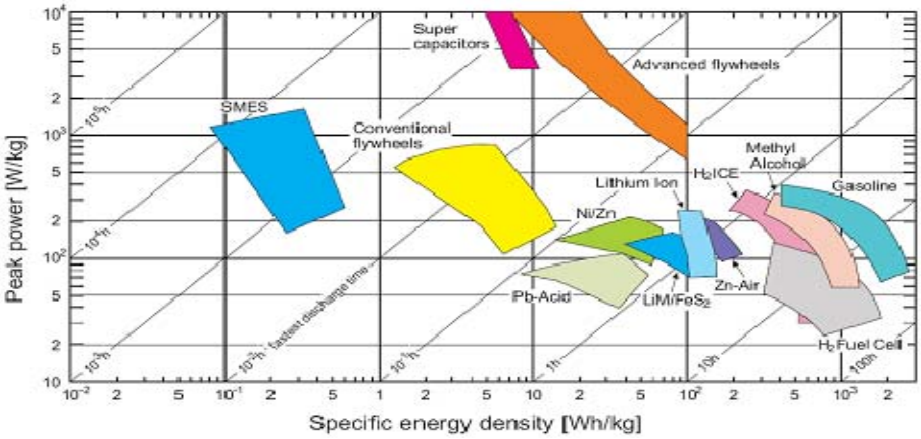


Figure 65. Specific Energy Density and Peak Power of Energy Storage Methods (From [5]).

### 1. Lithium-ion and Lithium–Polymer Batteries

Batteries are normally comprised of two dissimilar metals serving as the anode and cathode separated by an electrolyte. Lithium-ion (Li-ion) batteries have been the standard chemistry used in military and consumer electronics for some time now. In these batteries, lithium ions move between the anode and cathode during discharge and in the reverse during charge. Lithium-polymer batteries are an improved version of lithium ion that uses a polymer gel rather than a liquid for the electrolyte. This type of battery has several advantages over other commonly used types such as lead acid, nickel cadmium (Ni-Cd), and nickel metal hydride (Ni-mh) [5], [94].

In general, lithium-ion batteries have three distinct advantages over pre-existing chemistries. The first is that they do not develop a "memory" like other batteries. Essentially, they can be charged and recharged, to any level within their normal operating range, without concern for reduced performance. Prior technologies have required complete discharge, or "deep cycling," to maintain performance. Li-ion batteries do not need to be "deep cycled"; in fact it damages the battery [94].

Low self-discharge is the second big improvement of Li-ion batteries compared to other types. When batteries are in storage, or otherwise not used they lose some of their charge. The rate at which this self-discharge occurs depends on the storage conditions and the battery chemistry. For Li-ion batteries this can be 5% per month or lower, while Ni-Cd cells can lose 10% per month and Ni-mh cells can lose 30% [94].

The last major improvement is in the battery's voltage and energy density. Li-ion's voltage is nominally 3.7 V, while the voltage in Ni-mh and Ni-Cd is only about 1.2 V [5]. Figure 66 shows a comparison some commonly used batteries. Note that Li-ion batteries far exceed the previous technologies in energy density per volume and weight. This makes them the obvious choice for battery-powered UAVs as well as many other military and consumer applications. The RQ-11 uses lithium-polymer batteries, which typically have 20% greater energy density than Li-ion and are much lighter. Lithium-polymer batteries use flexible foil casings rather than rigid metal. This makes them lighter and gives greater flexibility in the application design.

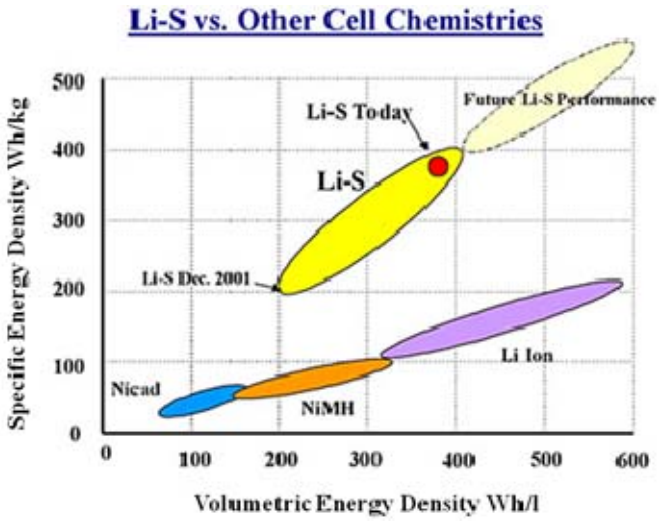


Figure 66. Specific and Volumetric Energy Density of Common Battery Types (After [95]).

### 2. Lithium-Sulfur Batteries

As Figure 66 shows, a newer battery chemistry, lithium-sulfur (Li-S) has a much higher specific energy density than Li-ion or Li-po. Li-S batteries with a specific energy of 350 Wh/kg were used in the record-setting solar UAV flight of QinetiQ's Zephyr [96].

Not only have these batteries been used for an experimental HALE UAV, but they have also been used as a replacement for the Li-po battery in the Raven during a test. Using these Li-S batteries, an RQ-11 that normally flies for 60–90 minutes, flew for nearly seven hours. This incredible improvement is due to the higher specific energy of the Li-S pack, which boasts 260 Wh/kg compared to 155 Wh/kg with the existing Li-po pack [95].

Lithium-sulfur batteries still have some drawbacks, such as greater volume for a given energy compared to Li-po batteries. However, as Figure 66 shows, as the technology matures, much greater performance is expected. One certainty is that, regardless of the specific emerging technology, battery energy density is continuing to improve at a rapid pace.

## E. CHAPTER SUMMARY

In this chapter, we looked at the most significant power considerations for a solar UAV implementation. First, we examined power conversion systems and efficiencies, and noted the importance of minimizing energy conversion losses in system design. Next, we described solar arrays in general, including two important design elements, the blocking and bypass diodes. Then we detailed some of the causes of varying power from solar cells, such as reduced irradiance due to latitude and angle of incidence, and explained the need for power optimization using an MPPT. We also included some of other functions that should be included in a well-designed MPPT, like voltage regulation, DC-DC conversion, and charge control to prevent damage to the battery or load. Lastly, we talked about batteries, from a functional description, to current technology used in UAVs (Li-po), to potential improvements using Li-S.

THIS PAGE INTENTIONALLY LEFT BLANK

# V. DESIGN AND ASSEMBLY

As previously stated, the goal of this research is to determine the practicality of applying commercially available thin-film photovoltaic cells to Unmanned Aerial Vehicles to increase their endurance, and/or capabilities. According to the latest Defense Department forecast, "…key technologies that will enable future UAS include lightweight, long endurance battery and/or alternative power technology…" [1].

We've presented a history of solar flight, looked at unmanned flight through the years, and chosen the RQ-11 Raven as the current U.S. aircraft best suited for testing. We then gave background on photovoltaic fundamentals, described thin-film alternatives to rigid silicon, and decided on CIGS cells as the best choice among the three commercially available options. Next we described some of the important considerations for intalling solar cells, including optimization.

With background firmly established, the next phase was to integrate solar cells on a proof-of-concept aircraft for testing. Testing was conducted during many of the assembly stages described in the following sections. That experimentation will be discussed in Chapter VI.

## A. CONSTRAINTS

Time and funding were major constraints to this research. Much of the early work on this project devoted to establishing contact with potential stakeholders within the Services, and a vain search for sponsorship. Unfortunately, the testing conditions envisioned were impractical due to lack of significant funding and compressed experimentation timeline caused by material delays. Some of the specific challenges to ideal testing conditions will be addressed in the following sections.

## B. AIRCRAFT

The RQ-11 was the target airframe for this research, but a Raven could not be secured in time for experimentation. As such, we needed to procure an off-the-shelf remotely piloted vehicle (RPV), commercially known as a "remote-controlled airplane."

In order to best approximate the effect of applying solar cells to an RQ-11, we needed to find an aircraft whose wing surface area was at least the same, that was similar in weight, about 4.2 lbs (1.9 kg), and which also used lithium-polymer batteries.

Before shopping for aircraft, we needed first to determine the wing surface area of the Raven in order to match it with an RPV test aircraft. Figure 67 shows an approximation of the main-wing area of the RQ-11. Due to the absence of a Raven for testing, or detailed specifications, this estimate was arrived at through measurement of scaled images using Microsoft Visio. The first measurement shown is the ideal coverage with 100% of the wing surface covered by solar cells. The second measurement, called "Large Rectangle" is a more realistic coverage estimate. Since CIGS solar cells are manufactured using a roll-to-roll process, they are sold in strip or rectangle form.

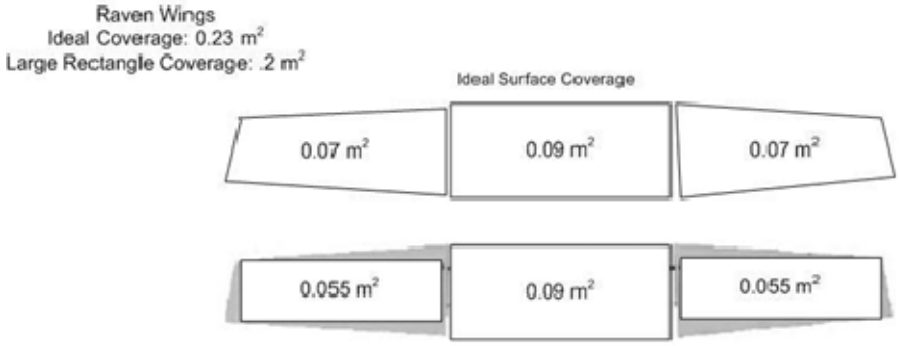


Figure 67. Approximate Wing Surface Area of RQ-11 Raven.

Besides using a large-rectangle area for the main wings, we also did not consider the use of other surfaces aside from the main wing in order to present a conservative performance estimate.

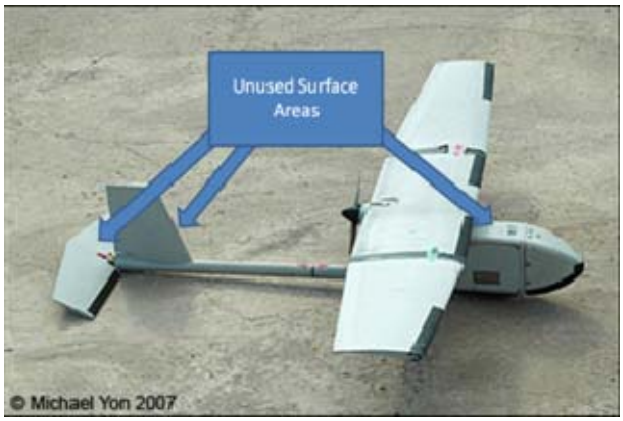


Figure 68. Possible Additional Surface Area for Solar Cells on RQ-11 Raven (After [97]).

Due to time constraints and the author's lack of experience as an RPV pilot, we also wanted to make sure our aircraft would be quick to assemble and easy to fly. With these criteria, we searched for a commercially available Raven, or similar aircraft. Unfortunately, nothing like the Raven was found after many days of searching. We quickly decided to purchase a ready-to-fly aircraft that was reasonably priced and easy to fly. At a minimum it would need to meet our most essential constraint; having surface area equal to, or greater than that of the RQ-11. After scouring the internet, we selected the Parkzone Radian, shown in Figure 69.


Figure 69. Parkzone Radian Remotely Piloted Vehicle (From [98]).

Given the lack of sponsorship, one major advantage for this choice was the price. It was relatively inexpensive at approximately $250, compared to $35,000 for a Raven [99]. It was also ready-to-fly (RTF), meaning it had all necessary parts included in one kit. Essentially, to get the aircraft flying, the wings and tail needed to be attached and

control rods inserted, the battery needed to be charged, and the included transmitter needed to be "bound" to the aircraft receiver. This model was also chosen for its simplicity of operation since it only had three channels, to control the motor speed, elevators, and rudder. Like the Raven, the Radian used Li-Po batteries, though

Without detailed specifications on the wing shape, a similar method to the one used for the Raven was applied to find the approximate wing dimensions. In each case, the wingspan was readily available, so images of the wings were set to that size to produce a scaled image. Again, we used Microsoft Visio to generate surface area estimates, which is shown in Figure 70.

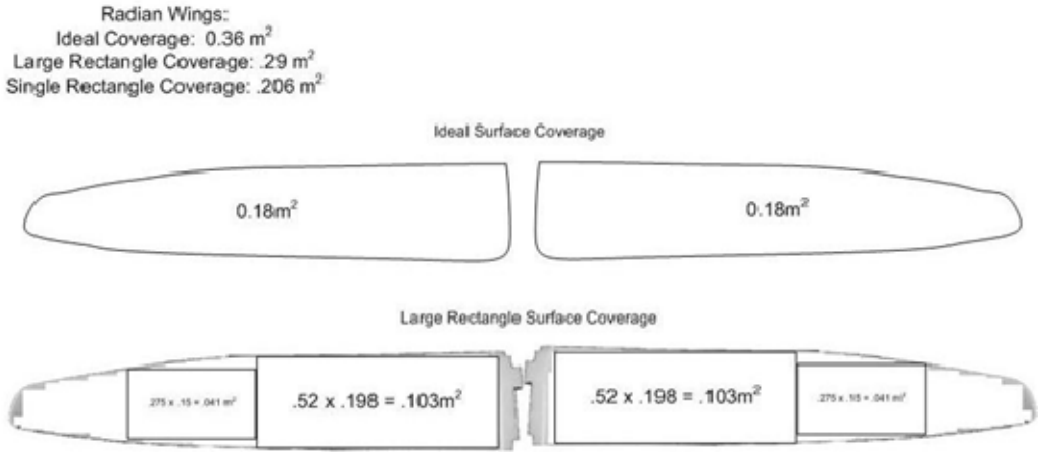


Figure 70. Parkzone Radian Wing Geometry with Ideal and Realistic Solar Coverage Regions.

Though the Radian has a much larger ideal surface area than the Raven, if only the central "large rectangle" area is used, both aircraft can accommodate approximately 0.2 $m^2$ of solar cells.

## C. SOLAR CELLS

In Chapter III, we described why CIGS solar cells are the best choice for this application. There are numerous CIGS manufacturers in the U.S. and around the world, but relatively few of them have verified production cells efficiencies over 10%. Two of these, Honda Soltec in Japan, and Germany's Wurth Solar have CIGS cells measured at greater than 10% efficiency, but they do not have flexible thin-film products publicly

available. Within the United States, there are several companies that are producing CIGS on flexible substrates, including Ascent Solar (polyimide substrate), and Nanosolar (aluminum substrate). At the time of this research, neither company had consumer ready products available for purchase, nor did they have the confirmed efficiency of our final selection Global Solar Energy.

### 1. Preferred Thin-film Product

Global Solar Energy (GSE) is one of the leading flexible CIGS manufacturers. Their headquarters is in Tucson, Arizona and they have a second manufacturing plant in Germany. Together, these facilities are capable of producing 75 MW of solar cells annually. The product best suited to this research was identified as their flexible G2 Thin-Film Strings, shown in Figure 71. This product, as with their building integrated photovoltaics (BIPV) is targeted at corporate partnerships, whereby Global Solar provides the solar cells tailored to meet a particular secondary manufacturer's needs [66].

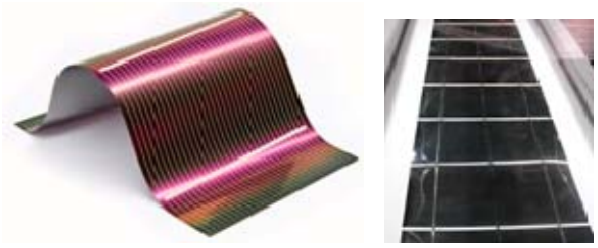

(a) (b)

Figure 71. Global Solar 10 cm x 20 cm CIGS Cell (a) and Thin-Film String (From [66]).

As shown, these "raw" cells would have been the best choice since they are extremely flexible and lightweight in this configuration. A string is normally constructed of 18 individual cells, wired together in series. Based on the size of the Raven's wings, one string would have provided more than enough solar cells. These cells would need to have been cut and rewired to provide greater coverage. As shown in Figure 72, if left in 10cm x 21 cm cells, and using just the main wing surface, only 0.168 $m^2$ would be

covered. Depending on the new cell sizes, an MPPT or DC-DC converter would be needed to increase the voltage. Each cell is only about 0.5 volts, but the Raven's battery is rated at 25.2 V.

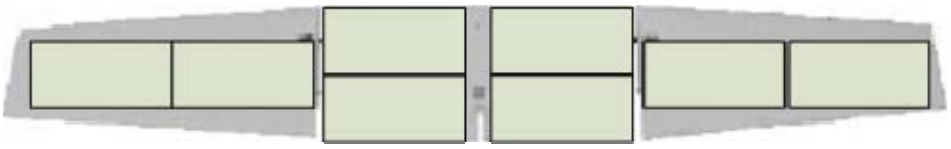

Figure 72. Estimated Solar Coverage of Raven Wings Using Uncut GSE Cells.

Unfortunately, individual cells or strings could not be purchased initially. During the procurement, design, construction, and testing phases of this research, the least quantity available from Global Solar was 50 strings of 18 cells, or about 75 times more than we needed to test the concept. Since our limited budget did not support such extravagant spending, we had to look at other alternatives.

Other less established companies were manufacturing CIGS cells on flexible substrates, like Ascent Solar and Nanosolar. Neither of these companies sells products directly to consumers, nor could we find any products from secondary manufacturers that made use of their cells, nor did they respond to web or email inquiries.

Thus Global Solar was our only viable option given the scale, timeline, and funding of the project.

### 2. Best Alternative

Since we were unable to reach an agreement with Global Solar to obtain a small quantity of 11% efficient, lightweight cells in a timely manner, we decided to purchase an off-the-shelf battery charger that used GSE's CIGS cells. This would require a great deal more work to ready the cells for installation, but was necessary to complete some level of experimentation. Figure 73 shows the 6.5-watt and 12-watt Global Solar SUNLINQ portable chargers we ordered.

(a) (b)

Figure 73. Global Solar SUNLINQ 6 Watt (a) and 12 Watt (b) Chargers (From [89] [100]).

These chargers are flexible and foldable, making them well suited for many civilian and military applications. In fact, GSE has produced several versions of their FLEX portable chargers for military use, like those shown in Figure 74, and tested them against military standards (MIL-STD-810). These chargers would make an excellent addition to a complete Raven system to serve as an alternative power source for the ground control station (GCS), or battery charger for the aircraft.

(a) (b)

Figure 74. Global Solar P3 Portable Power Pack, Folded (a), and Deployed (b) (From [101]).

### 3. Harvesting

The process of removing the solar panels from the battery chargers was incredibly time consuming and difficult. The images in the following sections give an overview of the steps involved. First, the thin fabric cut from the edges, then pulled away from the laminated top of the panel sections. Figure 75, shows the 6-watt charger with most of the

cloth edge trimmed from the left-most panel and a long strip of fabric removed from the top edge. This revealed a large metal contact region for termination of a strip of five shingled cells and for interconnection between strips.

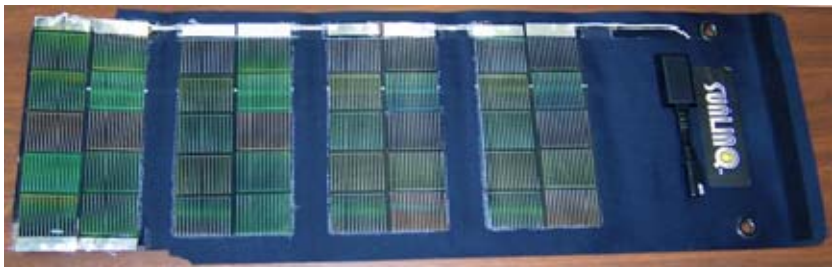

Figure 75. 6-Watt Panel with Partial Trimming and Some Top Fabric Removed.

Next, we needed to strip the backs of the panels. The solar arrays would be significantly heavier if the fabric and adhesive could not be removed. The effort illustrated by Figure 76 involved several hours of work during which many different tools and methods were used. This included the use of chemical solvents and heat. Eventually we abandoned these efforts. The progress shown in Figure 76 (a) and (b) took approximately one hour and was viewed as very likely to damage the thin CIGS cells. We used a heat-gun to loosen the underlying adhesive to speed up the process, but this resulted in the top-surface delamination, shown in (c).

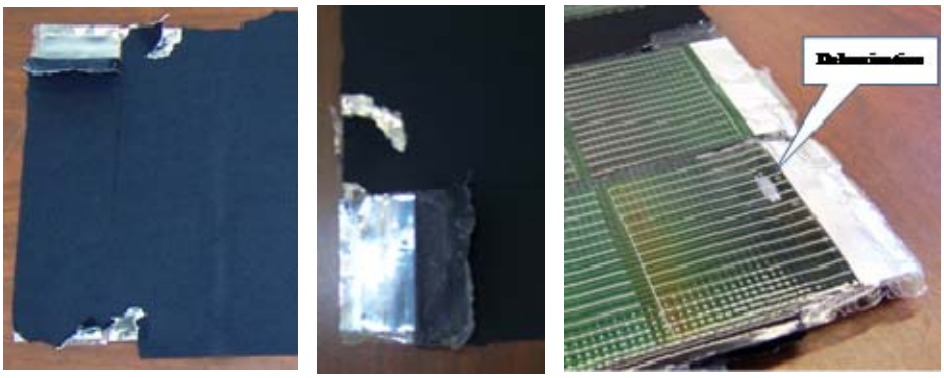

(a) (b) (c)

Figure 76. Attempts to Remove Fabric and Adhesive from Back of 6-watt Panel.

We made a fortunate discovery while removing the remaining fabric and adhesive from the front and sides, we found that the cloth on the backs of the panels was not adhered directly to solar cells; there was an additional layer of lamination between. Without realizing this, we had inadvertently tried to remove the lamination rather than just peeling the cloth from its surface.

Though removing the unwanted layers from the backs of the cells would take about 12 additional hours, it resulted in a significant reduction in weight. Between the two battery chargers, there were 12 panels total. The panels that were stripped on the front only weighed 25 grams each or 300 grams total. After the layers above the lamination were removed from the panel backs, they weighed a mere 18 g each, which was reduced to about 17.5 g by trimming excess lamination around the perimeter. So through the removal of the back cloth and adhesive and further trimming, the total weight of the pre-installed cells was reduced from 300 to 212 grams, or nearly 30 percent.

### 4. Installation

With the solar cells removed from the battery charger, the next stage would be to wire them together. We needed to configure the cells to provide the correct load voltage while minimizing the additional wiring needed in order to reduce the additional weight added to the plane. As mentioned in Chapter IV, individual cell voltage is usually quite low so they are connected in series to increase the total voltage.

Also discussed in Chapter IV were blocking and bypass diodes. Since all the cells would be aligned in the same horizontal plane, and the separate sections were very unlikely to be individually shaded, we did not install bypass diodes. They will be needed in future testing or production models if solar cells are applied to other surfaces. The SUNLINQ battery chargers included a small circuit board shown in Figure 77, which contained a blocking diode in addition to a limited the voltage to fewer than 15 volts.

Figure 77. Voltage Limiter and Blocking Diode.

Unlike the GSE's thin-film strings, the CIGS used in the battery chargers were not large 100 cm x 210 cm cells, but rather smaller cells shingled upon each other to form higher voltage strips. This would permit the use of these panels without a DC-DC converter to "step-up" the voltage. Each solar cell has a voltage of approximately 0.5 volts. The cells in the 6-watt charger were about half the size of those in the 12-watt charger, so they added up to the same voltage in a smaller area when put in series. This is shown in Figure 78.

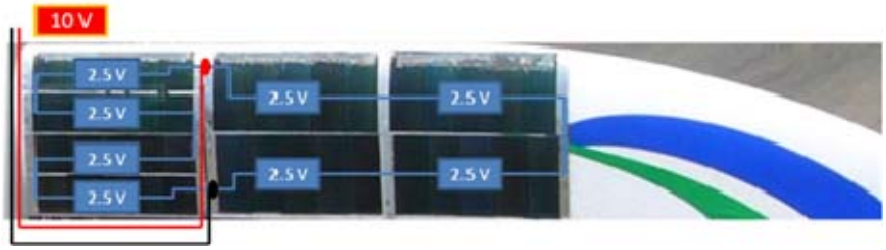


Figure 78. Solar Cell Wing Configuration.

With this configuration, the two wings would be connected in series to sum the voltages to approximately 20 volts. Thus, the plane could be tested with and without an MPPT since the baseline voltage would exceed 12.6 without a DC-DC converter.

The cell strips were connected using the existing flat wire braid attached to the large metal contacts at the end of each strip. Much smaller contact area and thinner, lighter wiring could be used in future testing with this aircraft, or installation of solar cells on the Raven or other UAV.

Since we were unsure if better cells would be procured during testing, we decided to attach the solar cells so they could be easily removed without damage to the wings or cells. The edges and seams were adhered to the wing using double-sided tape. The interior seams between the panels were covered with thin strips of clear tape and wider clear "packing" tape was applied to the leading and trailing edges.

## D. MPPT

As discussed in the previous chapter, an MPPT should be used in most solar applications to allow the cells to function at the best operating point, rather than being held to the voltage of the load. An ideal MPPT for this research would incorporate power-point tracking, voltage conversion, voltage regulation, charge control – including cell balancing, would be small and very lightweight, and would have high efficiency and very low quiescent power consumption.

There was not sufficient time or funding to design a build the ideal circuit so in keeping with the aim of using inexpensive off-the-shelf products for a practical application we began to research commercial MPPTs.

Unfortunately, very few MPPTs are designed for use in this type of application. An overwhelming majority of photovoltaic applications are terrestrial, so size and weight are typically not concerns for designers. One candidate was the photovoltaic power converter (PVPC) designed by Atira Technologies and tested at NPS, but it does not appear to have gone into production [92].

Another MPPT we considered was from Solar Converters. Their smallest charge controller, shown in Figure 79, can be purchased for 12 or 24-volt applications.


Figure 79. Solar Converters Charge Controller with MPPT (From [102]).

This unit meets most of the requirements stated previously. It can be factory configured for a specific application. As Table 5 shows, this unit was slightly less expensive than our final selection, but was heavier and drew more current.

| | Solar Converters | Genasun |
|---|---|---|
| Max Array Voltage (V) | 50 | 27 |
| Max Output (A) | 3 | 4 |
| Self Consumption (mA) Charging | 20 | 1 |
| Self Consumption (mA) Quiescent | 10 | 0.09 |
| Setpoint Tolerance (+/-) | 0.05 | - |
| Float Setting **(V) | 14.1 | 12.5 |
| Efficiency (%) | 96 | 94–98 |
| Max Temp °C | 60 | - |
| Weight (g) | 136 | 80 |
| Price ($) | 72 | 110 |

Table 5. MPPT Comparison [Data from [102][103]).

We selected the Genasun GV-4 Low-Power MPPT/Charge Controller (Figure 80) as the best alternative of readily available products that met our specifications. Another potential source was Solarmppt.com, but a custom product would have been needed to meet our voltage and weight parameters. The best MPPT for a solar modified RQ-11 would probably be very similar to the one used on the Sky-Sailor. After several iterations, the final design for that aircraft was 95–97% efficient, could produce up to 30 watts, and weighed only 7 grams.


Figure 80. Genasun GV-4 Low-Power MPPT/Charge Controller.

The Genasun MPPT was initially 80 grams, which would be much too heavy for this aircraft. The greater load would have negated any additional efficiency gains. Figure 81 shows the disassembly of the GV-4. The first image (a) shows the MPPT with the top cover removed. The second image (b) shows the MPPT without the base plate and mounting screws. It now weighed only 29 grams.

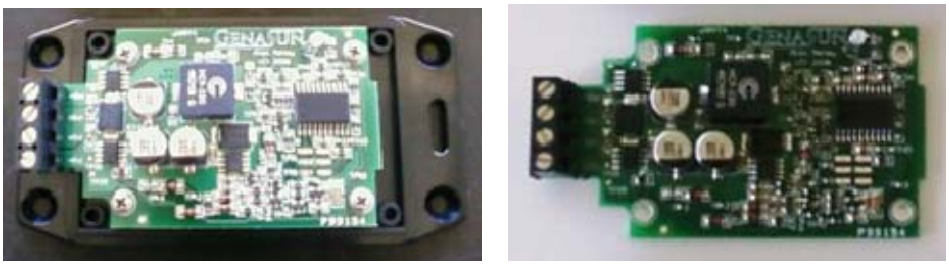

(a) (b)

Figure 81. Disassembled Genasun GV-4.

## E. SYSTEM INTEGRATION

With all components in hand, the next step was to integrate them all within the plane's canopy and begin system testing. The intended system design is shown in Figure 82.

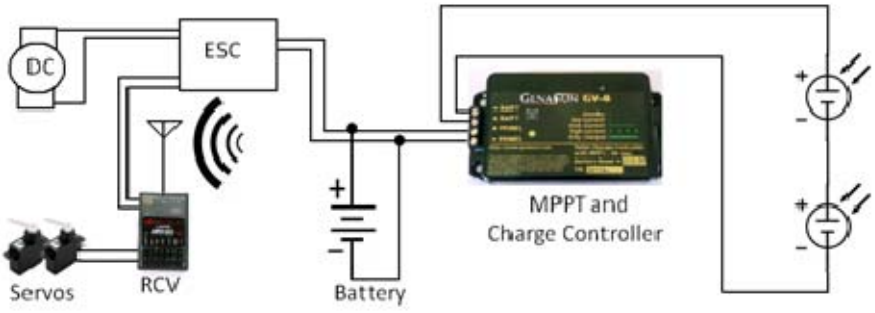


Figure 82. Planned Thin-Film Flyer Configuration.

Unfortunately, the MPPT suffered a catastrophic casualty during preliminary testing, so could not be incorporated in the full system testing. The diagram in Figure 83 shows the actual aircraft electrical configuration. Without the built-in protection of the

MPPT, it was important to add a blocking diode back into the circuit. The small circuit board from one of the battery chargers served that purpose, as well as limiting the voltage from the cells to 15 V.

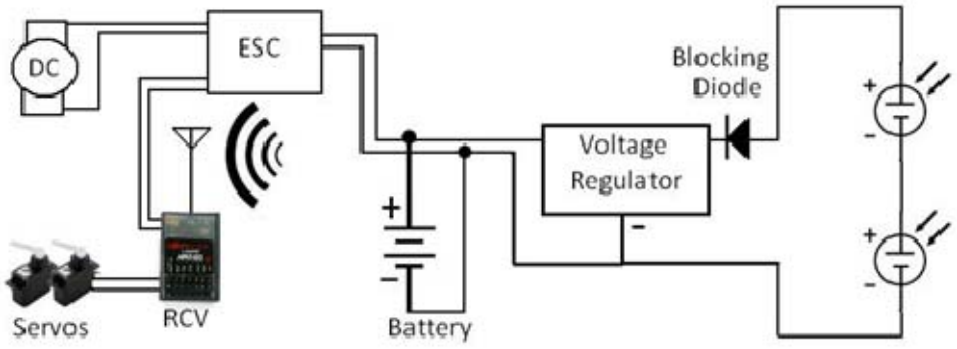


Figure 83. Actual Thin-Film Flyer Configuration.

The individual components were chosen and optimized for weight, then installed. Figure 84 (a) shows the open canopy with the battery connector on the left, wired in parallel with the output of the voltage regulator and the solar cell connectors. Figure 84 (b) shows the cockpit area with the battery and solar cells connected.

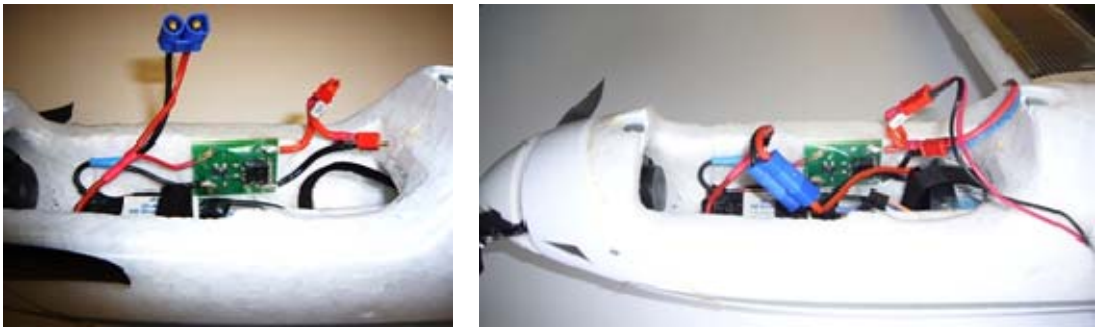

(a) (b)

Figure 84. Thin-Film Flyer Integrated Electronics.

The images in Figure 85 are of the final assembled aircraft. Figure 85 (a) shows the front of the aircraft with the canopy closed. In order to maintain the strength of the fuselage, we did not create holes for the wires from the solar arrays. Instead, we used a small piece of tape to reduce their drag on the surface. The second image (Figure 85 (b)) demonstrates the ability of the propeller to fold during gliding to reduce drag.

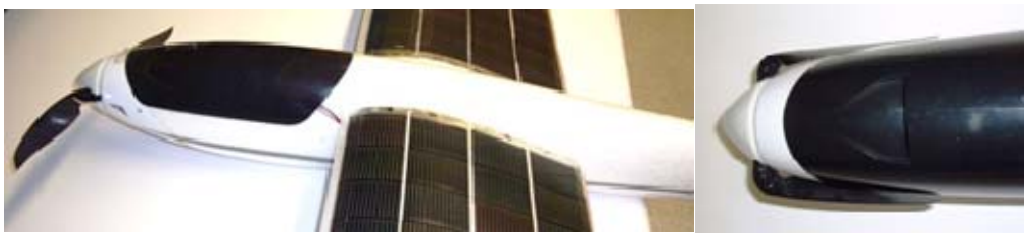

(a) (b)

Figure 85. Assembled Thin-Film Flyer with Canopy Closed.

The final image (Figure 86) is an overhead view of the fully assembled Thin-Film Flyer.

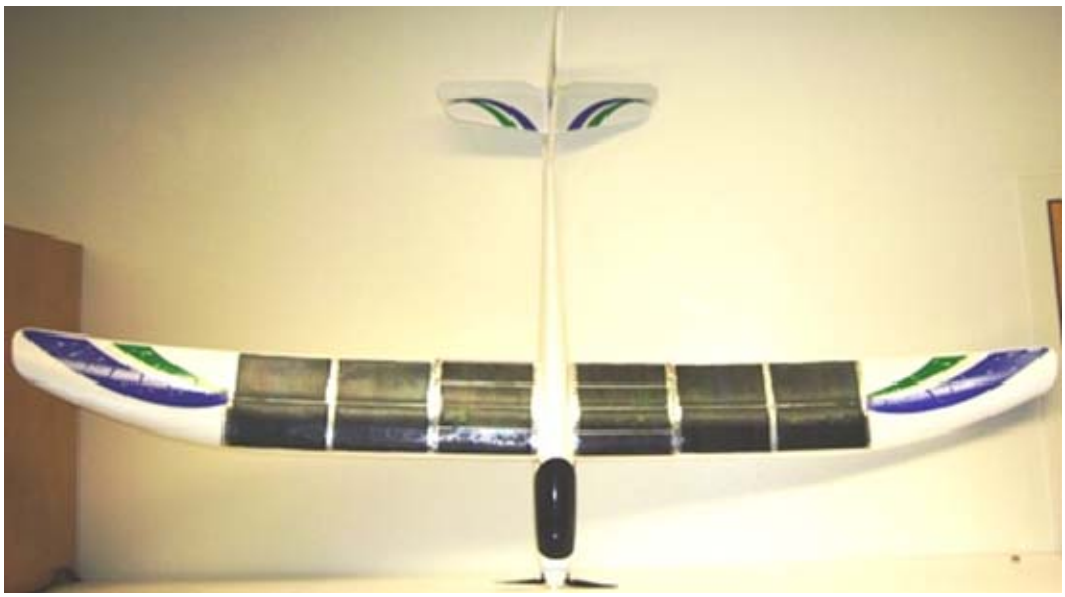

Figure 86. Thin-Film Flyer Fully Assembled.

## F. CHAPTER SUMMARY

In this chapter, we described the most significant constraints on the scope of this research, namely time and funding. We described how an inexpensive commercial-off-the-shelf (COTS) remotely piloted vehicle was used as a proof-of-concept demonstrator in place of an RQ-11 Raven. Next, we explained the reason for using the CIGS cells harvested from a battery charger and explained how they were connected and installed on the wings. We then detailed our MPPT selection process and showed our selection from

Genasun. We showed our system design as originally intended, and the implemented design used after the MPPT failed. Lastly, we showed our final aircraft configuration with all elements integrated.

# VI. TESTING AND ANALYSIS

As stated in the previous chapter, we conducted testing on individual components and sub-circuits prior to system testing and installation. The first components we tested were the batteries.

## A. BATTERIES

The Parkzone Radian RTF plane kit came with a 3-cell Li-po battery with a nominal voltage of 11.1 V. A battery charger was also included that could be plugged into a cigarette-lighter adapter in a car. We chose to purchase an aftermarket universal battery charger that came with an AC-DC wall adapter. This charger featured Li-po charging, discharging, and cell balancing. It could monitor battery temperature during charging and could export data to a computer with a USB cable (though not simultaneous with temperature monitoring). The Venom AC/DC Pro Balance Battery Charger is also capable of charging NiCd and NiMH batteries. The Parkzone and Venom chargers are pictured in Figure 87.


(a) (b)

Figure 87. Parkzone and Venom Balanced Chargers (From [104]).

A single 11.1 V, 1.3 Ampere-hour (Ah) battery came with the Radian kit. Two additional batteries of similar size, and one rated at 4.0 Ah, would be tested during this project. This larger sample size would help to eliminate battery malfunction or performance variations from affecting testing analysis.

Table 6 shows the four batteries we used for the remainder of this research. Though there are slight anomalies due to quality and manufacturing differences, in general, larger batteries have higher energy density.

| Battery | Ah | Mass (kg) | Specific Energy Density Wh/Kg |
|---|---|---|---|
| 1 Sapac | 1.20 | 0.104 | 128.1 |
| 2 Park Zone | 1.30 | 0.099 | 145.8 |
| 3 Thunder Power | 1.35 | 0.104 | 144.1 |
| 4 Thunder Power (large) | 4.00 | 0.265 | 167.5 |

Table 6. Lithium-Polymer Battery Parameters.

All these batteries are made of individual 3.7 V cells wired together in series, as in Figure 88 (a). Each pack has a large main connector for drawing large currents from the pack when connected to a load, and a smaller connector for monitoring and balancing the cells during charging. If a second set of three cells is placed in parallel with the first set (Figure 88 (b)), the voltage will remain the same, but the current will double, thereby doubling the power of the battery pack. Since a second set of connectors is not needed, only a small amount of internal wiring is added. The amount of packaging for a larger battery increases only slightly and additional internal protective circuits are not needed. Therefore, while the power doubles, the overall increase in pack weight is proportionally much less. Therefore, the specific energy of larger battery packs is better than smaller.

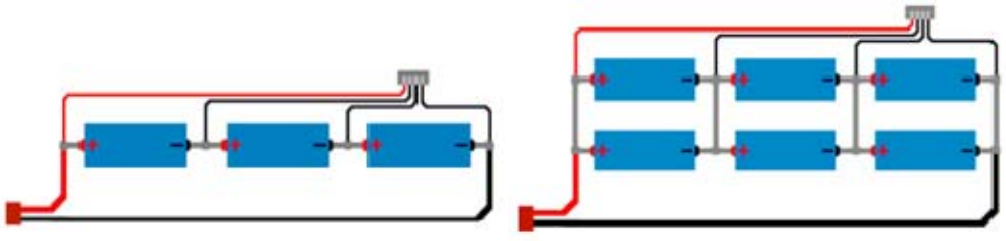

(a) (b)

Figure 88. Internal Wiring of 3s1p (a) and 3s2p (b) Lithium Polymer Packs (From [105]).

### 1. Bench Charge and Discharge Testing

The first test we conducted was to determine the general charge characteristics of Li-po batteries. Though similar data was available, we wanted to confirm the behavior with our charger and battery. The nominal voltage of each of the three cells in a pack is 3.7 V. During charging, they are charged at a constant current, this case 1.0 A, until the individual cells are 4.2 V. This is shown as the point in Figure 89 where the voltage remains constant at 12.6 volts. After the desired voltage is reached, charge current continues to decrement until the total battery's capacity is reached.

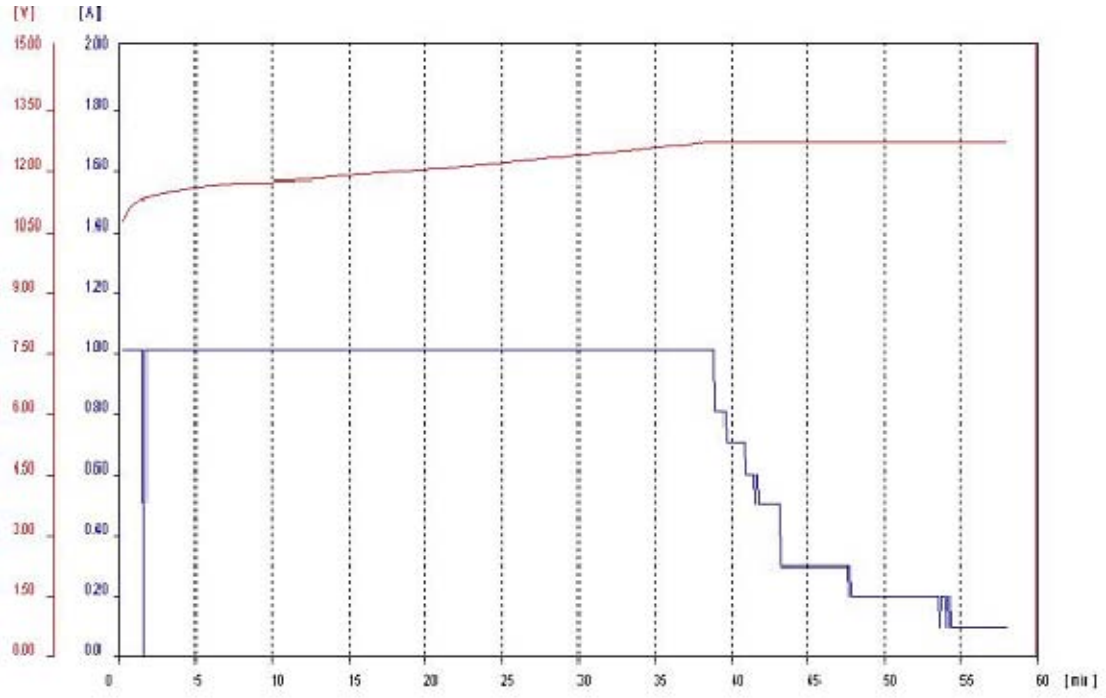


Figure 89. 11.1 V Lithium Polymer Battery Charge Cycle Using Venom Pro Charger.

From previous research (Chapter III), we knew that most battery-powered UAVs have an endurance of 30–60 minutes. From the Radian's documentation, we knew that flights were likely to be in the same range as well. For these reasons, we set our plane's throttle at such a level that a battery would be discharged in approximately the same time during bench testing as it would during a normal flight.

We found an approximate current using the current capacity of the battery and the desired run-time

$$\frac{1.35\text{Ah}}{.75\text{h}} = 1.8\text{A} \tag{6.1}$$

Figure 90 shows the aircraft bench-test configuration. We decided to increase the throttle slightly for our initial current measurement so the throttle lever could be positioned at an easy to find reference point. This would enable us to set the throttle to the same point for bench, rooftop, and field testing. The initial measured current was approximately 1.96 V at the start of each subsequent test. This corresponded to setting the throttle to one "notch" below centerline on our controller.

Figure 90. Battery Bench-testing Setup.

The voltage of Li-po batteries decreases as they discharge. The electronic speed control circuit (ESC) on the airplane takes advantage of this fact to determine when the battery's capacity is critically low. The ESC also reduces the current to the motor, hence the speed, as the battery voltage decreases. For uniformity, we decided to set the initial current to the same value for all tests. We would not be able to monitor the current while the plane was airborne to make continual adjustments to counteract the ESC.

As stated, Li-po batteries have a maximum voltage of 4.2 V per cell and should be discharged to no less than 3.0 V per cell. Therefore, our 3-cell packs would start at 12.6 V and were allowed to discharge to 9.0 V. The results of our battery voltage characterization test are shown in Figure 91.

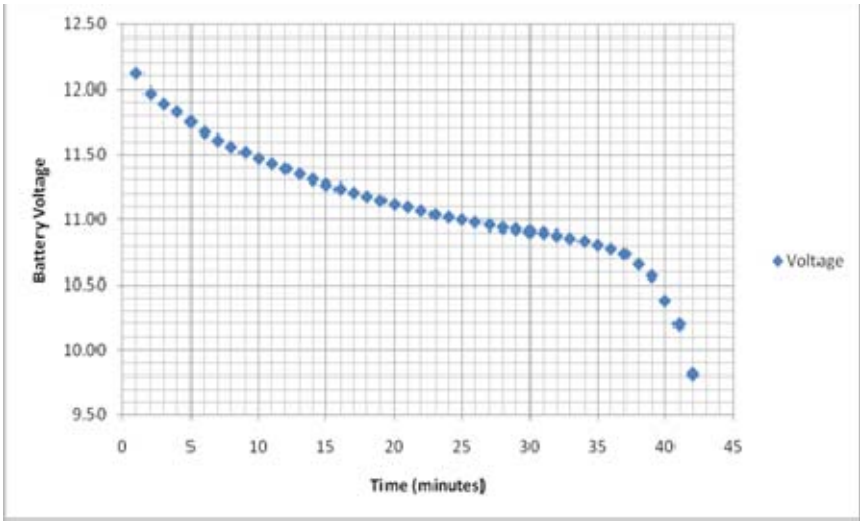


Figure 91. 1.3 Ah Lithium Polymer Battery Discharge at Initial Current of 1.96 A.

This discharge curve is typical of that in the literature. As seen in Figure 91, once the voltage on a Li-po battery goes below 10.5 V, it drops very quickly. To avoid permanent damage, the battery should not be discharged much further from this point. Therefore, the ESC forces the planes motor into a pulsating mode when the voltage drops too low. In practice, this gives the pilot on the ground a signal of the impending loss of power. Once the battery is discharged beyond this stage, power to the motor is cut off completely. However, the battery is not completely dead. The ESC is programmed to turn off the motor while leaving enough power in the battery to operate the servos. Thus, a pilot still has a chance to steer the plane toward a desired landing area.

We used this function of the ESC in all further testing. We ended tests when the motor started to pulsate, indicating a battery voltage of approximately 9.5 V.

### 2. Aircraft Bench Testing

Prior to testing the aircraft with solar cells installed, we needed to establish baseline endurance for each of the batteries. According to the literature that accompanied the Thunder Power Li-po batteries, they should be conditioned by running at a lower initial current, 3C-5C for the first few flights. “C” in this case is capacity in Amp-hours. So for a 1.3 Ah battery, the initial discharge cycles should not draw more than 5 x 1.2 Ah, or 6 Amps. We were only testing at two amps or less, so this would not cause damage.

However, we decided that in the interest of thoroughness, we would test the batteries ten times to determine if there was a difference in performance after a "break-in" period.

There was a distinct break-in period for two of the batteries as Figure 92 demonstrates. Batteries 1 and 4 showed a significant drop in endurance, steadily decreasing from test 1 to 5, then both batteries endurance became more stable. Batteries 2 and 3 did not noticeably demonstrate this same behavior.

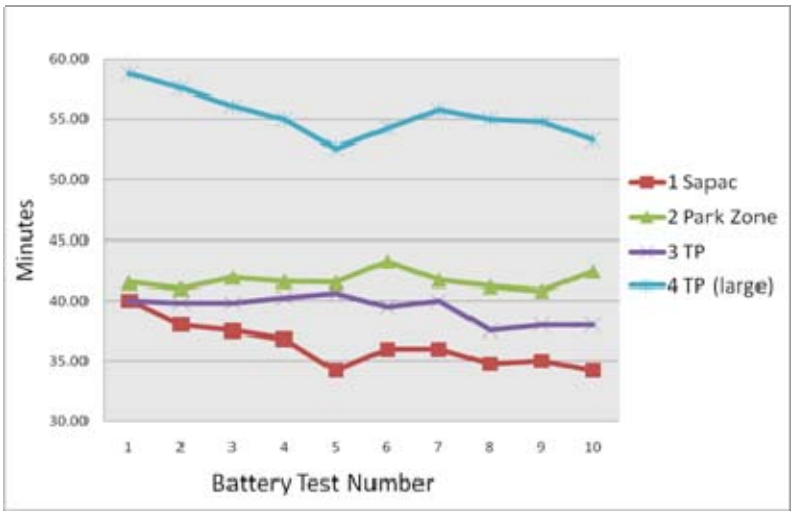


Figure 92. Bench Battery Endurance Tests.

For this reason, we would use an average of the last five battery tests as a baseline for each (Table 7).

| Test / Battery | 6 | 7 | 8 | 9 | 10 | Average of last 5 |
|---|---|---|---|---|---|---|
| 1 Sapac | 36.0 | 36.0 | 34.8 | 35.0 | 34.2 | 35.2 |
| 2 Park Zone | 43.3 | 41.7 | 41.2 | 40.8 | 42.4 | 41.9 |
| 3 TP | 39.5 | 40.0 | 37.5 | 38.0 | 38.0 | 38.6 |
| 4 TP (large) | 54.3 | 55.8 | 55.0 | 54.8 | 53.3 | 54.6 |

Table 7. Baseline Battery Endurance Tests (Run-time in Minutes).

## B. CHARACTERIZATION OF SOLAR PANELS

Per our discussion in Chapter III, solar cells are typically characterized by an I-V curve established under solar simulator with AM0 or AM1.5 irradiance. There was no solar simulator of sufficient size at NPS to test a solar array as large as those from the

battery chargers, nor was it possible to cut them into manageable sample sizes, since all cells would be used on the aircraft. In order to determine the efficiency of the cells we used, we needed to calibrate a reference cell that would fit in the solar simulator. A reference cell, shown in Figure 93, would also be used to measure the solar irradiance during rooftop and field-testing.

### 1. Reference Solar Cell

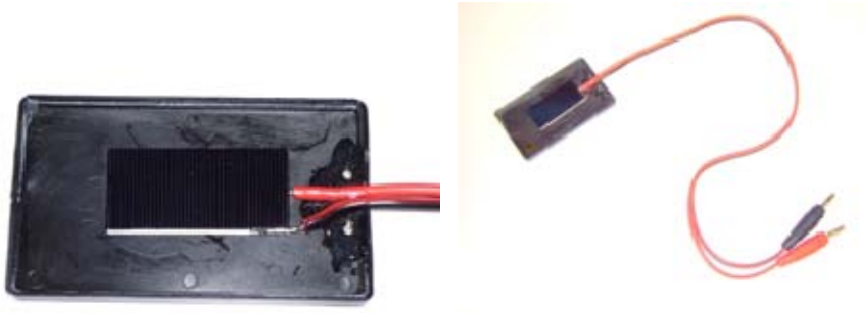

Figure 93. Reference Solar Cell with Multimeter Leads.

In order to find the voltage and current of this cell, we first had to calibrate the solar simulator. We used a laboratory-calibrated cell with known short-circuit current ($I_{SC}$) and open-circuit voltage ($V_{OC}$). The cooling system for the simulator was not functioning, so we used the simulator's built-in shield to block the light while the cell and mounting base cooled to 25°C. We tested the temperature with a digital thermocouple mounted on the testing surface near the cell. Luckily, the ambient temperature in the lab was almost perfect for testing, so the non-operational cooling system did not make a significant difference. At standard test conditions, the cell should be 25°C. We were able to cool our samples to 25.3°C, and took measurements immediately after the lamp was exposed.

Unfortunately, when we compared the readings taken throughout or outdoor tests, both on the roof and prior to flight tests, we discovered that the parameters from the "calibrated" solar cell we used were incorrect. Therefore, the solar simulator characterization of our reference cell was inaccurate. Though we took $V_{OC}$ and $I_{SC}$ readings throughout each stage of our testing, we were not able use those readings to

establish the incident radiation during testing. The measurements were not essential to the fundamental aims of the current research; however, they would have provided a better indication of the effectiveness of this approach at different levels of irradiance. The measurements will be available for analysis in follow-on research at Naval Postgraduate School.

### 2. Global Solar "SUNLINQ" Chargers

Prior to disassembling the battery chargers to harvest their cells for use on our aircraft, we wanted to determine their electrical parameters. We tested the $V_{OC}$ and $I_{SC}$ of both the 6.5 W and 12 W chargers. Global Solar determined these ratings under ideal test conditions, rather than what could be expected during practical use. They state that 6.5 watts is the maximum power, [100] though typical power under standard test conditions (1000 $W/m^2$) is only 5.5 W. In testing, our 6.5 W charger yielded a maximum of approximately 4.5 W. Though we knew some of this was due to non-ideal irradiance, this was nearly 20% less power than the typical power listed on the specification sheet, and about 30% of the power rating of the charger.

We had assumed that the advertised power rating of the battery charger was under ideal normal operating conditions. Instead, we learned that these ratings were at STC with the charger cooled to 25°C. Global Solar explains the temperature dependence of the battery chargers as follows:

> The panels are rated at room temperature (25C) and the power drops at 0.5% of the rated power for each degree of temperature increase...Under direct noon sunlight the panels operate at approximately 40 C above ambient air temperature with no wind. On a day when outdoor air temperature is 25C (77 F) the panel will heat to approximately 65C, causing a power decrease of 20% (i.e. 80% of rated power). [106]

This realization accounted for the significant difference in performance from our expectations. Figure 94 shows Global Solar's typical I-V curve of the 6.5 W charger. Also shown is the abrupt cut-off of voltage, as the SUNLINQ chargers have a built-in limiter to keep the solar charger's voltage in the range of a typical "cigarette lighter

adapter" (CLA). Most rechargeable consumer electronics can be charged from this type of adapter, so GSE designed its chargers to be limited near the CLA typical voltage maximum of 14.5 V [100].

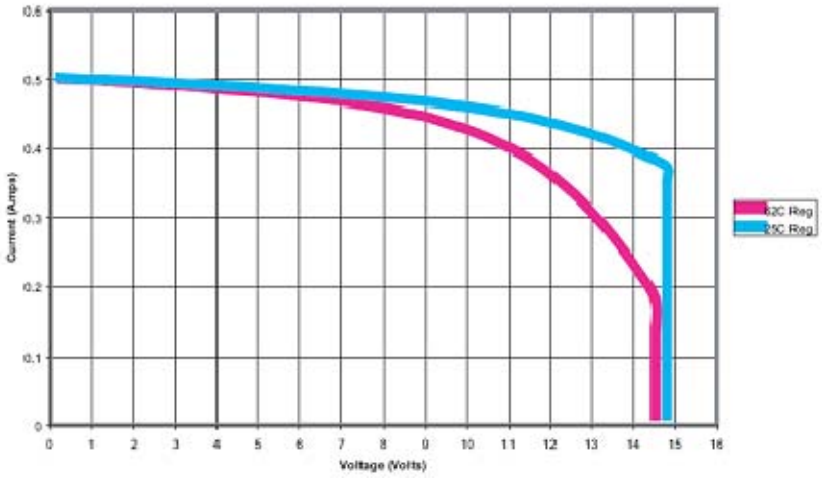


Figure 94. I-V Curve of Global Solar 6.5 Watt Charger at STC and at Higher Temperature (After [100]).

Our second charger was rated at 12 W by GSE. The I-V curve of this charger is shown in Figure 95. The shaded area of Figure 95 indicates the operating voltage of our Li-po battery. At STC, without a maximum power point tracker, the solar cells will be forced to operate between points (1) and (2), while the approximate maximum power point is at a higher voltage "M." At 62°C, the maximum power point is at least within our operating range, between points (3) and (4). In this case, the MPPT is not as critical, but still would provide additional power. In subsequent testing, we would confirm that the MPPT from Genasun actively drew approximately 2 mA of current, which equates to about 22 mW at our nominal voltage of 11.1 V.

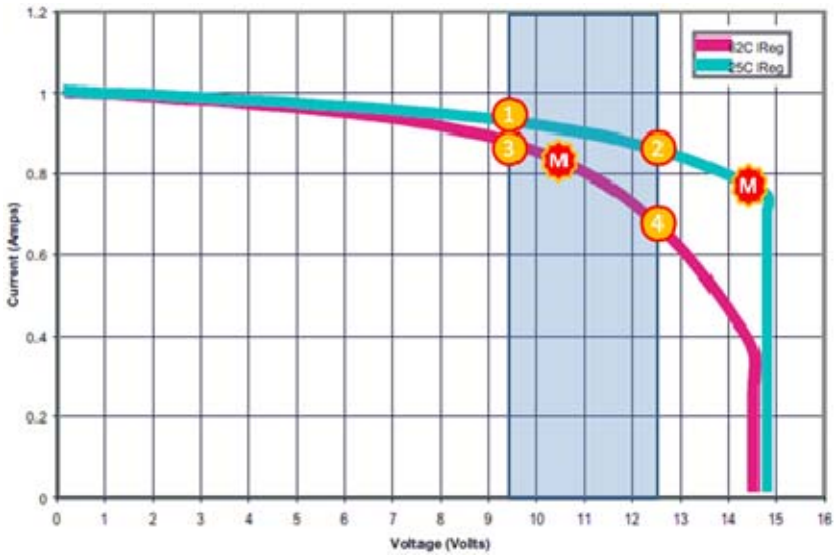


Figure 95. I-V Curve of Global Solar 12 Watt Charger at STC and at Higher Temperature (After [89]).

Though we did not have the means to measure the cells operating temperature in flight, we expected the cells to operate at some temperature considerably lower than 62°C, but higher than 25°C. To estimate the potential benefit of the MPPT, we compared approximate power using the 25°C GSE curve provided. Without an MPPT, the power from this charger at (2) would be approximately 12.5 V x 0.85 A, or 10.63 W. The power at (1) would be approximately 9.5 V x 0.93 A, or 8.84 W. For comparison, at the maximum power point "M," the power would be about 14.5 V x .77 A, or 11.17 W. If the MPPT draws 2 mA at this voltage, its active power consumption would be 29 mW. The added power gained from using an MPPT, less the power it consumes would be an additional 511 mW at (2), and 2.3 W at (1). That equates to greater than 25% more power at the lower voltage.

We knew that even when mounted on the wings with significant convection cooling in flight, the solar cells would probably operate at a temperature greater than 25°C. Even at a temperature closer to 62°C, it still appeared that the additional weight and cost of an MPPT would be offset by the added power that it produced.

## C. SOLAR CHARGING BATTERIES

Prior to removing the cells from the chargers and mounting them on the wings, we tested the battery chargers for their intended purpose; we conducted tests to determine how long it would take to recharge batteries. This would show the added benefit of solar modified UAV to "self-charging" on the ground between flights. These chargers could also be used in their original configuration to supplement power for the UAV ground control station, to recharge additional batteries, or for other electronics.

We decided in the interest of time to test only the three similarly sized batteries, forgoing experiments with the much larger battery for a later date.

We tested three combinations of solar chargers. First, we tested the charge time using a smaller 6.5 W (rated) charger, then using the 12 W charger, and finally, using both chargers in parallel. This configuration is shown in Figure 96.

Figure 96. Battery Charge Testing Configuration Using 6.5 W and 12 W GSE Chargers.

Though the rated value of these chargers is a combined 18.5 W, as discussed previously, the operating power would be significantly lower. Using the I-V curves in Figures 94 and 95, under 1000 W/m$^2$ of irradiance at 62°C, our chargers would produce a combined 13.2 W. We knew the irradiance during our tests would be lower due to our frequently overcast weather in Monterey, the lower angle of the sun to Monterey, which is at approximately 36°N latitude, and the varying times of day, we estimated our charging power would be 9–12 W.

Table 8 summarizes the results of these tests. Using our MPPT connected in series with the combined battery chargers, we found that batteries could be charged in 2–3 hours in less than ideal conditions.

| Battery | Time 6.5 W | Time 12 W | | | Time 18.5 W |
|---|---|---|---|---|---|
| | | Test 1 | Test 2 | Average | |
| 1 | 307 | 212 | 170 | 191 | X |
| 2 | X | 195 | 218 | 206.5 | 158 |
| 3 | 377 | 183 | 194 | 188.5 | 123 |
| | | | | 195.3 | 140.5 |

Table 8. Summary of Solar Battery Charging Tests.

## D. OUTDOOR PLANE BENCH TEST WITH SOLAR

### 1. Simulated Flight Tests with MPPT

Our next step was to connect the chargers to the plane in our planned configuration previously shown in Figure 82. The physical arrangement of equipment for this phase is shown in Figure 97.

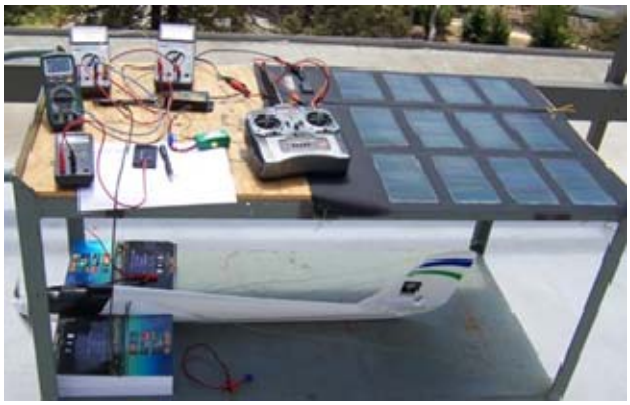

Figure 97. Plane Endurance Testing with MPPT and Combined 18.5 W Solar Chargers.

The results of these tests are summarized in Table 9. There was a lot of variation in due to Monterey weather and time of day. On a cloudy day, our worst test resulted in an endurance increase of only about 12 minutes, or 31%. Our best test on a sunny afternoon was 66 minutes, which was nearly double the pre-solar time.

| Battery | Test 1 | Test 2 | Average | Without Solar | Increase | Increase |
|---|---|---|---|---|---|---|
| 1 | 66 | 60 | 63 | 35.2 | 27.8 | 79.0% |
| 2 | 65 | 60 | 62.5 | 41.9 | 20.6 | 49.2% |
| 3 | 55 | 50.5 | 52.75 | 38.6 | 14.15 | 36.7% |

Table 9. Endurance Testing with MPPT and Combined 18.5 Watt Chargers.

Though we saw some significant improvement, we had expected better results. We suspected the MPPT may have malfunctioned, and after inspecting the circuit board, discovered that a component had obviously failed. Genasun covered the MPPT under warranty so we sent the device for repair. Meanwhile, due to an already compressed time schedule, we decided to continue experimenting without the MPPT, though we would not be able to show the greatest potential performance gain without power point tracking.

### 2. Simulated Flight Tests without MPPT

Besides optimizing the operating point and acting as a DC-DC converter, our MPPT had served several other important roles. It protected the solar cells from being forward biased, limited the output voltage to approximately 12.5 V, and monitored the charge-state of the battery to prevent overcharge. Without the MPPT, at a minimum, we would need to limit the output voltage and provide "blocking" protection to prevent the battery from forward biasing the solar cells. This would provide a low-impedance discharge path that could damage the battery or solar cells.

Fortunately, we were able to use the built-in circuit protection board from the solar battery chargers in place of the MPPT to provide those two important functions. This revised configuration was shown in Figure 83. There was a blocking diode on the circuit board that we installed, and a voltage limiter that kept the output below 15 V as it had in the battery charger.

Using this new configuration, we immediately saw a marked improvement in simulated flight endurance. On a somewhat cloudy day, we started our first test without MPPT at 1400. Though this is past daily solar-max, we observed an endurance of 83 minutes, 17 minutes longer than our previous best, and twice as long as the battery-only endurance.

We conducted two tests on each of three batteries, summarized in Table 10. Again, due to significant differences in start times and weather, there was a great deal of variation in our tested endurances. We did not have the luxury of traveling to more suitable climate and testing only during solar max hours, nor did we desire to do so. We wanted to present realistic rather than ideal results to prove the practicality of the concept.

We observed from these tests that even without a working MPPT, our battery endurance increased significantly. Our endurance test that yielded the least improvement was begun at 10:26 a.m., and conducted under 100% cloud cover for the duration of the test. Even under these conditions, we saw a 43% improvement in endurance.

Our best test commenced at 1255 under partly cloudy conditions. During this test, our battery lasted 108 Minutes, over three times the pre-solar average.

| Battery | Test 1 | Test 2 | Average | Without Solar | Increase | Increase % |
|---|---|---|---|---|---|---|
| **1** | 57.5 | 108 | 82.75 | 35.2 | 47.55 | 135.09% |
| **2** | 83.5 | 60 | 71.75 | 41.9 | 29.85 | 71.24% |
| **3** | 68.5 | 78 | 73.25 | 38.6 | 34.65 | 89.77% |

Table 10. Endurance Testing with Combined 18.5 Watt Chargers but without MPPT.

### 3. Flight-Ready Aircraft Simulation

Once we completed our testing with separate components, we needed to integrate our system design into a complete aircraft. Details of the labor-intensive process of harvesting and installing the solar cells and connecting the components were presented in Chapter V.

At this point, we were unsure if lighter, more efficient solar cells would be procured in time to use in this project. Therefore, the solar panels from the SUNLINQ chargers were attached using double-sided tape and clear packing tape. An improved version of this test aircraft, or certainly a solar-enhanced production model UAV, will be much lighter and more aerodynamic using strong spray-on adhesives.

The final aircraft ground testing configuration is shown in Figure 98.

Figure 98. Thin-Film Flyer Pre-Flight Test Configuration.

We were constrained by time, and only conducted one test with this configuration. The main goal was to ensure that the previously tested system worked once the solar arrays and circuits were hard-wired in place. An additional set of interesting data points would have been to discover the change in cell operating temperature compared to the previous readings. In previous tests, while the cells were still embedded in the chargers and laying flat on the wooden surface, we measured the temperature underneath the charger near the center of a solar cell. Had we considered this before attaching the cells to the wings, we would have mounted a thermocouple wire beneath a panel on each wing in order to take temperature measurements for comparison. We tried to insert a thermocouple under a panel during this experiment, but were unable to do so without potentially damaging the cells and wing surface.

This final pre-flight test started at 1400, past daily solar max, but it still lasted 91 minutes, over 2.5 times longer than pre-cell endurance.

Measurements taken before and after modification show that our aircraft weight grew from 763 grams to 990 g. Its weight increased by 227g, or an additional 30%. Next, we needed to determine if the additional weight would counterbalance the additional power provided by the cells.

## E. FLYING TESTS

The final, most important stage of this research was to fly our proof-of-concept aircraft to determine if the net effect of adding CIGS cells and related wiring and circuit would result in improved endurance. The author of this research was not a pilot and did not wish to destroy the aircraft while learning to fly (Figure 99). Therefore, we enlisted the aid of Don Meeks, a retired NPS employee with decades of experience flying remote-controlled planes, and who has tested UAVs for various Department of Defense components. He expertly flew the plane, volunteering many hours, and protecting the plane from the author.

Figure 99. William Hurd with the Thin-Film Flyer.

### 1. Benchmark Flights Using Thermal Updrafts

On July 31, 2009, during the bench-testing phase of our research, we began flight-testing. We sought to establish baseline endurance for the aircraft prior to the solar

modification. We wanted to fly a number of test flights taking advantage of our plane's gliding capabilities. The Parkzone Radian is a sailplane, and as such is designed to take advantage of thermal updrafts, or simply "thermals." Depending on the weather conditions, thermals can provide significant lift to the aircraft. Sailplanes have the ability to fly for hours under the right conditions. Like other sailplanes, the Radian can be lifted to high altitudes while riding an updraft. After the lift is gone, the plane can glide for a long time, with the hinged propeller folding back to reduce drag.

Though we attempted several flights, the first two were cut short due to high winds. Unfortunately, at this location there are typically afternoon winds that coincide with daily temperature increases, which is also the best time to fly a solar-powered plane from an irradiance standpoint. Our last flight attempt without solar cells was on August 3. The plane stayed aloft for 95 minutes by exploiting thermals. The pilot was able to find significant lift for several minutes at a time, and then allow the plane to simply glide for 5–10-minute stretches without using throttle.

### 2. Solar Flight Using Thermal Updrafts

We installed our solar cells and related circuitry, and headed back to the airstrip on August 7 for the first solar aided flight of the Thin-Film Flyer. However, once again, our testing was shortened due to wind. High winds not only make it increasingly perilous to keep the aircraft flying, but they also prevent the use of thermals for extended flight. Though we had an abbreviated first solar flight, it still showed the aircraft was still airworthy and flew well even with 30% greater weight. We started the flight well before solar max at 10:02 a. m. Our pilot reported that there were no thermals and he had to use a lot more throttle due to the wind. As the wind speed increased, we decided to land the plane at 11:04 a.m. After a flight of just over one hour, we measured the voltage in the battery at 11.42 V.

Referring back to our battery discharge characterization in Figure 91, 11.42 V corresponded to 11 minutes of run-time. This was just less than 27% of the total battery endurance. Carrying this proportional comparison forward to our flight test, if the same

flight profile were continued in the similar conditions, and 11.42 V corresponds to only 27% of the total battery life, the plane could theoretically have remained aloft for a total of 229 minutes.

On August 10, we flew the plane again with solar cells. Once again, we started earlier than the most favorable time to try to avoid the higher winds at midday. We launched the plane at 10:25 a.m. in moderate winds of five mph, gusting to seven. There was very little lift from thermals on this day and, after one hour, the wind had strengthened to a steady 8 mph, gusting to 10 mph. This eliminated even more potential lift and required our pilot to use more throttle. The flight was completed at 12:12 p.m., or 107 minutes after launch. This was a longer flight than the pre-solar "thermalling" flight, but it was obvious that our test method needed to be revised. Because the unpredictable wind conditions made such an impact on the thermal updrafts, and therefore, endurance of our flights, we decided to try to minimize their affect on our experimentation.

### 3. Benchmark Constant-Throttle Flights

We realized that by trying to use thermals to extend our flights we were introducing a great deal more variation. It would have taken a relatively large number of flights with each configuration to try to sift out the proportion of extended endurance was due to solar cells. One a good day, an experienced pilot can exploit thermal activity to extend a sailplane's endurance to several hours.

Besides reducing variation, we needed to change our flight profile to make it more consistent with a typical UAV mission. The military does not use UAVs like sailplanes; flying wherever the updrafts are best, but rather they have a particular location, activity, or vehicle to monitor or they have predetermined surveillance flight path. Therefore, we decided to conduct our flight tests as we had done our bench and rooftop testing; we would set the throttle to a certain level for each flight. The only difference for the flight tests would be the initial power used. At launch, the throttle would have to be higher to get the aircraft to a safe altitude, approximately 200–400 ft above ground level (AGL).

At this point, we had already modified our plane, so to produce a new baseline we attached a spare set of wings from the same model, again courtesy of Don Meeks. We would not remove the additional wiring and small circuit board from the cockpit of the plane, but the additional weight was only about 10 grams, or approximately 1–2% of the original weight.

We did not have onboard telemetry equipment to monitor the current and voltage during our testing and transmit it to the ground. We did however know the throttle position at which we had done all static testing that equated to an initial current of approximately 1.95 A. So once the plane was at a safe altitude, our pilot set the throttle to one notch below midpoint and flew the plane back and forth across the wind.

On August 12, 2009, we went back to the field for our new baseline flights and possible additional flights with the solar wings. We did two tests using the method described previously. The first test, using Battery 2 (1.3 Ah) lasted 33 minutes, and the second test, using Battery 3 (1.35 Ah), lasted 37 minutes. While we waited for our first battery to recharge for a possible solar-assisted flight, the wind picked up considerably. When we began our flights the wind was only 3–5 mph, but less than three hours later, it had strengthened to a steady 10 mph, with gusts reaching 14 mph, which precluded further testing that day.

#### 4. Solar Constant-Throttle Flight

Our next available flight was August 17. We mounted the solar wings on the plane and launched the Thin-Film Flyer with Battery 2 at 10:56 a.m. The wind speed was an acceptable 4 mph. Our constant-throttle solar-aided flight completed at 12:29 p.m., 93 minutes after launch. This is an endurance of 2.5 times greater than the pre-solar flight.

We were unable to conduct additional flights on this day. We decided that this flight and the thermalling solar flights had confirmed the airworthiness of the aircraft. More importantly, these flights confirmed the validity of our more extensive rooftop testing in projecting the improved endurance of our plane.

## F. ENERGY CALCULATIONS

From the bench-discharge test pictured in Figure 91, we used our voltage and current measurements to find the power at one-minute intervals. As shown in Figure 100 we used a Riemann sum to approximate the integral of the power during the test. This resulted in a calculated energy of 13.7 watt-hours (Wh), or 49,320 J. Our battery was rated at 1.3 ampere-hours (Ah) at a nominal 11.1 V, or 14.43 Wh.

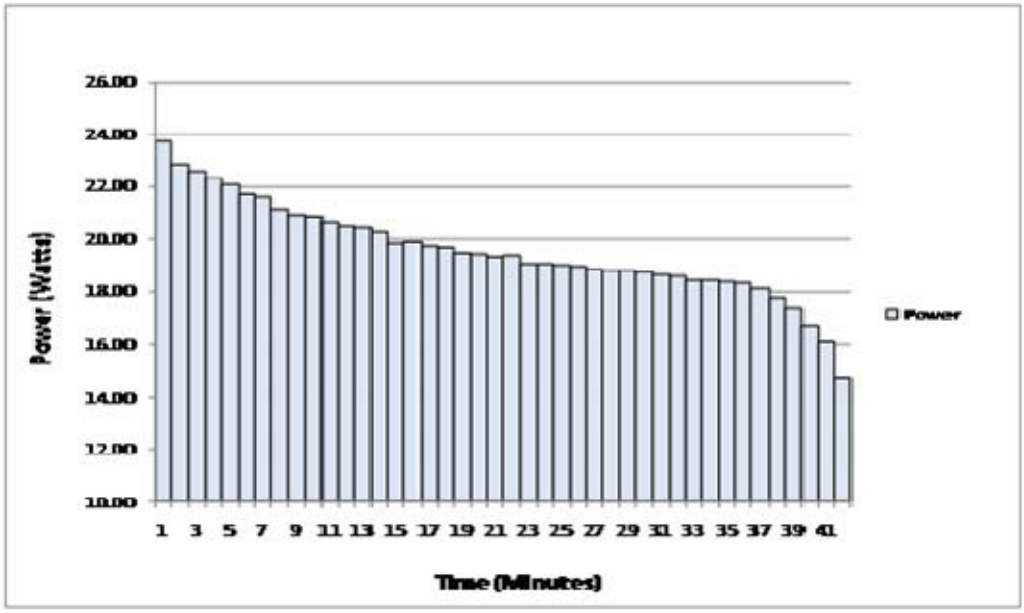


Figure 100. Battery Discharge (Power vs. Time)

During our final flight test, the level-flight power was approximately 20 W. Since the plane flew for 93 minutes, or 1.55 hours, the total energy used during the flight was

$$20\text{W}(1.55\text{ hours}) = 31\text{ Wh} \tag{6.2}$$

Since the battery can provide about 13.7 W-h, the remaining 17.3 W-h was provided by the solar cells. This means our solar cells were providing approximately

$$\frac{17.3\text{Wh}}{1.55\text{h}} = 11.16\text{ W} \tag{6.3}$$

With an efficiency of 11%, rather than 8% efficient, production line Global Solar cells will produce about 37.5% greater power under a given irradiance. Using our final flight test as an example, the solar cells would produce

$$11.16\text{W}(1.375) = 15.35\text{ W} \tag{6.4}$$

The aircraft will still require the same or less power, about 20 W, since the more efficient cells will weigh the same or less than the current cells. Therefore, the power required from the battery will be on average about

$$20\text{W} - 15.35\text{W} = 4.65\text{ W} \tag{6.5}$$

We found our battery could provide approximately 13.7 Wh, so by extension, we estimate that under the same irradiance, the aircraft would fly for

$$\frac{13.7\text{Wh}}{4.65\text{W}} = 2.95\text{ h (177 minutes)} \tag{6.6}$$

This would be 1.9 times better than the current configuration, and 4.8 times longer endurance than the same plane before the addition of solar cells.

## G. RAVEN COMPARISON

To extend our results from our proof-of-concept aircraft to the RQ-11 Raven, we first note that the Raven is significantly heavier. It also has greater in-flight power consumption due to its payload. Though it is heavier, it also has a much larger battery than that we used in our plane. With the 8% cells we used, crudely attached, and without an MPPT, the improvement in the Raven's endurance would be much less significant that what we achieved. However, with better cells, an integrated high-efficiency, lightweight MPPT, and better aerodynamics, we believe that Raven could achieve a proportionally equivalent gain in endurance.

Because the solar cells we used were only 8% efficient and had heavy lamination, they only had a power density of 75 W/kg. Global Solar has 11% efficient production cells that have a power density nearly 350 W/kg [66]. Using these cells would provide nearly 40% more power for a given irradiance than those we used, and they are much lighter. The net effect of using lighter, more efficient cells would be a power density nearly five times greater. This means the UAV would have greater power, with much less additional weight than our demonstrator would.

Aside from better, lighter CIGS solar cells, an implementation on the Raven or other UAV would also include an MPPT. As previously discussed, an MPPT can provide an additional 30% or more power compared to solar installations without power point tracking.

## H. COST ESTIMATE

The cost of the RQ-11 Raven is approximately $35,000 per aircraft [99]. Though we were not able to purchase a larger quantity of cells, Global Solar quoted a price of $5,000 for 50 strings of cells, with each string made of 18 cells. The cells are each 0.021 $m^2$, so approximately 10 cells could be used on the wings of a Raven ($0.2m^2$). For that order size, there would be 900 cells total, or ideally enough for 90 RQ-11s, at a per unit cost of just over $55. However, Global Solar cells can be as little as one dollar per watt for larger purchases [107], and a contract to produce enough cells for each of the 10,000 Ravens would certainly bring the cost-per-watt closer to this price.

At $30 per unit for CIGS solar cells, $100 for each MPPT, $50 for adhesive, wiring, and other miscellaneous items, and perhaps $500 per unit for re-engineering and assembly labor, we estimate that solar-modification of the RQ-11 Raven would cost less than $1,000 per unit.

## I. CHAPTER SUMMARY

We began this chapter by describing our battery characterization tests, showing the I-V curves of Lithium-polymer batteries during charge and discharge. We reviewed our constant-throttle bench-top battery tests, which showed that many Li-po batteries have a “break-in” period that affects their run time. Once we established our baseline battery endurance, we conducted stationary rooftop tests with a maximum power point tracker. This demonstrated that our solar cells provided significant improvement, but less than expected.

Next, we showed that by removing the faulty MPPT our rooftop testing produced much better results. With the defective circuit removed, the plane's endurance increased up to three times the pre-solar level. We also described our final rooftop test, with our components crudely attached to the plane.

We described our series of experiments that consisted of two distinctly different flight profiles. The first test flights attempted to make use of thermal updrafts to take advantage of our sailplane's design for extended flights. These tests revealed that this method was far too volatile due to day-to-day weather changes that affected performance. Our second set of airfield experiments was conducted under constant throttle, so were more consistent with real-world UAV missions. These experiments showed that with far from ideal materials and construction, a battery-powered plane's endurance increased 2.5 times.

We concluded the chapter showing how these performance results could be extended to the Raven, which could be modified with CIGS cells for $1,000 per plane.

THIS PAGE INTENTIONALLY LEFT BLANK

# VII. CONCLUSIONS

This thesis examined the history of solar flight, including recent advances that have produced several aircraft capable of multiday flights. It examined the current inventory of U.S. unmanned aerial vehicles to determine best candidate for solar modification. It chose the RQ-11 Raven as the target aircraft due to the large number in use and projected future employment.

Next, it reviewed the fundamentals of photovoltaics and described the advantages of thin-film solar cells for aviation applications. It compared the three most practical thin-film cells: amorphous silicon, cadmium telluride, and copper indium gallium diselenide. CIGS cells were chosen as they have the greatest research and production-line efficiency, have the greatest potential for future improvement, and have better specific energy density than any other type of cell, thin-film or otherwise.

Solar cell configuration and optimization was described, including the importance of using a circuit to track the maximum power point for greatest efficiency. Current and near-term battery options were also described. Next it reviewed the aircraft chosen as a proof-of-concept aircraft in lieu of an RQ-11, and detailed the system design, construction, and testing using heavier and lower efficiency cells than would be used in a UAV modification.

Experiments were conducted in three stages; bench, rooftop, and flight. These tests first established baseline battery endurance under constant throttle. Then rooftop testing showed that the batteries used in this aircraft could be recharged between flights in as little as two hours using the solar cells that would be installed. Next, pre-installation tests showed that with 8% efficient CIGS, the endurance of the test plane could be extended up to three times its pre-solar baseline.

Finally, using a constant-throttle flight to approximate the mission profile of a UAV, the aircraft flew 2.5 times longer with solar cells than without. Table 11 gives a summary of the results obtained.

| | Battery Alone | Battery and Solar Cells |
|---|---|---|
| Battery Charging | Requires External Power | 140.5 Minutes average time to charge. No external source needed. |
| Stationary Plane Endurance Test | 38.6 Minutes average | 75.9 Minutes average |
| | 43.25 Minutes best | 108 Minutes best |
| Level Flying | 37 Minutes | 93 Minutes |
| Calculated Level Flight with 11% Efficient CIGS | 37 Minutes | 177 Minutes |

Table 11. Summary of Testing Results

We showed that our plane flew for 37 minutes on battery alone, 93 minutes once 8% efficient CIGS cells were installed. We then calculated that under the same irradiance, the plane would fly 177 minutes with available 11% efficient CIGS cells. This would be 4.8 times greater endurance for a UAV than on battery alone.

Comparison between our test aircraft and the RQ-11 revealed that, although the Raven is much heavier and has greater power consumption due to its payload, similar endurance improvements might be seen using better 11% rather than 8% CIGS cells, much improved construction, and a maximum power point tracking circuit. Lastly, this thesis estimated the cost of such a solar modification to be less than $1,000 per aircraft, about 3% of the initial cost of a single Raven.

## A. RESEARCH CONTRIBUTIONS

To the author's knowledge, no existing military UAVs use solar cells, and no research on any type of aircraft has examined the utility of CIGS thin-film cells. Since CIGS cells have greater specific energy density than any other type of cell, they are the best choice in applications where weight is a critical factor.

This research also showed the additional benefit of allowing a solar UAV to self-charge on the ground between flights. When not needed to recharge the onboard battery, the wing-mounted cells can connected through adapters to power other mobile electronics in the field. Additional lightweight CIGS battery chargers could be added to a UAVs kit to power the ground station, transmitter, and other electronics.

## B. RECOMMENDATIONS

There are many ways this research can be continued and improved. In order to show even better performance with this specific application, the aircraft can be tested using lighter, more efficient Global Solar, or possibly CIGS on polyimide from Ascent Solar. Any further testing should include a comparison using the repaired Genasun MPPT.

An overall system design approach such as that presented by Dr. Noth could prove incredibly beneficial in the design or modification of a UAV [5]. This simulation program takes into account a myriad of aerodynamic, mechanical, and electrical parameters to forecast the endurance of a solar UAV.

### 1. Improved MPPT

A significant improvement of this application would be to procure or design an MPPT more suitable for use in UAVs. As previously discussed, this circuit would include solar cell protection, power point tracking, charge control, and lithium-polymer cell balancing. The best design would be integral to the existing UAV electronics, or be easily integrated without significant system redesign. A system-on-a-chip design would provide the best combination of features necessary as it would be lightweight, low power, and much smaller than current designs.

### 2. Test on RQ-11 Raven

An RQ-11 Raven should be obtained in order to fully test the concept of this research and to provide a realistic design. Without the complete drawings, specifications, and performance data of the Raven, it is impossible to accurately forecast the true impact of solar modification. Knowing the physical and electrical configuration of the Raven will permit the integration of an existing or newly designed MPPT. In addition, application of thin-film cells to other surfaces like the fuselage and stabilizers could be examined. Furthermore, a multi-disciplinary project can explore the possibility of redesigning optional wings for the RQ-11 to provide greater surface area upon which to mount solar cells.

### 3. Design or Modification of More Suitable UAV

Another intriguing extension of this research would be to find, or design UAV with larger surface area, and thus better optimized for solar modification. An existing aircraft that might suit this purpose is the tandem wing DraganFly Tango, shown in Figure 101.

Figure 101. DraganFly Tango Tandem-Wing Commercial UAV (From [108]).

"Flying wings" or "delta wing" designs would be an excellent choice for solar integration, since the aircraft would provide a very large proportion of surface area to weight. Examples are the current AeroVironment Wasp, or larger battery-powered designs like the Strix, shown in Figure 102.

Figure 102. Strix Flying Wing UAV from Selex Galileo (After [109]).

### 4. CIGS and Lithium-Sulfur Batteries

As discussed in Chapter IV, Lithium-Sulfur batteries have a much higher specific energy than Lithium-polymer. When used in an RQ-11, these batteries permitted a flight of nearly seven hours. If these batteries were used in conjunction with CIGS solar cells on a large-surface area UAV, multiday flights would be possible even in tactical UAVs. The best configuration would minimize support materials and surfaces by incorporating batteries in the main wing and fuselage and using the solar cells as the top surface material, rather than layering them upon a superstructure.

THIS PAGE INTENTIONALLY LEFT BLANK

# LIST OF REFERENCES


[1] Office of the Secretary of Defense, "FY2009–FY2034 Unmanned Systems Integrated Roadmap," *Office of the Under Secretary of Defense for Acquisition, Technology and Logistics*, Apr. 2009. [Online]. Available: http://www.acq.osd.mil/uas/docs/UMSIntegratedRoadmap2009.pdf. [Accessed Aug. 16, 2009].

[2] DARPA, "News Releases 2008," *DARPA* Apr. 2008. [Online]. Available: http://www.darpa.mil/news/2008/vulture.pdf. [Accessed Aug. 19, 2009].

[3] R. J. Boucher, "Project Sunrise," presented at AIAA/SAE/ASME 15th Joint Propulsion Conference Las Vegas, Nevada, 1979.

[4] AC Propulsion, *AC Propulsion's Solar Electric Powered SoLong UAV*. AC Propulsion. Jun. 2005. [Online]. Available: http://www.tu.no/multimedia/archive/00024/SoLong_info_24122a.pdf. [Accessed Sept. 23, 2009].

[5] Andre Noth, "Design of Solar Powered Airplanes for Continuous Flight," PhD Thesis, Autonomous Systems Lab, ETH Zurich, Dec. 2008. [Online]. Available: http://www.sky-sailor.ethz.ch/docs/Thesis_Noth_2008.pdf. [Accessed May 13, 2009].

[6] Niels Diepeveen, "The Sun Surfer: Design and construction of a solar powered MAV," M.S. Thesis, Swiss Federal Institute of Technology, Zurich, 2007.

[7] R. J. Boucher, "History of Solar Flight," presented at AIAA/SAE/ASME 20th Joint Propulsion Conference, Cincinnati, OH, 1984.

[8] Experimental Aircraft Association, Inc., "UFM-Mauro Solar Riser," *EAA AirVenture Museum – Oshkosh, WI.* [Online]. Available: http://www.airventuremuseum.org/collection/aircraft/UFM-Mauro%20Solar%20Riser.asp. [Accessed Aug. 21, 2009].

[9] NASA, "Albatross ECN-13413: Solar-powered Gossamer Penguin in flight," NASA. Feb. 2002. [Online]. Available: http://www.dfrc.nasa.gov/Gallery/Photo/Albatross/HTML/ECN-13413.html. [Accessed Aug. 22, 2009].

[10] AeroVironment, "UAS Advanced Development Center: Solar Challenger Detail," *AeroVironment.* May 2009. [Online]. Available: http://www.avinc.com/uas/adc/solar_challenger/. [Accessed Sept. 20, 2009].

[11] G. Palmisano, & R. Ciriminna, *Flexible Solar Cells*. (2008). Weinheim: Wiley-VCH.

[12] T. E. Noll, J. M. Brown, M. E. Perez-Davis, S. D. Ishmael, G. C. Tiffany, & M. Gaier, "Investigation of the Helios Prototype Aircraft Mishap," *NASA* (2004). Hampton: NASA.

[13] Douglas Barrie, "Qinetiq Fine-Tuning Zephyr For Longer Flights," *Aviation Week* Aug. 2008. [Online]. Available : http://www.aviationweek.com/aw/generic/story_channel.jsp?channel=defense&id=news/ZEPHYR082508.xml&headline=Qinetiq%20Fine-Tuning%20Zephyr%20For%20Longer%20Flights. [Accessed Aug. 26, 2009].

[14] Sion Power, "Advanced Energy Storage : Technology Overview," *Sion Power Corporation.* May 2008. [Online]. Available: http://www.sionpower.com/technology.html. [Accessed Aug. 26, 2009].

[15] QinetiQ, "Zephyr - Unmanned Aerial Vehicle (UAV)," *QinetiQ*. [Online]. Available: http://www.qinetiq.com/home/products/zephyr.html. [Accessed Aug. 26, 2009].

[16] DARPA, "Vulture," *Darpa - Tactical Technology Office*. Aug. 2009. [Online]. Available: http://www.darpa.mil/TTO/programs/vulture/index.htm. [Accessed Aug. 26, 2009].

[17] SunPower, "SunPower Launches High-Efficiency Photovoltaic Modules in North America," *SunPower*. Oct. 2004. [Online]. Available: http://investors.sunpowercorp.com/releasedetail.cfm?releaseid=179414. [Accessed Aug. 26, 2009].

[18] NOVA. "Spies That Fly," *PBS*. Nov. 2002. [Online]. Available: http://www.pbs.org/wgbh/nova/spiesfly/uavs.html. [Accessed Aug. 27, 2009].

[19] John DeGaspari, "Look Ma, No Pilot!" *Mechanical Engineering Magazine - MEMagazine.* Nov. 2003. [Online]. Available: http://www.memagazine.org/backissues/membersonly/nov03/features/lookma/lookma.html. [Accessed Aug. 17, 2009].

[20] Edward S. Marek, "Old Herc a pioneer in laser guided bombing." *Talking Proud.* Aug. 2009. [Online]. Available: http://www.talkingproud.us/ImagesMilitary/BlindbatLGB/DC130.jpg. [Accessed Sept. 24, 2009].

[21] United States Navy, "The US Navy - Fact File," *United States Navy*. Feb. 2009. [Online]. Available: http://www.navy.mil/navydata/fact_display.asp?cid=1100&tid=2100&ct=1 [Accessed Aug 28, 2009].

[22] Laurence R. Newcome, *Unmanned aviation: a brief history of unmanned aerial vehicles.* Reston, VA: American Institute of Aeronautics and Astronautics, 2004.

[23] William Park, "North America > Low Altitude Short Range UAV," Mar. 2006. *William Park's UAV(UAS) Center.* [Online]. Available: http://www.uavcenter.com/english/wwuavs/north_america/eSR.asp. [Accessed Sept. 20, 2009].

[24] Bill Yenne, Attack of the drones: a history of unmanned aerial combat. St. Paul, MN: Zenith Press, 2004.

[25] Ed Wolski, "Unmanned Aircraft Systems," Wired, Jan. 2009. [Online]. Available: http://www.wired.com/images_blogs/dangerroom/files/Wolski.pdf. [Accessed Sept. 23, 2009].

[26] Northrop Grumman, "X-47B UCAS," *Northrop Grumman Corporation*. (2009) [Online]. Available: http://www.as.northropgrumman.com/products/nucasx47b/index.html. [Accessed Aug. 31, 2009].

[27] G. Warwick, & G. Norris, "Blue Sky Thinking: DARPA is 50 years old and still looking 20 years into the future," *Aviation Week and Space Technology,* pp. 2–6. Aug. 2008.

[28] Andreas Parsch, " Leading Systems Amber," *Designation-Systems.Net.* Jun. 2004. [Online]. Available: http://www.designation-systems.net/dusrm/app4/amber.html. [Accessed Sept. 20, 2009].

[29] D. W. Jaquish, "Uninhabited Air Vehicles for Psychological Operations," *Air and Space Power Journal - Español, Cuarto Trimestre 2005.* Nov. 2005. [Online]. Available: http://www.airpower.maxwell.af.mil/apjinternational/apj-s/2005/4tri05/jaquish.html. [Accessed Sept. 20, 2009].

[30] T. V. Brook, "Faster, deadlier pilotless plane bound for Afghanistan," *USA Today*. Aug. 27, 2007.

[31] General Atomics Aeronautical, "GA-ASI Successfully Executes First Flight of Predator C Avenger," *General Atomics Aeronautical Systems Inc.* Apr. 2009. [Online]. Available: http://www.ga-asi.com/news_events/index.php?read=1&id=186&page=1. [Accessed Sept. 1, 2009].

[32] Graham Warwick, "New Predator C Hints At Stealth, Weaponry," *Aviation Week.* Apr. 2009. [Online]. Available: http://www.aviationweek.com/aw/generic/story_channel.jsp?channel=defense&id=news/AVENGE041509.xml. [Accessed Sept. 20, 2009].

[33] U. S. Air Force, Air Combat Command, Public Affairs Office, “Factsheets : RQ-4 Global Hawk Unmanned Aircraft System,” *The Official Website of the U. S. Air Force*. Oct. 2008. [Online]. Available: http://www.af.mil/information/factsheets/factsheet.asp?fsID=13225. [Accessed Sept. 1, 2009].

[34] FlightInternational, “US budget watchdog calls for suspension of Northrop Grumman RQ-4B UAV full production,” *Flightglobal*. Mar. 2006. [Online]. Available: http://www.flightglobal.com/articles/2006/03/16/205482/us-budget-watchdog-calls-for-suspension-of-northrop-grumman-rq-4b-uav-full.html [Accessed Sept. 21, 2009].

[35] John Wilson, "The Next Age in Aviation," *Approach*, pp. 3–4, Jul.-Aug. 2009. [Online]. Available: http://safetycenter.navy.mil/media/approach/issues/julaug09/Jul-Aug09_Approach.pdf. [Accessed Aug. 31, 2009].

[36] INSITU, “Resources” *Insitu, Inc*. Aug. 2009. [Online]. Available: http://www.insitu.com/press-resources. [Accessed Sept. 22, 2009].

[37] Army Technology, “Shadow 200 RQ-7 Tactical Unmanned Aircraft System, USA – Army Technolog,” *Army Technology*. Sept. 2009. [Online]. Available: http://www.army-technology.com/projects/shadow200uav/. [Accessed Sept. 22, 2009].

[38] Glenn W. Goodman Jr., "Three Tiers - The Marine Corps takes a key step this summer to modernize its UAVs," *Seapower*, p. 18, Jul. 2006. [Online]. Available: http://www.navyleague.org/sea_power/jul06-18.php. [Accessed Aug. 31, 2009].

[39] California Literary Review, “Fallujah_Drone_200.jpg,” *California Literary Review*. Jan. 2008. [Online]. Available: http://calitreview.com/images/falluja_drone_200.jpg. [Accessed Sept. 22, 2009].

[40] Michael Guillory, “Up, Up and Away,” *United States Army Homepage*. Nov. 2006. [Online]. Available: http://www.army.mil/-slideshows/2006/11/22/720-up-up-and-away/. [Accessed Sept. 22, 2009].

[41] Defense Update, “Wasp III MAVs for Marine Corps' Platoons,” *Defense Update Defence Industry News Military Technology Magazine.* May 2009 [Online]. Available: http://defense-update.com/newscast/1107/news/221107_wasp.htm. [Accessed Sept. 22, 2009].

[42] Doug Roles, “GMAV Pilots Bring 'hover and Stare' Capability to Battlefield,” *Stryker Brigade News*, Aug. 2009. [Online]. Available: http://www.strykernews.com/archives/2009/08/03/gmav_pilots_bri.html [Accessed Sept. 2, 2009].

[43] Nathan Hodge, “Nat’l Guard Gets Spying, ‘Flying Beer Keg’ for Iraq,” *Wired*. Nov. 2008. [Online]. Available: http://www.wired.com/dangerroom/2008/11/national-guard/. [Accessed Sept. 22, 2009].

[44] Darrell Brock, “MQ-8B Fire Scout Vertical Unmanned Aerial System.” *Northrop Grumman.* Sept. 2008. [Online]. Available: http://www.as.northropgrumman.com/products/mq8bfirescout_army/assets/FS-Fact-Sheet.pdf. [Accessed Sept. 23, 2009].

[45] Gidget Fuentes, “Frigate hosts latest trials for unmanned helo,” *Navy Times.* Jun. 2009. [Online]. Available: http://www.navytimes.com/news/2009/06/navy_fire_scout_062709w/. [Accessed Sept. 22, 2009].

[46] U.S. Department of Energy, “Solar Energies Technology Program: Solar Cell Structures,” *U.S. Department of Energy. 2005.* [Online]. Available: http://www1.eere.energy.gov/solar/solar_cell_structures.html#heterojunctions. [Accessed Sept. 23, 2009].

[47] Jonathan G. Dorn, “Solar Cell Production Jumps 50 Percent in 2007,” *Earth Policy Institute.* Dec. 2007. [Online]. Available: http://www.earthpolicy.org/index.php?/indicators/C47/. [Accessed Sept. 22, 2009].

[48] Mark Winter. WebElements. [Online]. Available: http://www.webelements.com/silicon/. [Accessed Sept. 3, 2009].

[49] Christiana Honsberg and Stuart Bowden, *PVCDROM* . Oct. 2008. [Online]. Available: http://pvcdrom.pveducation.org/SEMICON/SEMICON.HTM. [Accessed Sept. 6, 2009].

[50] Pieter Kuiper, “Electronic band structure,” *Wikipedia.* Sept. 2009. [Online]. Available: http://en.wikipedia.org/wiki/Electronic_band_structure. [Accessed Sept. 22, 2009].

[51] Robert F. Pierret, *Semiconductor Device Fundamentals*. Reading, Mass: Addison-Wesley, 1996.

[52] Matt Britt, “Semiconductor,” *Wikipedia.* Sept. 2006. [Online]. Available: http://en.wikipedia.org/wiki/Semiconductor. [Accessed Sept. 6, 2009].

[53] Carsten Deibel, “March – 2008,” Notes on Disordered Matter. Mar. 2008. [Online]. Available: http://blog.disorderedmatter.eu/2008/03/. [Accessed Sept. 22, 2009].

[54] Department of Physics – Durham University, "Solar cell research at Durham," Durham University. Dec. 2003. [Online]. Available: http://www.dur.ac.uk/~dph0www5/solar.html. [Accessed Sept. 22, 2009].

[55] Solar Buster, "Solar Buster – Technology," *Solar Buster*. Jun. 2009. [Online]. Available: http://solarbuster.com/technology. [Accessed Sept. 22, 2009].

[56] H. S. Rauschenbach, *Solar Cell Array Design Handbook*, Volume 1. Pasadena, CA, USA: NASA – Jet Propulsion Laboratory, 1976.

[57] Eye Lighting International of North America, Inc. "Solar Energy," Eye Lighting International of North America, Inc. Dec. 2008. [Online]. Available: http://www.eyesolarlux.com/Solar-simulation-energy.htm. [Accessed Sept. 5, 2009].

[58] Robert A. Rohde, "File:Solar Spectrum.png," *Global Warming Art*. Jun. 2007. [Online]. Available: http://www.globalwarmingart.com/wiki/File:Solar_Spectrum_png. [Accessed Sept. 23, 2009].

[59] Jenny Nelson, *The Physics of Solar Cells*. London: Imperial College Press, 2003.

[60] Luigi Pistoni and Massimiliano Merisio, "Solar LED lighting solutions for rural areas," *Power Management Design Resource for Electronic Engineers*. Mar. 2009. [Online]. Available: http://www.powermanagement-europe.com/215800654;jsessionid=RONJUC2ICCTMVQE1GHPSKHWATMY32JVN?pgno=2. [Accessed Sept. 23, 2009].

[61] Advanced Energy, "AE PV Sun Times E-Newsletter," *Advanced Energy*. Jun. 2009. [Online]. Available: http://www.advanced-energy.com/en/PV_Sun_Times.html. [Accessed Sept. 23, 2009].

[62] Sherif Michael, "EC3230 Space Power and Radiation Effects Solar Cell Basics," 2009. [Class Notes – Unpublished].

[63] Solar Horizon, "Solar Power For Your Home," *Solar Horizon*. Feb. 2009. [Online]. Available: http://www.solarhorizon.com.au/SolarCells.html. [Accessed Sept. 23, 2009].

[64] Tom's Hardware, "Wafer Fabrication – Review Tom's Hardware : Semiconductor Production 101," Jul. 2007. [Online]. Available: http://www.tomshardware.com/reviews/semiconductor-production-101,1590-3.html. [Accessed Sept. 22, 2009].

[65] Emcore Corporation, “Triple-Junction Solar Cell for Terrestrial Applications,” *Emcore*. Oct. 2008. [Online]. Available: http://www.emcore.com/assets/photovoltaics/CTJ_B_Web.pdf. [Accessed Sept. 6, 2009].

[66] Global Solar Energy, “G2 Thin Film String Data Sheet,” *Global Solar*. Jul. 2008.

[67] Gavin Conibeer, "Third Generation Photovoltaics," *Electronics Systemintegration Technology Conference*, 2008. Greenwich, IEEE, 2008, pp. 45–50.

[68] Solarbuzz, "Solar Photovoltaic, PV Module, Panel Prices," *Solarbuzz*. Jun. 2009 [Online]. Available: http://www.solarbuzz.com/Moduleprices.htm. [Accessed Jun. 17, 2009].

[69] Bob Haavind, “Industry execs hear about bright days ahead in energy,” *ElectroIQ.com*. Jan. 2009. [Online]. Available: http://www.electroiq.com/index/display/article-display/350771/s-articles/s-solid-state-technology/s-applications/s-solar/s-2009/s-01/s-industry-execs-hear-about-bright-days-ahead-in-energy.html. [Accessed Sept. 22, 2009].

[70] B. Von Roedern, “NREL: Thin Film Partnership Program - Latest Updates,” *NREL*. Mar. 2009. [Online]. Available: http://www.nrel.gov/pv/thin_film/docs/SPECSHEETrat0309pub.DOC. [Accessed Jun. 17, 2009].

[71] Alison J. Breeze, “Next Generation Thin-Film Solar Cells,” *University of California, Santa Cruz*. Apr. 2008. [Online]. Available : http://physics.ucsc.edu/~galers/stuff/2E-2.ppt. [Accessed Sept. 7, 2009].

[72] Emcore, “Space and Satellite Solar Cells,” *Emcore*. 2009. [Online]. Available: http://www.emcore.com/solar_photovoltaics/space_solar_cells. [Accessed Sept. 7, 2009].

[73] Spectrolab, “Products - Space – Cells,” *Spectrolab*. [Online]. Available: http://www.spectrolab.com/prd/space/cell-main.asp. [Accessed Sept. 7, 2009].

[74] Lawrence Kazmerski and Don Gwinner, “Solar Cell,” *Wikepedia*. Nov. 2007. [Online]. Available: http://en.wikipedia.org/wiki/Solar_cell. [Accessed Sept. 22, 2009].

[75] Rutgers University, “Solar Cell Design and Processing Class,” 2005. [Online]. Available: http://www.rci.rutgers.edu/~dbirnie/solarclass/amorphousSi.pdf. [Accessed Jun. 17, 2009].

[76] PowerFilm, “Technology,” *PowerFilm*. May 2008. [Online]. Available: http://www.powerfilmsolar.com/about/technology/. [Accessed Sept. 22, 2009].

[77] PowerFilm, “PowerFilm Solar OEM Components,” *PowerFilm.* Dec. 2008. [Online]. Available: http://www.powerfilmsolar.com/downloads/pdf/297774%20OEM%20Flysheet_p1.pdf [Accessed Sept. 7, 2009].

[78] A. Kolodziej, "Staebler-Wronski Effect in Amorphous Silicon and its Alloys," *Opto-electronics Review*, pp. 21–32, 2004.

[79] Tonio Buonassisi, “Signal Lake (from MIT course),” *Computer Communication Technical Innovation-Finance Innovation.* Jan. 2007. [Online]. Available: http://www.signallake.com/innovation/BuonassisiJan07.pdf. [Accessed Jun. 17, 2009].

[80] Global Solar Energy, "Technology," *Global Solar Energy.* Jul. 2009. [Online]. Available: http://www.globalsolar.com/technology/. [Accessed Sept. 24, 2009].

[81] A. J. Breeze, "Next generation thin-film solar cells," in *Reliability Physics Symposium, 2008.*, Phoenix, IEEE International, 2008, pp. 168–171.

[82] Karsten Otte, Liudmila Makhova, Alexander Braun, and Igor Konovalov, "Flexible Cu(In,Ga)Se2 thin-film solar cells for space application," *Thin Solid Films*, pp. 613–622, 2006.

[83] UC - Santa Cruz, “Energy Conversion,” *University of California, Santa Cruz.* May 2009. [Online]. Available: http://www.ic.ucsc.edu/~wxcheng/envs23/lecture17/conversion_efficiency.html. [Accessed Sept. 23, 2009].

[84] Polar Power Inc., “Different types of photovoltaic systems,” *Polar Power Inc.* Feb. 2000. [Online]. Available: http://www.polarpowerinc.com/info/operation20/operation23.htm. [Accessed Sept. 23, 2009].

[85] Martin A. Green, "General Temperature Dependence of Solar Cell Performance and Implications for Device Modelling," *Progress in Photovoltaics: Research and Applications*, pp. 333–340, 2003.

[86] Ben Gorman, “Electrical Characteristics of Solar Panels or PV Modules,” *AltE.* Mar. 2008. [Online]. Available: http://www.altestore.com/howto/Electrical-Characteristics-of-Solar-Panels-PV-Modu/a87/. [Accessed Sept. 23, 2009].

[87] William Pentland, “Solar Energy,” *Knol.* Oct. 2008. [Online]. Available: http://knol.google.com/k/william-pentland/solar-energy/1g0rrsoesmjko/2?version=125. [Accessed Sept. 23, 2009].

[88] Richard A. Cullen, “Frequently Asked Questions & Technical Tips.” *Blue Sky Energy Inc.* Apr. 2004. [Online]. Available: http://www.blueskyenergyinc.com/uploads/pdf/BSE_What_is_MPPT.pdf. [Accessed Sept. 9, 2009].

[89] Global Solar, “SUNLINQ Portable Solar Panel - 12 Watt,” *Global Solar*. Mar. 2008. [Online]. Available: http://www.globalsolar.com/download.php?f=sl_12_spec_sheet.pdf [Accessed Sept. 17, 2009].

[90] Maxim Integrated Products, “Switch-Mode, Linear, and Pulse Charging Techniques for Li+ Battery in Mobile Phones and PDAs,” *Maxim/Dallas Semiconductor*. Dec., 2001. [Online]. Available http://pdfserv.maxim-ic.com/en/an/AN913.pdf. [Accessed Sept. 9, 2009].

[91] RCHeliSite, “Lipo Battery Charging & Safety Guide,” *RCHeliSite*. Feb. 2008. [Online]. Available: http://www.rchelisite.com/lipo_battery_charging_and_safety_guide.php. [Accessed Sept. 9, 2009].

[92] Randyll R. M. Fernandez, "A Novel Photovoltaic Power Converter for Military And Space Applications," M.S. Thesis, Naval Postgraduate School, Monterey, California, 2005.

[93] Office of the Secretary of Defense, "Unmanned Aircraft Systems Roadmap," *Office of the Secretary of Defense*. Aug. 2005. [Online]. Available: http://fas.org/irp/program/collect/uav_roadmap2005.pdf. [Accessed Sept. 23, 2009].

[94] Aaron Moore, “Lithium Polymer (Lipo) Battery Guide,” *ProtoTalk.net*. Nov. 2008. [Online]. Available: http://prototalk.net/forums/showthread.php?t=22. [Accessed Sept. 10, 2009].

[95] Sion Power Corporation, “Applications for Unmanned Systems,” *Sion Power Corporation*. Apr. 2009. [Online]. Available: http://sionpower.com/applications/unmanned.html. [Accessed Sept. 10, 2009].

[96] Yu. Mikhaylik, I. Kovalev, J. Xu, and R. Schock, "Rechargeable Li-S Battery with Specific Energy 350," *213th Electrochemical Society Meeting, Abstract #112*, Phoenix, 2008.

[97] Michael Yon, “Bird’s Eye View,” *Michael Yon - Online Magazine.* Jul. 2007. [Online]. Available: http://www.michaelyon-online.com/birds-eye-view.htm. [Accessed Sept. 22, 2009].

[98] RC Flyer, “Parkzone Radian P'N'P Electric Powered Sailplane,” *RC Flyer*. Nov. 2008. [Online]. Available: http://rcflyer.com.au/shop/catalog/product_info.php?cPath=31&products_id=384. [Accessed Sept. 23, 2009].

[99] Raymond Piper, “Small UAV provides eyes in the sky for battalions.” *Global Security* Feb. 2005. [Online]. Available: http://www.globalsecurity.org/intell/library/news/2005/intell-050216-arnews01.htm. [Accessed: Sept. 11, 2009].

[100] Global Solar, “SUNLINQTM Portable Solar Panel - 6.5 Watt,” *Global Solar*. Mar. 2008. [Online]. Available: http://www.globalsolar.com/download.php?f=sl_6.5_spec_sheet.pdf. [Accessed Sept. 17, 2009].

[101] Global Solar Energy, “Products – Information,” *Global Solar*. Jul. 208. [Online]. Available: http://www.globalsolar.com/download/mil-std-810.pdf. [Accessed Sept. 12, 2009].

[102] Solar Converters Inc., “3 Amp Charge Controller Model: PT 12/24–3,” *Solar Converters Inc.* Mar. 2008. [Online]. Available: http://www.solarconverters.com/sp12_3.htm. [Accessed Sept. 12, 2009].

[103] Karen E. Robinson, GV-4 Flyer, *Genasun*, Oct. 2008. [Online]. Available: http://www.genasun.net/gv4flyer.pdf. [Accessed Sept. 12, 2009].

[104] Tower Hobbies, “Venom AC/DC Pro Charger,” *Tower Hobbies*. Apr. 2008. [Online]. Available: http://www3.towerhobbies.com/cgi-bin/wti0001p?&I=LXUAB8&P=7#tech. [Accessed Sept. 23, 2009].

[105] Brian Gosselin, “R/C Calculations,” *ScriptAsylum*. Aug. 2009. [Online]. Available: http://scriptasylum.com/rc_speed/_lipo.html. [Accessed Sept. 23, 2009].

[106] Bob Butcher, "Temperature and Light Level Effects on CIGS Solar Panels," *Global Solar*. Feb. 2007. [Document].

[107] Eric Fuentes of Global Solar in a private telephone conversation Jun. 2009.

[108] Draganfly, “Photo Gallery - Draganfly Tango,” *Draganfly*. Aug. 2008. [Online]. Available: http://www.draganfly.com/uav-airplane/tango/gallery/pictures/picture-4.php. [Accessed Sept. 23, 2009].

[109] Air Force Public Information Office, “Il colonnello Sicuso prima di un lancio di un UAV Strix.jpg,” *Air Force Public Information Office (Italy).* Oct. 2008. [Online]. Available: http://stampa.aeronautica.difesa.it/tih08_fotogallery/imagepages/image35.htm. [Accessed Sept. 23, 2009].

THIS PAGE INTENTIONALLY LEFT BLANK

# INITIAL DISTRIBUTION LIST

1. Defense Technical Information Center
   Ft. Belvoir, Virginia

2. Dudley Knox Library
   Naval Postgraduate School
   Monterey, California

3. Chairman, Department of Electrical and Computer Engineering
   Naval Postgraduate School
   Monterey, California

4. Dr. Sherif Michael, Code EC/Mi
   Department of Electrical and Computer Engineering
   Monterey, California

5. Dr. Todd Weatherford, Code EC/Wt
   Department of Electrical and Computer Engineering
   Monterey, California

6. Dr. Kevin Jones
   Department of Electrical and Computer Engineering
   Monterey, California

7. CAPT Vincente Garcia USN (Ret.)
   Department of Electrical and Computer Engineering
   Monterey, California

8. LtCol James Roudebush USMC
   Naval Air Systems Command (PMA-263)
   Patuxent River, Maryland

9. Maj James Lee USMC
   Marine Corps Systems Command (PG-11)
   Quantico, Virginia

10. Robert Wolfe
    Army PEO Aviation (Unmanned Aircraft Systems)
    Redstone, Alabama

11. Bruce Fowler
    Army PEO Aviation (Unmanned Aircraft Systems)
    Redstone, Alabama